Rheinland-Pfälzische Technische Universität Kaiserslautern Landau

Addressing the redundant roles of phytotoxic proteins in the necrotrophic infection of *Botrytis cinerea* by multi-knockout mutagenesis

vom Fachbereich Biologie

der Rheinland-Pfälzischen Technischen Universität Kaiserslautern-Landau

zur Verleihung des akademischen Grades Dr. rer. nat. genehmigte

Dissertation

von

Nassim Safari, M.Sc., geb. in Teheran

Mündliche Prüfung: 29.09.2025

Dekan:	Prof. Dr. Stefan Kins
Promotionskommissionsvorsitzender:	Prof. Dr. Michael Schroda
Berichterstattende:	Prof. Dr. Matthias Hahn
	Prof. Dr. Ekkehard Neuhaus

D386

Related Publications:

Klug K, Zhu P, Pattar P, Mueller T, **Safari N**, Sommer F, Valero-Jiménez CA, van Kan JA, Huettel B, Stueber K, Scheuring D. Genome comparisons between *Botrytis fabae* and the closely related gray mold fungus *Botrytis cinerea* reveal possible explanations for their contrasting host ranges. Journal of Fungi. 2024 Mar 14;10(3):216.

Müller T, Bronkhorst J, Müller J, **Safari N**, Hahn M, Sprakel J, Scheuring D. Plant infection by the necrotrophic fungus Botrytis requires actin-dependent generation of high invasive turgor pressure. New Phytologist. 2024 Oct;244(1):192-201.

Leisen T, Werner J, Pattar P, **Safari N**, Ymeri E, Sommer F, Schroda M, Suárez I, Collado IG, Scheuring D, Hahn M. Multiple knockout mutants reveal a high redundancy of phytotoxic compounds contributing to necrotrophic pathogenesis of *Botrytis cinerea*. PLoS pathogens. 2022 Mar 3;18(3):e1010367.

Table of Contents

1. Introduction

1.1 The gray mold pathogen *Botrytis cinerea*

Botrytis cinerea, an ascomycete fungus belonging to the family *Sclerotiniaceae* (order *Helotiales*) is widely recognized as the primary causative agent of gray mold disease, a serious problem in many important crop systems (Dean et al., 2012). *B. cinerea* infects more than 1,400 plant species, by killing host cells and exploiting the resulting necrotic tissue (Elad et al., 2016). It attacks many commercially important crops, including vegetables (e.g., celery, zucchini, lettuce), ornamental flowers (e.g., sunflower, rose, tulip), bulbs (e.g., garlic and various flower bulbs), and fruits (e.g., grapevine, strawberry, kiwifruit). Global annual losses linked to this pathogen are conservatively placed between 10 and 100 billion USD (Weiberg et al., 2013). The fungus produces vast quantities of multinucleate conidia on branched conidiophores, giving lesions their characteristic gray appearance and enabling efficient wind, insect, and mechanical dispersal (Webster et al., 2009; Agrios, 2005). Field populations frequently evolve resistance to multiple fungicide classes because of marked genetic plasticity (Hahn, 2014). These combined traits necrotrophy, exceptionally wide host range and high adaptability, have established *B. cinerea* as one of the most studied plant pathogens (Dean et al., 2012; Elad et al., 2016).

1.2 Life and infection cycle of *B. cinerea*

As a representative of the Ascomycota, *B. cinerea* exhibits three defining traits: (i) formation of stromatic ascocarps (apothecia); (ii) production of ascospores within asci; and (iii) generation of asexual micro- and macroconidia on conidiophores (Deacon, 2006). Although apothecia are rarely observed in nature, they can be produced readily on artificial media (Spada et al., 2024). Conidia arising from aerial mycelium on host surfaces constitute the main inoculum: they are dispersed over long distances by wind and can cross continents through latent plant infections (Deacon, 2006). Both spores and sclerotia occur virtually everywhere and are formed continuously throughout the year (Jarvis, 1977).

Airborne spores first adhere to the plant cuticle through weak hydrophobic interactions that are rapidly reinforced by a secreted polysaccharide matrix (Doss et al., 1993; Doss et al., 1995). Germ tubes then penetrate directly via appressorium-like infection cushions or enter through wounds and stomata; both strategies are supported by cutinases and pectin-degrading enzymes (Gourgues et al., 2004; ten Have et al., 1998; van Kan, 2006; Choquer

et al., 2007, 2021). Once inside, the fungus releases a coordinated arsenal of cell-wall-degrading enzymes, low-molecular-weight phytotoxins and small interfering RNAs that silence host-defence genes, ensuring rapid tissue maceration and nutrient acquisition (van Kan, 2006; Choquer et al., 2007; Weiberg et al., 2013; Porquier et al., 2021). Under adverse conditions the mycelium switches from conidiation to formation of melanised sclerotia, long-lived structures that persist in soil or plant debris (Jarvis, 1977). After fertilization by spermatia, sclerotia can produce apothecia that release ascospores; although seldom observed in nature, this sexual phase introduces novel allele combinations into field populations (Williamson et al., 2007; Atwell et al., 2015; Fillinger et al., 2018).

Latent infection and genetic diversity: In many fruit and ornamental hosts the fungus may remain quiescent until ripening, senescence or abiotic stress reactivates aggressive growth, an asymptomatic period that complicates disease forecasting and post-harvest control (Williamson et al., 2007). Comparative genomics reveals extensive intraspecific polymorphism, explaining both the breadth of the host range and the rapid emergence of fungicide resistance (Atwell et al., 2015).

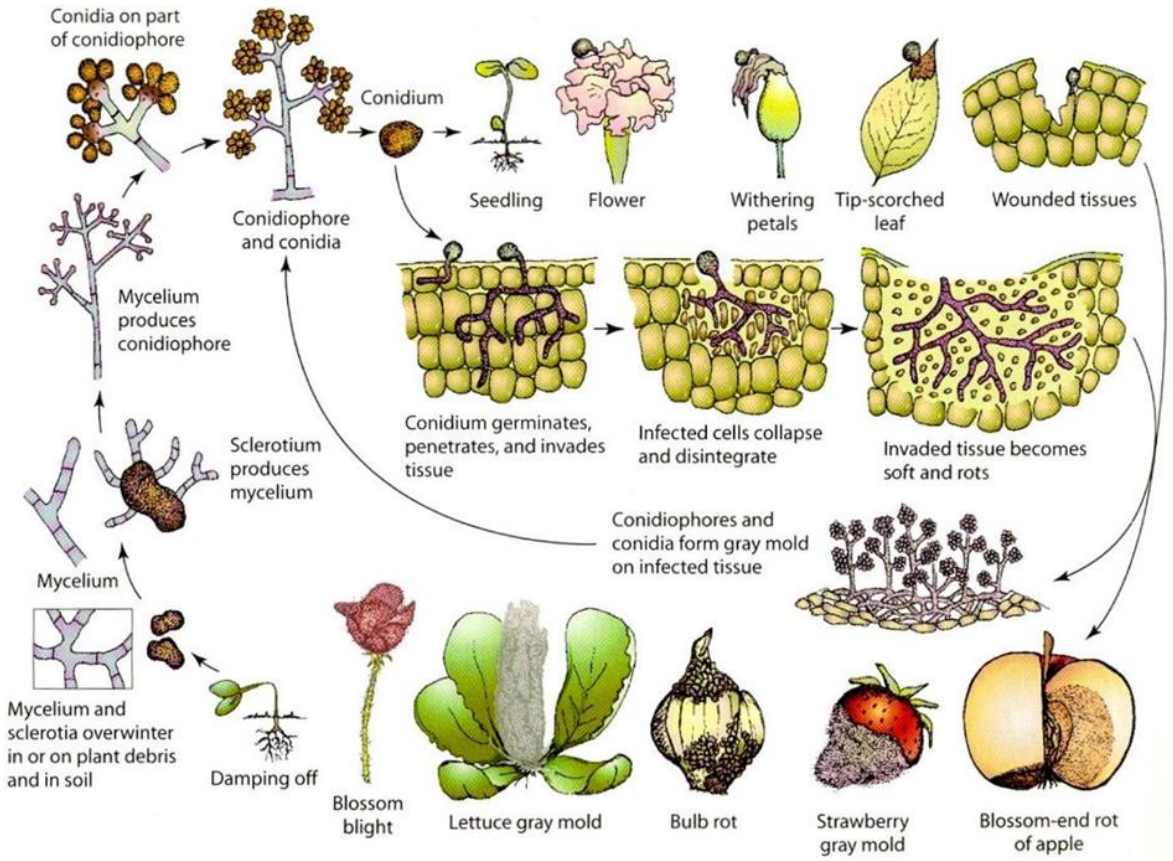

Figure 1. Life and infection cycle of *B. cinerea*. Conidia land on host surfaces, germinate, and infect plant tissues by penetrating through wounds, stomata, or directly breaching intact epidermal layers. After colonizing host tissue, the fungus forms conidiophores that produce conidia, which disseminate

and perpetuate the cycle. In some cases, the fungus produces sclerotia as a survival structure that can later give rise to either new mycelia or, more rarely, sexual fruiting bodies (apothecia). Figure adapted from Agrios (2005).

Despite extensive research, the molecular mechanisms that trigger host-cell death and govern the shift from a quiescent to an aggressive fungal lifestyle remain poorly defined (Fillinger et al., 2016). In particular, the complex crosstalk among fungal effectors, host defence signaling pathways, and the precise timing of cell-death induction demands further elucidation (Müller et al., 2018; Wang et al., 2018; Veloso et al., 2018). Clarifying these processes is essential to achieve our goal of developing durable, integrated disease-management solutions, ranging from RNA interference-based fungicides and improved biocontrol agents to the deployment of resistant crop varieties.

1.3. Plant defence mechanisms and plant-pathogen interaction

Plants continually face various environmental threats. To defend themselves passively, they produce preformed antimicrobial compounds for protection and have a waxy cuticular layer that makes tissue penetration by invaders difficult (Jones and Dangl, 2006). The plant immune system involves two distinct lines of defence: the first line, called pathogen-associated molecular pattern (PAMP)-triggered immunity (PTI), initiates immediately upon pathogen attack. PTI recognizes PAMPs, such as the bacterial flagellin protein flg2, using cell-surface pattern recognition receptors (PRRs) (Zipfel, 2008). These PRRs typically have extracellular domains characterized by leucine-rich repeats, LysM, or S-lectin domains (Yuan et al., 2021). Receptors are membrane-associated and include receptor-like kinases (RLKs), which contain kinase domains, and receptor-like proteins (RLPs), which lack kinase domains and instead form complexes with cytosolic kinases like SOBIR1 (Suppressor of BIR1-1) for signal transduction (Yuan et al., 2021). Both RLKs and RLPs can interact with co-receptors, such as BAK1 (BRI1-Associated Kinase 1) (Yuan et al., 2021). Upon ligand binding, auto- and transphosphorylation events occur, activating receptor-like cytoplasmic kinases (RLCKs) such as BIK1 (Botrytis-induced kinase 1) (Ngou et al., 2022; Yuan et al., 2021). RLCKs initiate immune responses including calcium influx, reactive oxygen species (ROS) production, stomatal closure, callose, mitogen-activated protein kinase (MAPK) cascades, production of defence-related hormones and transcription of PTI-responsive genes (Ngou et al., 2022; Yuan et al., 2021). However, pathogens can suppress PTI, prompting plants to employ a second, intracellular defence mechanism known as effector-triggered

immunity (ETI). ETI involves nucleotide-binding domain leucine-rich repeat-containing receptors (NLRs), which detect intracellular effectors either directly or indirectly, leading to a more robust immune response than PTI (Yuan et al., 2021). These NLRs, also known as resistance (R) proteins, include three types classified based on their N-terminal domains: coiled-coil NLRs (CNLs), Toll/Interleukin-1 receptor NLRs (TNLs), and RPW8-like CC domain NLRs (RNLs) (Yuan et al., 2021). In *Arabidopsis thaliana*, specific CNLs have been found to assemble after recognition of bacterial effector into the ZAR1 resistosome, which then relocates to the plasma membrane to initiate defence signaling (Ngou et al., 2022). Once embedded in the membrane, the ZAR1 complex functions as a calcium-permeable channel, driving a massive influx of Ca^{2+} ions. The sudden rise in cytosolic calcium triggers calcium-dependent protein kinases (CDPKs), ultimately leading to induction of strong ETI defence responses and hypersensitive cell death (Gao et al., 2022; Ngou et al., 2022). Although PTI and ETI share many downstream events, such as reactive oxygen species production and gene activation, the timing and magnitude of these responses can differ markedly between the two layers of plant immunity.

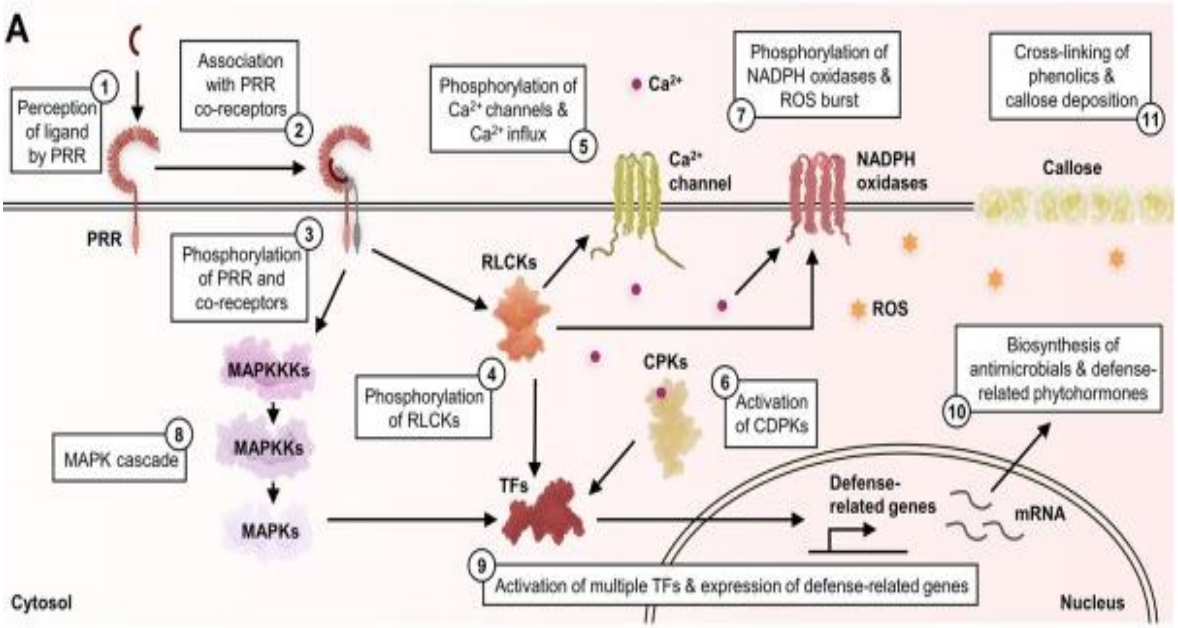

Figure 2. Signalling pathways involved in PAMP-triggered immunity. Pathogen-associated molecular patterns (PAMPs) are detected by pattern recognition receptors (PRRs), which activate a cascade of mitogen-activated protein (MAP) kinases and receptor-like cytoplasmic kinases (RLCKs), to activate defence-related transcription factors (TF). This activation triggers a series of immune responses, including calcium influx, production of reactive oxygen species (ROS), expression of defence-related genes, and deposition of callose in the cell wall (Ngou et al., 2022).

1.4. Botrytis strategies to kill host cells

B. cinerea is a necrotrophic fungus that acquires nutrients by actively killing host tissues or colonizing senescent plant parts (Williamson et al., 2007; van Kan, 2006). The pathogen employs an aggressive lifestyle, systematically destroying host cells and exploiting necrotic or dying tissues to sustain rapid growth and expansion (van Kan, 2006). The infection process relies on a coordinated network of virulence factors, including cell wall–degrading enzymes (CWDEs), phytotoxic metabolites, various effector proteins, and small RNAs. These factors enable *B. cinerea* to effectively overwhelm plant defences (Choquer et al., 2007; Weiberg et al., 2013). Notably, redundancy among these virulence determinants is common, allowing the fungus to compensate effectively when specific pathogenic mechanisms are compromised (Leisen et al., 2022).

In a recent review, Bi and Sharon (2023) delineated a three-phase infection sequence (Figure 3). In the initial early phase (0–36 h post-inoculation), fungal germ tubes, appressoria, and infection cushions form on the host surface. During this period, the secretion of cell death-inducing proteins (CDIPs) results in localized epidermal cell death, establishing a nutrient-rich microenvironment for fungal colonization (Bi et al.,2023). The intermediate phase (36–48 hpi) involves penetration pegs that breach the plant cuticle and primary cell wall, initiating a process of regulated cell death (RCD) in both fungal hyphae and adjacent host cells. Concurrently, the fungus develops radiating hyphae (RH) on the plant surface, promoting lateral spread. During this critical window, the pathogen actively detoxifies host-produced phytoalexins such as camalexin by activating its detoxification and stress-tolerance pathways (Shlezinger et al., 2012; Bi et al.,2023). In the late infection stage (>48 hpi), rapid radial expansion of necrotic lesions occurs, often exceeding growth rates of 0.5 mm per hour under favorable conditions, accompanied by dense fungal mycelial colonization of dead tissues behind the expanding front. Although this model is based on recent research data, it still needs to be considered preliminary and applicable only to standardized infection conditions.

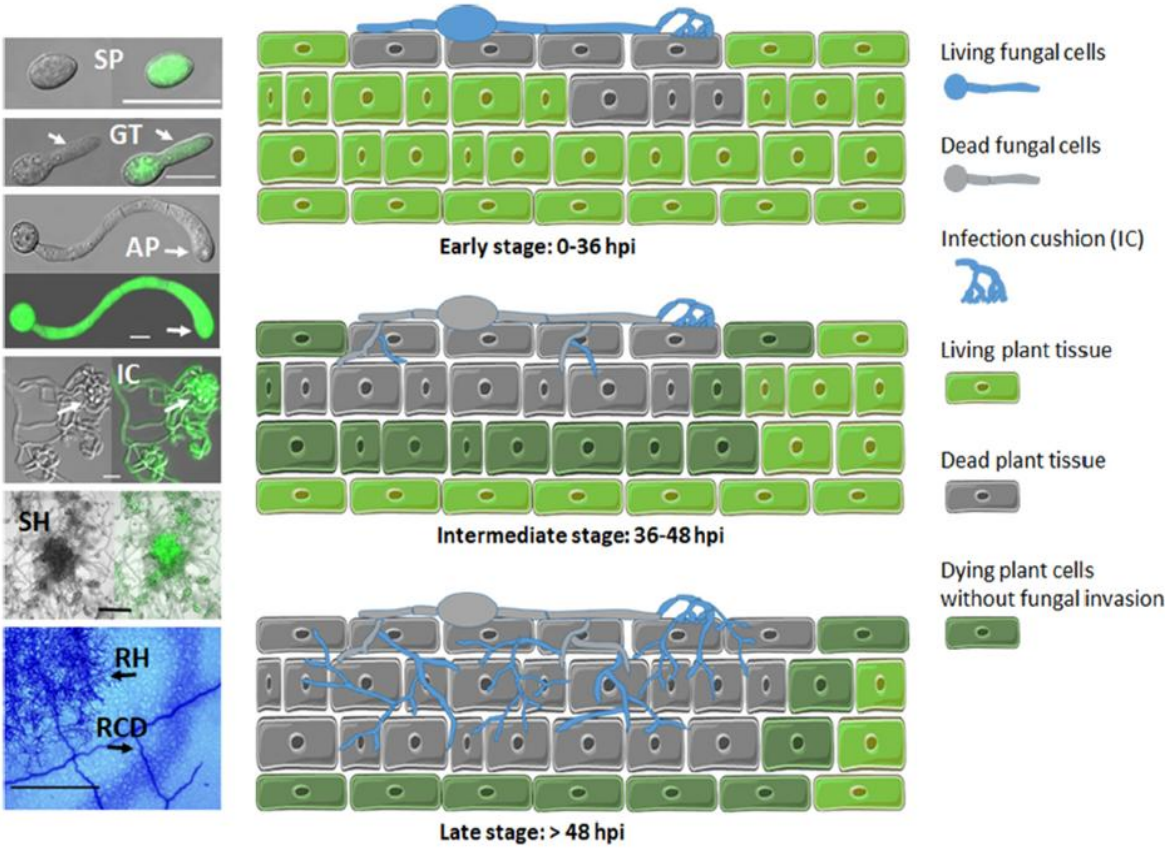

Figure 3. Schematic of early, intermediate, and late infection phases of *B. cinerea*. Three-phase infection sequence of *B. cinerea*: (i) early epiphytic growth and first CDIP-triggered epidermal cell death (0–36 hpi), (ii) penetration with a narrow band of host- and hypha-regulated cell death (36–48 hpi), and (iii) radial lesion expansion as necrotic tissue fuels dense mycelial growth (> 48 hpi) (Bi and Sharon, 2023).

Biotrophic pathogens depend on living host tissues for survival and thus typically avoid or actively suppress the plant's hypersensitive response (HR), a defence mechanism involving localized cell death. In contrast, necrotrophic pathogens, which benefit from host cell death, often deliberately trigger HR to enhance infection. For instance, *B. cinerea* effectively exploits this mechanism by secreting specific molecules, effectors and PAMPs to stimulate plant defences and induce HR intentionally, which provides dead tissue for fungal nutrition (Govrin and Levine, 2000). However, for plants, activating HR presents a complex trade-off; it can either protect against biotrophic pathogens or inadvertently facilitate infections by necrotrophs, depending on the invading pathogen type (Kliebenstein et al., 2008). Therefore, an evolutionarily optimal threshold for HR activation is maintained in plants, shaped by environmental pressures exerted by either biotrophic or necrotrophic pathogens (Jones and DAngl, 2006; Kliebenstein et al., 2008).

Another model by Veloso and van Kan (2018) proposed fungal manipulation of two main pathways of host programmed cell death (PCD): autophagy (AU) and apoptosis-like PCD (AP). This manipulation directs the host-pathogen interaction along one of three trajectories (Figure 4): (A) Strong, early activation of autophagy results in host resistance by confining the pathogen; (B) A balanced state between autophagy and apoptosis enables asymptomatic, biotrophic colonization that can persist until the host becomes senescent or stressed; (C) Early suppression of autophagy followed by subsequent strong activation of apoptosis (>16 hpi) leads to widespread host cell death and facilitates the pathogen's necrotrophic switch and severe infection (Veloso and van Kan, 2018). Research has shown that plants unable to perform autophagy are significantly more vulnerable to infection by Botrytis (Lai et al., 2011). During infection, the fungus temporarily suppresses the plant's autophagic response. Additionally, fungal genes like BcBIR1 help prevent premature fungal cell death, enabling the pathogen to manage cell death timing in a way that benefits its infection process (Shlezinger et al., 2017).

These insights explain why *B. cinerea* possesses substantial redundancy in its virulence factors; if one pathogenic route is blocked, the fungus can utilize alternative mechanisms or manipulate different host cell death pathways (Leisen et al. 2022). Furthermore, they provide insight into why the host's classical hypersensitive response (HR), a form of programmed apoptosis, paradoxically promotes *B. cinerea* infection by supplying dead tissue necessary for fungal nutrition (Govrin and Levine, 2000). Finally, they highlight the potential for targeted intervention strategies that either enhance early host autophagy or inhibit apoptosis-inducing fungal effectors, offering narrow yet critical windows of opportunity to limit lesion progression during intermediate infection stages.

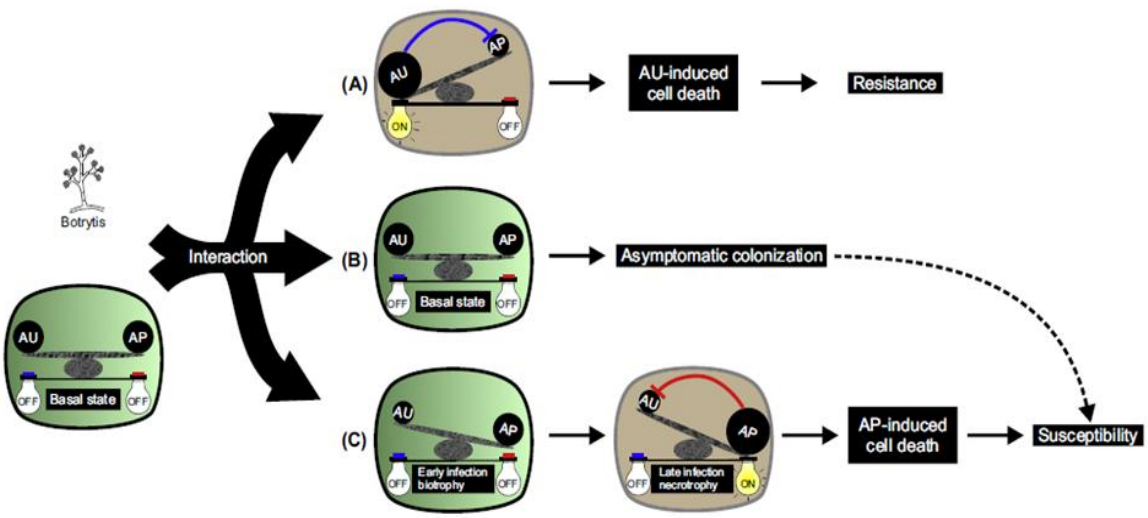

Figure 4. Outcomes of the AU/AP balance in plants during *B. cinerea* infection. Outcome of the host autophagy (AU), apoptosis-like PCD (AP) balance: strong early AU → resistance; AU≈AP → asymptomatic colonisation; early AU suppression followed by AP surge → extensive host apoptosis and full necrotrophy (Veloso and van Kan, 2018).

1.4.1. Cell wall–degrading enzymes

A principal mechanism by which *B. cinerea* achieves tissue invasion is the production of cell wall degrading enzymes (CWDEs), including cutinases, pectinases, and xylanases (van Kan, 2006). By breaking down structural polymers within the plant cell wall, these enzymes both facilitate penetration and release simple carbohydrates upon which the fungus thrives. The two major polygalacturonases, **PG1** and **PG2**, can induce measurable tissue maceration; however, single knockouts typically result in only partial reductions in virulence due to the fungus's extensive enzymatic redundancy (ten Have et al., 1998; Kars et al., 2005; Leisen et al., 2022). Furthermore, polygalacturonases (PGs) contribute to cell wall degradation by breaking down pectin, and they are known to interact with PRRs. In Arabidopsis, the receptor RLP42, together with the co-receptors BAK1 and SOBIR1, specifically recognizes a conserved 9-amino-acid fragment (pg9(At)) from fungal endopolygalacturonases (Zhang et al., 2021).

In multi-gene knockout experiments, the collective absence of several CWDEs can significantly diminish *B. cinerea* pathogenicity (Leisen et al., 2022). Yet even then, residual virulence often persists, reflecting the fungus's multi-layered approach to host cell destruction (Veloso & van Kan, 2018).

1.4.2. Phytotoxic metabolites

In tandem with CWDEs, *B. cinerea* secretes phytotoxic metabolites to expedite cell death (Fillinger & Elad, 2015). Two notable families botrydial (sesquiterpenoid) and botcinins (polyketides) are linked to host tissue necrosis. When both toxin biosynthesis pathways are interrupted, the fungus shows markedly reduced virulence, demonstrating their synergistic contribution to pathogenic success (Dalmais et al., 2011; Leisen et al., 2022).

Botrydial is a sesquiterpenoid phytotoxin produced by *B. cinerea* during plant infection, causing chlorosis and cell death (Pinedo et al., 2008). Its biosynthesis is governed by the *BOT* gene cluster (BcBOT1–BcBOT7), with BcBOT2 encoding a sesquiterpene synthase initiating the pathway (Pinedo et al., 2008; Porquier et al., 2016). The transcription factor BcBOT6, a Zn (II)$_2$Cys$_6$ protein, is the pathway-specific activator of this cluster (Porquier et

al., 2016). Despite its phytotoxicity, botrydial's contribution to virulence is strain-dependent and functionally redundant with another phytotoxin, botcinic acid (Dalmais et al., 2011).

Botcinic Acid, a polyketide, is synthesized via two polyketide synthases (*Bcboa6* and *Bcboa9*) within a subtelomeric gene cluster, and its expression is positively regulated by the Zn $(II)_2Cys_6$ transcription factor BcBoa13 (Porquier et al., 2019). Like botrydial, botcinic acid does not have a known specific plant receptor, and its mode of action in the host remains unclear. As mentioned above, only mutants deficient in both toxins show significantly reduced virulence (Dalmais et al., 2011).

1.4.3. Cell Death–Inducing Proteins (CDIPs)

CDIPs are believed to represent a key virulence mechanism utilized by *B. cinerea* to induce rapid collapse of host cells, thereby facilitating nutrient acquisition required for its necrotrophic lifestyle (Bi et al., 2021). These secreted proteins are broadly categorized into two main functional groups. The first group comprises enzymatic CDIPs, predominantly characterized by glycoside hydrolase or transglycosylase activities that compromise the integrity of the plant extracellular matrix. However, specific members, notably Gs1 and RAE1, have cytotoxic properties despite targeting substrates beyond the cell wall, underscoring considerable functional diversity within this catalytic group (Zhang et al., 2015; Zhang et al., 2024). The second group consists of non-enzymatic, small cysteine-rich CDIPs. Despite the absence of identifiable catalytic domains, these proteins consistently trigger programmed cell death pathways across various dicotyledonous hosts (Jeblick et al., 2023). Recent studies have demonstrated that representatives from both functional classes can be recognized by plant plasma membrane-localized pattern-recognition receptor (PRR) complexes and silencing these receptor components effectively suppresses the necrotic response initiated by CDIPs, confirming their essential role in the recognition, and signaling processes leading to host cell death (Jeblick et al., 2023; Nie et al., 2021).

CDIPs with cell wall-degrading activity can also have phytotoxic activity. For example, **Xyn11A** is a glycosyl hydrolase family 11 (GH11) xylanase secreted by *B. cinerea*, degrades xylan, a major hemicellulosic polysaccharide, was found to play a role in virulence through the induction of plant defence responses, including necrosis and the hypersensitive response (HR) (Frías et al., 2019). Importantly, this activity of Xyn11A is independent of its enzymatic function, and even a short, 25-residue peptide (Xyn25) was found to be sufficient to fully trigger host cell death (Frías et al., 2019). Notably, Xyn11A is recognized by the tomato receptor LeEix2, a leucine-rich repeat protein that normally mediates pattern-

triggered immunity but, in this case, contributes to a cell death response that benefits necrotrophic infection (Ron & Avni, 2004; Noda et al., 2010; Frías et al., 2019).

XYL1, a GH10 family xylanase, exhibits lower catalytic efficiency compared to other GH10 and GH11 xylanases identified from the same organism. Its primary enzymatic role is the hydrolysis of xylooligosaccharides into xylose, acting synergistically with other xylanases to efficiently degrade complex hemicellulosic substrates; yet, its phytotoxic activity seems independent on its catalytic activity, as a 26 aa fragment of Xyl1 was shown to be sufficient for inducing cell death (Yang et al., 2018a). **XYG1** is a secreted GH12 xyloglucanase that also induces cell death and immune responses in dicot plants independently from its enzymatic activity (Zhu et al., 2017). Its function as an immune elicitor specifically involves plant leucine-rich repeat receptor-like kinases (LRR-RLKs) co-receptors BAK1 and SOBIR1, which mediate cell death signaling upon XYG1 recognition. Moreover, specific exposed residues on XYG1 surface loops are crucial for triggering plant cell death, thereby underscoring the receptor-dependent nature of its immune recognition (Zhu et al., 2017).

Another enzymatic effector, **Gs1**, is a glucan 1,4-alpha-glucosidase classified within the glycosyl hydrolase family 15 (GH15), but without known cell wall degrading activity. Gs1 contains both GH15 and CBM20 domains, which are essential for its full elicitor activity (Zhang et al., 2015; Yang et al., 2018b). Together with its phytotoxic activity, it induces rapid plant defence responses, including necrosis, reactive oxygen species (ROS) production, lignin accumulation, cell wall strengthening, and systemic resistance against pathogens (Yang et al., 2018b).

Among the non-enzymatic CDIPs, **PLP1**, a cysteine-rich cell death-inducing protein (CDIP) secreted by *B. cinerea,* triggers strong plant immune responses, including necrosis and defence gene activation. Its cell-death-inducing activity on *N. benthamiana* depends on the co-receptors BAK1 and SOBIR1 (Zhang et al., 2013). RLP30, an Arabidopsis receptor-like protein, was previously shown to recognize the PLP1 homolog SCFE1 from *S. sclerotiorum*, also functioning with BAK1 and SOBIR1 as co-receptors (Zhang et al., 2013). Interestingly, a different receptor in *N. benthamiana*, called RE02, is involved in the recognition of another PLP1-SCFE1 homologue from the apple pathogen *Valsa mali*, VmE02, further highlighting the role of RLP30-like proteins in detecting fungal elicitors and initiating immune signaling (Nie et al., 2021). **Spl1** is a cerato-platanin protein and induces hypersensitive response (HR)-like cell death and defence gene expression in plants (Frías et al., 2011). It also triggers systemic acquired resistance (SAR) in tobacco, including salicylic acid accumulation and PR gene activation (Frías et al., 2013). Necrosis induction is partially reduced in Arabidopsis

bak1 mutants, indicating partial BAK1 co-receptor dependency (Frías et al., 2011; Frías et al., 2014). **IEB1** triggers necrosis upon leaf. However, its deletion doesn't significantly reduce virulence, suggesting other effectors can compensate (Frias et al., 2016). While not essential for infection, IEB1 likely enhances tissue collapse, acting more as an amplifier of cell death than a key virulence factor. Similarly, **Hip1** might contribute to the fungus's strategy to induce host necrosis. Jeblick et al. (2023) reported that most of the Hip1 protein sequence was required to induce necrosis, indicating that its tertiary structure is required for recognition by the postulated Hip1 receptor. While deletion of Hip1 did not have an effect on virulence, *B. cinerea* strains overexpressing Hip1 showed a slightly increased necrotic activity (Jeblick et al., 2023). In addition, the non-enzymatic effector **CDI1**, which has been identified as a CDIP of a variety of fungi, is secreted during infection and interacts with host plasma membranes to trigger cell death (Franco-Orozco et al., 2017; Zhu et al., 2023). NEP-like proteins such as **Nep1** and **Nep2** are widely distributed among fungi, oomycetes and even bacteria. They represent a special group of CDIPs because their cell-death inducing activity has been precisely defined: They form pores in the plasma membranes of dicotyledonous cells by interacting with specific membrane sphingolipids (Lenarčič et al., 2017). In addition to their cytolytic activity, they are recognized by the receptor PLP23. Binding to PLP23 initiates defence signaling that paradoxically facilitates the necrotrophic lifestyle of the pathogen (Qutob et al., 2006; Ottmann et al., 2009; Albert et al., 2015).
Leisen et al. (2022) knocked out up to twelve CDIP-encoding genes in *B. cinerea* and found that, despite reduced virulence, the fungus still caused noticeable lesions. This shows these proteins are highly redundant and implies there are other, uncharacterized factors helping it kill host cells. In other words, no single CDIP is essential, *B. cinerea* likely relies on a flexible set of these proteins to ensure host cell death across different conditions and plant species.

1.4.4. Small RNA–mediated interference

Beyond toxins, CDIPs, and cell wall–degrading enzymes (CWDEs), *B. cinerea* employs small RNAs (sRNAs) to undermine plant defences (Müller et al., 2018). These sRNAs enter the host's cells and co-opt the plant's RNA interference (RNAi) machinery, leading to the silencing of key immunity-related genes (Weiberg et al., 2013; Wang et al., 2016). As a result, defensive responses are dampened, thus promoting fungal infection (Veloso & van Kan, 2018). Recent findings highlight the breadth of cross-kingdom RNA trafficking, indicating that these fungal sRNAs may target a wide range of host signaling networks, from

hormone pathways to stress-response genes (Cai et al., 2018). However, the significance of cross-kingdom siRNA trafficking for *B. cinerea* infection has been challenged recently, indicating that it might not play a major role for its interaction with its host plant (Qin et al., 2023).

1.5. Using CRISPR/Cas9 for efficient genetic editing in *B. cinerea*

CRISPR/Cas9 technology, originally identified as a bacterial adaptive immune mechanism, enables precise genetic modifications by inducing targeted double-strand breaks (DSBs) in DNA. These breaks are repaired through either error-prone non-homologous end joining (NHEJ) or precise homology-directed repair (HDR). The development of the simplified Cas9-single-guide RNA (sgRNA) system greatly advanced genome editing, allowing researchers to disrupt or precisely alter genes of interest (Mali et al., 2013; Shalem et al., 2014; Nødvig et al., 2015). The advent of CRISPR/Cas9 technology has revolutionized the field of functional genomics by enabling rapid, precise, and marker-free genetic modifications in a wide range of organisms, including fungi and oomycetes (Schuster and Kahmann, 2019). In the context of plant-pathogenic fungi, particularly *B. cinerea*, CRISPR/Cas9-based mutagenesis offers an unprecedented opportunity to dissect complex virulence mechanisms, including the role of secreted cell death–inducing proteins (CDIPs). In our laboratory, Leisen et al. (2020) have established a robust CRISPR/Cas9 method tailored for *B. cinerea*. Their system is based on the introduction of pre-assembled Cas9, single guide RNA (sgRNA) ribonucleoprotein (RNP) complexes into fungal protoplasts. To enhance editing efficiency and facilitate screening for successful genome modifications, they developed a novel strategy combining RNP delivery with the introduction of transiently selectable telomere vectors (pTEL). These telomere vectors are autonomously replicating and, importantly, are rapidly lost in the absence of selection pressure, ensuring that resulting mutants are marker-free. The method achieves high editing yields with minimal off-target effects, as verified by whole-genome sequencing (Leisen et al., 2020). Furthermore, by applying short homology flanks (as little as 60 bp) to repair templates, they demonstrated that targeted homologous recombination is highly efficient in *B. cinerea*. This approach was further validated by the successful generation of knock-in GFP-tags to a superoxide dismutase (SOD1), and the one-step exchange of all codons at a critical position for fungicide resistance in the gene encoding the SdhB subuni of succinate dehydrogenase (Leisen et al., 2020).

Building upon this efficient marker-free system, Leisen et al. (2022) employed the CRISPR/Cas9-based mutagenesis platform to generate multiple deletion mutants in *B. cinerea*. By serially eliminating up to 12 genes encoding various phytotoxic compounds and CDIPs, their study revealed a remarkable redundancy within the fungal virulence arsenal. Although mutants lacking many known virulence factors exhibited significantly reduced lesion formation across several host tissues, residual pathogenicity persisted, indicating that additional, as yet unidentified, factors contribute to the necrotrophic lifestyle of *B. cinerea* (Leisen et al., 2022).

1.6. Objectives

The primary objective of this thesis was to investigate how the necrotrophic fungus *B. cinerea* utilizes secreted cell-death-inducing proteins (CDIPs) during plant infection. Using a highly efficient CRISPR/Cas9 editing system developed in our group, the roles of individual CDIPs as well as their full complement should be evaluated by continuing a systematic multi-knock-out mutagenesis approach.

The research aimed to expand the existing mutant collection by disrupting additional genes encoding newly identified CDIPs, with the final goal to eliminate all phytotoxic proteins of *B. cinerea*. Criteria for selection of new CDIPs for knock-out were their known roles in *B. cinerea* and related fungal species, their homology to known CDIPs, and their significant gene expression during infection.

The pathogenic roles of CDIPs should be assessed individually and in combination with other CDIPs through evaluations of a series of consecutive multiple mutants regarding their in vitro growth and particularly their ability to form expanding lesions in different plant tissues. This analysis should determine the importance of each CDIP in disease progression and reveal possible host-specific effects.

To complement the *in vivo* assays, comparative MS-based proteomic analyses and phytotoxicity assays were planned with the on planta secretomes from wild-type and CDIP-deficient mutants. This was expected to further clarify the individual and collective contribution of CDIPs to the pathogen's necrotrophic capabilities.

Because the final multi-knockout mutants still caused slowly expanding lesions and produced a secretome with residual phytotoxicity, a search for as yet undetected CDIPs was

undertaken, and the phytotoxic activity of novel CDIP candidates validated after their expression in E. coli and through *Agrobacterium* infiltration in *N. benthamiana*.

2. Materials and Methods

2.1. Microorganisms used

2.1.1. *B. cinerea* strains

The *B. cinerea* strains used and generated in this study are listed in Table 1.

Table 1. *B. cinerea* isolates used.

Strain/mutant	Gene	Genotype
13x	*Bcpg1*	*spl1 nep1 nep2 xyn11A hip1 xyg1 plp1 ieb1 xyl1 gs1 bot2 boa6 pg1*
14x	*Bccrh1*	*spl1 nep1 nep2 xyn11A hip1 xyg1 plp1 ieb1 xyl1 gs1 bot2 boa6 pg1 Crh1*
15x	*BcCDI1*	*spl1 nep1 nep2 xyn11A hip1 xyg1 plp1 ieb1 xyl1 gs1 bot2 boa6 pg1 CDI1*
16x	*Bccfem1*	*spl1 nep1 nep2 xyn11A hip1 xyg1 plp1 ieb1 xyl1 gs1 bot2 boa6 pg1 CDI1 Crh1 CFEM1*
17x	*Bcpg2*	*spl1 nep1 nep2 xyn11A hip1 xyg1 plp1 ieb1 xyl1 gs1 bot2 boa6 pg1 CDI1 Crh1 CFEM1 pg2*
18x	*BcSSP2*	*spl1 nep1 nep2 xyn11A hip1 xyg1 plp1 ieb1 xyl1 gs1 bot2 boa6 pg1 CDI1 Crh1 CFEM1 SSP2*
19x	*BcCDI2*	*spl1 nep1 nep2 xyn11A hip1 xyg1 plp1 ieb1 xyl1 gs1 bot2 boa6 pg1 CDI1 Crh1 CFEM1 pg2 SSP2 CDI2*
20x	*Bcsgp1*	*spl1 nep1 nep2 xyn11A hip1 xyg1 plp1 ieb1 xyl1 gs1 bot2 boa6 pg1 CDI1 Crh1 CFEM1 pg2 SSP2 CDI2 SGP1*
21x	*Bccrh4*	*spl1 nep1 nep2 xyn11A hip1 xyg1 plp1 ieb1 xyl1 gs1 bot2 boa6 pg1 CDI1 Crh1 CFEM1 pg2 SSP2 CDI2 SGP1 Crh4*
22x	*Bcxyg3*	*spl1 nep1 nep2 xyn11A hip1 xyg1 plp1 ieb1 xyl1 gs1 bot2 boa6 pg1 CDI1 Crh1 CFEM1 pg2 SSP2 CDI2 SGP1 Crh4 XYG3*
23x	*BcGAS5A*	*spl1 nep1 nep2 xyn11A hip1 xyg1 plp1 ieb1 xyl1 gs1 bot2 boa6 pg1 CDI1 Crh1 CFEM1 pg2 SSP2 CDI2 SGP1 Crh4 XYG3 GAS5A*
24x	*Bccdi3*	*spl1 nep1 nep2 xyn11A hip1 xyg1 plp1 ieb1 xyl1 gs1 bot2 boa6 pg1 CDI1 Crh1 CFEM1 pg2 SSP2 CDI2 SGP1 Crh4 XYG3 GAS5A CDI3*
25x	*Bcrrae1*	*spl1 nep1 nep2 xyn11A hip1 xyg1 plp1 ieb1 xyl1 gs1 bot2 boa6 pg1 CDI1 Crh1 CFEM1 pg2 SSP2 CDI2 SGP1 Crh4 XYG3 GAS5A CDI3 RAE1*
26x	*Bcfat1*	*spl1 nep1 nep2 xyn11A hip1 xyg1 plp1 ieb1 xyl1 gs1 bot2 boa6 pg1 CDI1 Crh1 CFEM1 pg2 SSP2 CDI2 SGP1 Crh4 XYG3 GAS5A CDI3 FAT1*
27x	*Bcxyl2*	*spl1 nep1 nep2 xyn11A hip1 xyg1 plp1 ieb1 xyl1 gs1 bot2 boa6 pg1 CDI1 Crh1 CFEM1 pg2 SSP2 CDI2 SGP1 Crh4 XYG3 GAS5A CDI3 RAE1 FAT1 Xyl2*
28x	*BcIEB2*	*spl1 nep1 nep2 xyn11A hip1 xyg1 plp1 ieb1 xyl1 gs1 bot2 boa6 pg1 CDI1 Crh1 CFEM1 pg2 SSP2 CDI2 SGP1 Crh4 XYG3 GAS5A CDI3 RAE1 FAT1 Xyl2 IEB2*
29x	*BcCELP1*	*spl1 nep1 nep2 xyn11A hip1 xyg1 plp1 ieb1 xyl1 gs1 bot2 boa6 pg1 CDI1 Crh1 CFEM1 pg2 SSP2 CDI2 SGP1 Crh4 XYG3 GAS5A CDI3 RAE1 FAT1 Xyl2 IEB2 CELP1*
Nep1-overexpressed	Bc22x-H2B-Nep1	22x background + [Nep1-H2B Promotor]
Nep1-overexpressed	Bc22x-His3-Nep1	22x background + [Nep1-His3 Promotor]

2.1.2. Bacteria and plasmids used

In this study, *E. coli* strains listed in Table 2 were employed for cloning and protein expression and *A. tumefaciens* for transient expression in *N. benthamiana*. The plasmids used in this study are summarized in Table 3.

Table 2. Microorganisms used.

Name	Strain	Genotype
Escherichia coli	DH5α	F^- φ80dlacZΔM15 Δ(lacZYA-argF)U169 recA1 endA1 hsdR17(r_K^- m_K^+) phoA supE44 λ^- thi-1 gyrA96 relA1
	Rosetta	F^- ompT hsdSB(r_B^- m_B^-) gal dcm [pRARE (Cam^R)]
Agrobacterium tumefaciens	GV3101::mp90	rifR, Ti plasmid pMP90 (disarmed), C58 chromosomal background

Table 3. Plasmids used in this study.

Plasmid	Feature	Antibiotic Resistance	Reference
IEB1-pET28		Kanamycin	this work
IEB2-pET28		Kanamycin	this work
XYG3-pET28		Kanamycin	Luoyu Wu (unpublished)
XYG3- pCold–TF		Ampicillin	this work
pTEL-Fen	Telomere vector with PtrpC promoter from *A. nidulans* & TniaD terminator from *B. cinere*	Ampicillin & Kanamycin for selection in *E. coli* Fenhexamid in *B. cinerea*	Leisen et al. (2020)
pET28	*E. coli* expression vector	Kanamycin	(Novagen, Munich, Germany)
pCold–TF	*E. coli* expression vector with Trigger Factor fusion protein	Ampicillin	(Takara Bio Inc., Shiga, Japan)
pGGC000	Entry vector	Ampicillin	(Lampropoulos et al., 2013)
pGGA004	35S promoter	Ampicillin	(Lampropoulos et al., 2013)
pGGB003	B-dummy	Ampicillin	(Lampropoulos et al., 2013)
pGGB006	Signal peptide	Ampicillin	(Lampropoulos et al., 2013)
pGGD-HA	3xHA-tag	Ampicillin	University of Heidelberg
pGGE001	RBCs terminator	Ampicillin	(Lampropoulos et al., 2013)
pGGF011	PM-mCherry marker	Ampicillin	(Stephani et al., 2020)
pGGZ003	Destination vector	Spectinomycin	(Lampropoulos et al., 2013)
pGGC000-IEB2	Entry vector+IEB2	Ampicillin	this work
pGGC000-RAE2	Entry vector+RAE2	Ampicillin	this work
pGGC000-XYL3	Entry vector+XYL3	Ampicillin	this work
pGGC000-CDI4	Entry vector+CDI4	Ampicillin	this work
pGGZ003-IEB2	Final vector for Agro	Spectinomycin	this work
pGGZ003-RAE2	Final vector for Agro	Spectinomycin	this work
pGGZ003-XYL3	Final vector for Agro	Spectinomycin	this work
pGGZ003-CDI4	Final vector for Agro	Spectinomycin	this work

2.2. Cultivation and harvesting of *B. cinerea* spores

B. cinerea was cultivated on ME or HA agar plates at 22°C under continuous fluorescent illumination supplemented with near-UV (black) light. Conidia were harvested aseptically from cultures aged 6–11 days and used for subsequent assays and transformation procedures.

2.2.1. Media used for cultivation

The media used for the cultivation of *B. cinerea* and *E. coli* are listed in Table 4

Table 4. Cultivation media used.

Medium	Composition	Remarks
1x HA agar (ME)	1.0% (w/v) malt extract (Neogen), 0.4% (w/v) glucose (Merck Millipore), 0.4% (w/v) yeast extract (Neogen), 1.5% (w/v) agar-agar (Neogen), pH 5.5, autoclaved	Solid full medium for conidia production and growth determination
4x HA agar	4.0% (w/v) malt extract, 1.6% (w/v) glucose, 1.6% (w/v) yeast extract, 1.5% (w/v) agar-agar, pH 5.5, autoclaved	Solid full medium for enhanced and rapid growth of the fungus
LB-Medium	1% (w/v) Trypton, 1% (w/v) NaCl, 0.5% (w/v) yeast extract, pH 7.2, autoclaved (with 1.5% w/v agar if solid medium needed)	Standard bacterial growth medium
Gamborg – Medium (50 mM Glucose)	0.305% (w/v) Gamborg Basal Salts, 0.136% (w/v) KH_2PO_4, 0.991% (w/v) Glucose, pH 5.5	Liquid Gamborg medium with 50 mM glucose
Gamborg – Medium (25 mM Glucose)	0.305% (w/v) Gamborg Basal Salts, 0.136% (w/v) KH_2PO_4, 0.495% (w/v) Glucose, pH 5.5	Liquid Gamborg medium with 25 mM glucose
Gamborg – Medium (No Glucose)	0.305% (w/v) Gamborg Basal Salts, 0.136% (w/v) KH_2PO_4, pH 5.5	Liquid Gamborg medium without glucose
Gamborg – Semi-Solid Medium	0.305% (w/v) Gamborg Basal Salts, 0.136% (w/v) KH_2PO_4, 0.991% (w/v) Glucose, 0.5% (w/v) agar, pH 5.5	Semi-solid Gamborg medium (≈50 mM glucose)

2.3. Transformation of *B. cinerea*

This transformation protocol was adapted from a previously established marker-free CRISPR/Cas9 genome editing method (Leisen et al., 2020) and relies on generating gene knockouts by introducing two double-strand breaks in the target locus without providing a repair template.

2.3.1. Used culture media, buffers, and solutions for *B. cinerea* transformation

Below is a table 5 summarizing the key buffers, solutions, and media used for *B. cinerea* transformations, including their compositions, final volumes, and relevant preparation notes:

Table 5. Culture media, buffers, and solutions used to transform *B. cinerea*.

Name	Volume	Recipe	Comment
Malt extract (ME/HA)	1 l	4 g Glucose, 4 g yeast extract 10 g malt extract pH 5.5, autoclave	Liquid medium for overnight culture
KCl 0.6 M / NaP 0.1 M		500 ml KCl 0.6 M + 50 ml Na(Pi) 1M pH 5.8, autoclave	Used for washing mycelium or conidia prior to enzyme digestion
KCl 0,6M	500 ml	22.37 g KCl, autoclave	For: KCl 0.6 M / NaP 0.1 M
NaP 1M	200 ml	15.8 ml Na_2HPO_4 1 M 184.2 ml NaH_2PO_4 1 M pH 5.8 (NaOH), autoclave	
Na_2HPO_4 1 M	50 ml	7.1 g Na_2HPO_4	
NaH_2PO_4 1 M	500 ml	68.99 g NaH_2PO_4	
TMS Buffer	500 ml	91 g Sorbitol (1M) 1045 mg MOPS pH 6.3 (NaOH), autoclave	Used for protoplast resuspension and washes
TMSC Buffer	100 ml	18.2 g Sorbitol (1M) 209 mg MOPS 588 mg $CaCl_2$ pH 6.3 (NaOH), autoclave	For final protoplast adjustment and transformation mix
MS (0.6 M Sorbitol)	100 ml	10.9 g Sorbitol (0.6 M) 209 mg MOPS, pH 6.3 (NaOH), autoclave	Used to prepare PEG solution
PEG 60%	2 ml	1.2 g PEG3350 + 800 µl MS Dissolve at 60°C Do not add water!	Prepare fresh; cool to room temp before use; enough for ~10 samples
SH Agar	200 ml	41.08 g Sucrose (0.6 M) 1 ml 1 M Tris-HCl (pH 6.5) 0.023 g $(NH_4)H_2PO_4$ 1.8 g Bacto-Agar (Becton-Dick.)	For plating protoplasts after transformation Aliquots a 50 ml / 200 ml
Tris-$CaCl_2$		10 mM Tris, 1mM EDTA 40 mM $CaCl_2$ (pH 6.3; NaOH)	For dissolving DNA
Enzyme Mix	20 ml	20 ml KCl 0.6 M / NaP 0.1 M 0.2 g Glucanex 0,02g Yatalase	Prepare freshly (30min incubation on Roller at RT before sterile filtration
sgRNA Cleavage Buffer	10 mL	47.7 mg HEPES (to yield 20 mM, adjust pH to 7.5), 111.8 mg KCl (to yield 150 mM), 1.5 mg DTT (to yield 1 mM; add fresh), 1 mL glycerol (10% v/v); RNase-free water to bring total volume to 10 mL	Provides optimal ionic and reducing conditions for sgRNA stability and RNP formati

Each solution was prepared under sterile conditions to minimize contamination. Whenever possible, filter sterilization (0.45 µm) was preferred for heat-sensitive components; otherwise, autoclaving at 121 °C for 15–20 min is recommended if the components are stable under those conditions.

2.3.2. Pre-culture

Conidia are typically harvested from 7–10-day-old *B. cinerea* colonies grown on malt extract solid media. These conidia (e.g., ~1 × 10^6 to 1 × 10^8 per mL, depending on the protocol) are inoculated into 50–100 mL of ME/HA medium in appropriately sized erlenmeyer flasks. Cultures are incubated at 20–22 °C for approximately 17–19 h with shaking (120–180 rpm). After this incubation, the mycelium is sufficiently developed for downstream protoplast isolation.

2.3.3. Protoplast formation

The mycelial biomass is first collected by centrifugation (e.g., 1,000 × g at approximately 18 °C) and subsequently washed with a 0.6 M KCl/0.1 M NaP buffer. Following washing, the mycelium is transferred into an enzyme mixture consisting of the same buffer (0.6 M KCl/0.1 M NaP) supplemented with Glucanex (0.2 g per 20 mL) and Yatalase (0.02 g per 20 mL). This mixture is then incubated at 25–28 °C for 1–2 h under gentle agitation (e.g., at 100 rpm or on a rocking platform). During the incubation, protoplast formation is periodically monitored under a microscope. Once a sufficient number of protoplasts has been observed (with the average time reaching adequate protoplast levels being approximately 1 hour and 30 min), the solution is filtered through a sterile nylon mesh with a pore size ranging from 30 to 60 µm to remove any debris. Subsequently, the filtrate is centrifuged at around 1,500 × g for 5–10 min at 4 °C. The pellet obtained from this centrifugation is then gently resuspended in TMS buffer. To further enhance purity, repeated cycles of centrifugation and washing may be performed, after which the pellet is resuspended in TMSC buffer. The final concentration of protoplasts is then determined using a hemocytometer and adjusted to approximately 5 × 10^7 to 2 × 10^8 protoplasts per mL (or about 2 × 10^7 protoplasts per reaction when employing multiple CRISPR/Cas9 ribonucleoproteins (RNP)). An average yield is obtained from a 100 mL culture inoculated with 10^7 protoplasts.

2.3.4. *B. cinerea* transformation

Aliquots of ~100 µL of protoplast suspension (in TMSC) are placed into 1.5 mL tubes and sometimes pre-chilled on ice for 10 min to improve stability. DNA (0.5–10 µg, e.g., pTel-Fen plasmid or repair templates, dissolved in ~60 µL Tris-$CaCl_2$) and, if desired, one to four pre-incubated ribonucleoprotein complexes (for CRISPR/Cas9 editing) are added. After a brief incubation on ice (~10 min), 160 µL of freshly prepared 60% PEG are introduced, and the mixture is incubated at 22 °C for ~20 min. The sample is then diluted with TMSC (e.g.,

680–800 µL), centrifuged at ~1,500 × g for 3–8 min at room temperature, and the pellet is gently resuspended in ~200 µL TMSC. This final suspension is used for plating.

2.3.5. Plating and initial selection

Approximately 50–200 mL of liquid SH agar cooled to ~39.5°C is supplemented with the relevant antibiotic or fungicide (e.g., fenhexamid) immediately before use. The full 200 µL transformation mixture is gently mixed into the molten agar, poured into 90 mm Petri dishes, and allowed to solidify at room temperature. The plates are then incubated at 20–22 °C (with or without light). After 3–5 days, individual colonies that appear on the surface are transferred to fresh non-selective high-nutrient medium agar (4x ME) to allow loss of pTEL-fen. In case of stable integration of constructs containing a fenhexamid or hygromycin resistance marker, the ME agar was supplemented with 35 µg/mL hygromycin or 1 µg/mL fenhexamid.

2.3.6. Isolation and confirmation of transformants

Putative transformants are grown for an additional 3–5 days to ensure sufficient biomass for genomic DNA extraction, followed by PCR analyses to confirm the presence or absence of specific transgenes or to verify gene edits (e.g., in CRISPR/Cas9-mediated knockouts). If a marker-free system is used, colonies may be streaked on nonselective medium to facilitate plasmid loss. Finally, strains showing correct deletions or edits are maintained on agar slants at 4 °C for short-term storage or preserved as glycerol stocks at −80 °C for long-term archiving.

2.3.7. RISPR/Cas9 mutagenesis and sgRNA synthesis

A single Cas9 variant protein, Cas9-Stux2, was used according to Leisen et al. (2020) and stored at −80 °C until use.

2.3.8. Design and selection of sgRNA targets

To edit genes in the fungus *B. cinerea* (strain B05.10), we engineered specific RNA molecules that guide the CRISPR-Cas9 system precisely to the target DNA sequence. These RNA guides either as single-guide RNA (sgRNA) or as a combination of CRISPR RNA (crRNA) and trans-activating CRISPR RNA (tracrRNA) are crucial for ensuring that Cas9 induces a cut at the desired gene location. For the design of these guide RNAs, we employed two online tools: GPP sgRNA Designer by the Broad Institute (https://portals.broadinstitute.org/gpp/public/) and CHOPCHOP (https://chopchop.cbu.uib.no/). These resources enabled us to select RNA sequences, known

as protospacers, that exhibit high on-target activity while minimizing the risk of off-target effects. To ensure that our selected sgRNAs would not bind to unintended sites within the *B. cinerea* genome, we performed a BLASTn search against the fungal genome database available on Ensembl: Ensembl Fungi, *Botrytis cinerea* (http://fungi.ensembl.org/Botrytis_cinerea/Info/Index). All RNA oligonucleotides (including crRNA, tracrRNA, and sgRNA) were synthesized at a concentration of 100 µM and stored at −80 °C until use.

Table 6. Oligonucleotides used for sgRNA synthesis.

KO order	**Strain/ mutant**	**Gene**	**gRNA lable**	**Oligonucleotides used (5'→3')**
13	13x	*Bcpg1*	TL294_Pg1_gRNA1	AAGCTAATACGACTCACTATAgTTGATGCGAAATGTTA ACAGGTTTTAGAGCTAGAAATAGCAAG
			TL296_Pg1_gRNA3	AAGCAATACGACTCACTATAGAAGAGAAGACTGATAA CAGGTTTTAGAGCTAGAAATAGCAAG
14	14x	*Bccrh1*	Chr1 L5	AAGCTAATACGACTCACTATAGAGTATTCACAAGAAA ATATGGTTTTAGAGCTAGAAATAGCAAG
			Chr1 R10	AAGCTAATACGACTCACTATAGCTCCTGTGAATATGGC AGTGTTTTAGAGCTAGAAATAGCAAG
15	15x	*BcCDI1*	Cdi1 L4	AAGCTAATACGACTCACTATAGATGGCATGTCTCTTGA CAGGTTTTAGAGCTAGAAATAGCAAG
			Cdi1 R4	AAGCTAATACGACTCACTATAGAAGAGTTTTCACCTAG ACCGGTTTTAGAGCTAGAAATAGCAAG
16	16x	*Bccfem1*	CFEM1-L4	AAGCTAATACGACTCACTATAGTGCCAACGAGCGACA AACAGTTTTAGAGCTAGAAATAGCAAG
			CFEM1-R7	AAGCTAATACGACTCACTATAGCAGAAATACATAAAG CCCATGTTTTAGAGCTAGAAATAGCAAG
17	17x	*Bcpg2*	gRNA pg2 L1	AAGCTAATACGACTCACTATAGACAATGGTTGATAACC ATGGTTTTAGAGCTAGAAATAGCAAG
			gRNA pg2 R5	AAGCTAATACGACTCACTATAGTACCAAGGAGAAAAC TCACGGTTTTAGAGCTAGAAATAGCAAG
18	18x	BcSSP2	gRNA PTP L1	AAGCTAATACGACTCACTATAGATCATGCGAGAAACCC GAATGTTTTAGAGCTAGAAATAGCAAG
			gRNA PTP R1	AAGCTAATACGACTCACTATAGAAGCAGTAAGAATCTC CGATGTTTTAGAGCTAGAAATAGCAAG
19	19x	*BcCDI2*	CDI2gRNA-L1	AAGCTAATACGACTCACTATAGAGTATCTAGAGTGTGT GTGGGTTTTAGAGCTAGAAATAGCAAG
			CDI2gRNA-NR2	AAGCTAATACGACTCACTATAGATTGAATTAAATAGAG ACCAGTTTTAGAGCTAGAAATAGCAAG
20	20x	*Bcsgp1*	SGP1 gRNA-L1	AAGCTAATACGACTCACTATAGAGAGCACAACACCCTT CCCTGTTTTAGAGCTAGAAATAGCAAG
			SGP1 gRNA-R3	AAGCTAATACGACTCACTATAGTATGAATGACATGTAC CGAAGTTTTAGAGCTAGAAATAGCAAG
21	21x	*Bccrh4*	Crh4 gRNA-L1	AAGCTAATACGACTCACTATAGTACGATCTAAGGCTAT CTGAGTTTTAGAGCTAGAAATAGCAAG
			Crh4 gRNA-R2	AAGCTAATACGACTCACTATAGGCACATCTGGATATAT GCCAGTTTTAGAGCTAGAAATAGCAAG
22	22x	*Bcxyg3*	XYG3 gRNA-L3	AAGCTAATACGACTCACTATAGAATGAATCACTTTGTC CGGGGTTTTAGAGCTAGAAATAGCAAG
			XYG3 gRNA-R3	AAGCTAATACGACTCACTATAGATAATCGTCGCGATTA CTGTGTTTTAGAGCTAGAAATAGCAAG
23	23x	*BcGAS5A*	Gltr1 gRNA-L1	AAGCTAATACGACTCACTATAGGAGATAACATATGGAT AGTGGGTTTTAGAGCTAGAAATAGCAAG
			Gltr1 gRNA-R1	AAGCTAATACGACTCACTATAGGAGGCATGGAGAGAG GCTGCGGTTTTAGAGCTAGAAATAGCAAG

24	24x	*Bccdi3*	CDI3 gRNA-L1	AAGCTAATACGACTCACTATAGGTTAAGCGGGACCAA GAGACGGTTTTAGAGCTAGAAATAGCAAG
			CDI3 gRNA-R3	AAGCTAATACGACTCACTATAGGCATCAACATGATGAT TGGAGGTTTTAGAGCTAGAAATAGCAAG
25	25x	*Bcrrae1*	RAE gRNA-L2	AAGCTAATACGACTCACTATAGGTTGTGGTGGGGGATC TGGAGTTTTAGAGCTAGAAATAGCAAG
			RAE gRNA-R2	AAGCTAATACGACTCACTATAGAGAATCTAGCTCGTAT TGAGGTTTTAGAGCTAGAAATAGCAAG
26	26x	*Bcfat1*	FAT gRNA-L2	AAGCTAATACGACTCACTATAGCAAGATCTGAACCCTC ATGTGTTTTAGAGCTAGAAATAGCAAG
			FAT gRNA-R2	AAGCTAATACGACTCACTATAGAAGGTTCGGAAAAAT GACAAGTTTTAGAGCTAGAAATAGCAAG
27	27x	*Bcxyl2*	Xyl2gRNA-L2	AAGCTAATACGACTCACTATAGACTTGTCATACAGAGC GCAAGTTTTAGAGCTAGAAATAGCAAG
			Xyl2gRNA-R1	AAGCTAATACGACTCACTATAGCAAGTCGACAAATAC GAGGTGTTTTAGAGCTAGAAATAGCAAG
28	28x	*BcIEB2*	IEB2 gRNA-L1	AAGCTAATACGACTCACTATAGGCTCACTCAATCGTAT GGGGGTTTTAGAGCTAGAAATAGCAAG
			IEB2 gRNA-R2	AAGCTAATACGACTCACTATAGACGCCGATGTATCAAC CCAGTTTTAGAGCTAGAAATAGCAAG
29	29x	BcCELP1	CELP1 gRNA-L2	AAGCTAATACGACTCACTATAGCGTGTAATTGCCATAT CATGGTTTTAGAGCTAGAAATAGCAAG
			CELP1 gRNA-R2	AAGCTAATACGACTCACTATAGTTGTTGTATGTACAAA TAGGGTTTTAGAGCTAGAAATAGCAAG

2.3.9. sgRNA synthesis via T7 transcription

Two complementary oligonucleotides were designed to form a double-stranded DNA (dsDNA) template incorporating the T7 promoter, the target-specific protospacer, and the sgRNA scaffold. The protospacer oligonucleotide contains the T7 promoter, the target region, and part of the sgRNA scaffold, while the constant oligonucleotide contains the remaining scaffold portion.

Annealing: Oligonucleotides are mixed according to Table 7, heated to 95 °C for 5 min, and then cooled gradually to 25 °C. A more detailed thermocycler program can be used (e.g., cooling from 95 °C to 85 °C at 2 °C/s, then from 85 °C to 25 °C, at −0.1 °C/s) if higher precision is required.

Table 7. Composition of the annealing reaction for sgRNA synthesis.

Component	**Volume**
Protospace Oligo (100 µM)	1 µl
Constant Oligo (100 µM)	1 µl
H2O (0.1% DEPC-treated)	13 µl
End Volume	15 µl total

T4 DNA polymerase extension: After annealing, the mixture is combined with T4 DNA polymerase components (Table 8) and incubated (at 20 min at 12 °C) to synthesize the fully double-stranded DNA template.

Once the extension is complete, the dsDNA product is purified (via a PCR cleanup kit), and its concentration is determined. An optional check on a 4% TBE gel (~100 ng) was occasionally done to confirm successful template formation.

Table 8. Composition of the T4 DNA Polymerase reaction.

Component	**Volume**
10 mM dNTPs	2.5 µl
NEB-Buffer 2.1	2.5 µl
DEPC-H2O	2.5 µl
T4-DNA Polymerase	1 µl
End Volume	10 µl total

In vitro transcription: The purified double-stranded template (~2 µg) is then transcribed using a HiScribe® T7 High Yield RNA Synthesis Kit (New England Biolabs, NEB) according to the manufacturer's instructions. Typical reaction components are shown in Table 9. The mixture is incubated at 37 °C for approximately 16 h (overnight).

Table 9. Composition of the T7 Polymerase reaction.

Component	**Volume**
NTPs (25 mM stock)	6 µl
T7 Buffer (10×)	1.5 µl
T7 Polymerase Mix	1.5 µl
DEPC-H2O	X µl
DNA Template	Y µl
End Volume	20 µl total

DNase treatment and purification: After in vitro transcription, DNase I was used to remove residual DNA. First, 14 µl of DEPC-treated water, 4 µl of 10× DNase I buffer, and 2 µl of DNase I were added directly to the reaction. The mixture was then incubated at 37°C for 30 min. Following the DNase treatment, the single-guide RNA (sgRNA) was purified with an RNA cleanup kit according to the manufacturer's instructions and eluted in RNase-free water. Occasionally, a small aliquot of the purified sgRNA was examined on a 10% denaturing polyacrylamide gel to confirm RNA integrity.

2.3.10. RNP formation

For each ribonucleoprotein (RNP) complex, 6 µg of Cas9Stux2 was combined with 2 µg of sgRNA in cleavage buffer, and the reaction volume was adjusted to 15 µl. This mixture was assembled in individual PCR tubes. The tubes were incubated at 37 °C for 30–60 min to

allow complete formation of the Cas9–sgRNA complex. Immediately following incubation, the pre-formed RNPs were used for fungal protoplast transformation, facilitating the nuclear entry of the complexes, and enabling targeted generation of double-strand breaks at the specified genomic sites.

2.3.11. Preparation of glycerol permanent cultures

For long-term storage of *B. cinerea* strains, we prepared a concentrated spore suspension (washed twice in sterile water), then mixed 500 µl of this suspension with 500 µl of sterile 60% glycerol solution in reaction tubes. Likewise, *E. coli* strains were stored by combining equal volumes of a freshly grown selective LB overnight culture and 60% glycerol. All glycerol stocks were then kept at −80 °C for future use.

2.3.12. Single-spore isolation

Homokaryotic isolates of *B. cinerea* were generated from transformants via single-spore isolation. Briefly, spores were collected from sporulating cultures, and 10 µl of this spore suspension was spread onto plates with a thin layer of selective ME-agar using a sterile Drigalski spatula. Plates were incubated overnight at 22°C. Individual germinated spores were then identified under an inverted microscope and transferred to appropriate media to obtain homokaryotic colonies.

2.4. Phenotypic analyses of *B. cinerea*

2.4.1. Vegetative growth assays

Vegetative growth was assessed on various media (listed in Table 4). Plates were inoculated centrally with 10 µl of spore suspensions adjusted to 1 × 10^5 spores/ml in sterile water. Cultures were incubated at 20°C in darkness or under low light, and radial expansion was recorded as needed.

2.4.2. Conidia formation on ME/HA plates

To induce conidia formation in *B. cinerea*, we placed 10 µl droplets of spore suspensions (1 × 10^5 spores/ml) onto ME/HA agar plates and incubated them at 22 °C for 10 days under continuous fluorescent illumination, supplemented with near-UV (black) light. After incubation, the conidia were collected aseptically by gently rubbing the colony surface with sterile water and passing the resulting suspension through glass wool to remove mycelial

debris. Conidial concentrations were then determined using a Neubauer counting chamber before further analyses.

2.4.3. Induction of sclerotia formation

Sclerotia formation was induced by inoculating ME/HA agar plates (as described in Table 4) in the center with 10 µl droplets of spore suspensions containing 1 × 10^5 spores/ml in sterile water. Plates were maintained in darkness at 22°C for a minimum of two weeks. After incubation, sclerotia formation was documented photographically to evaluate morphological characteristics and counting.

2.4.4. Infection tests with spore suspensions

Infectivity assays were conducted on various host tissues to evaluate the pathogenic potential of both wild-type (BcWT) and mutant *B. cinerea* strains. Unless stated otherwise, spore suspensions were prepared at a concentration of 1×10^5 conidia mL^{-1} in Gamborg minimal medium supplemented with 25 mM glucose (see Table x). Inoculation of tomato leaves (*Solanum lycopersicum cv. Money Maker*), bean primary leaves (*Phaseolus vulgaris cv. Münster*), and apple fruit (*Malus domestica*, cv. 'Golden Delicious') was performed by applying 20 µL drops of the spore suspension onto the plant surface. For quantitative comparisons, a pairwise inoculation approach was used: each leaf received one to two drops of the BcWT strain on one side of the midrib and an equal number of drops of the test isolate on the opposite side, enabling direct evaluation of infection deficits relative to the BcWT. For apple inoculations, the fruit surface was first surface-sterilized with 70 % ethanol; apples were immersed in 70% ethanol for 30 seconds and then allowed to dry. A wound approximately 2 mm deep was made using a 5 mm cork borer, and the resulting 5 mm-diameter plug of tissue was removed with a scalpel. The exposed wound site was then inoculated with the respective spore suspension. For *Arabidopsis thaliana* and maize (*Zea mays*), a 10 µL drop of Gamborg semi-solid inoculation medium (see below) containing conidia was applied directly to the leaf surface.

Tobacco leaves proved difficult to inoculate with conidia suspensions due to the hydrophilic leaf surface. Therefore, 10 µL of conidia were first placed on 5 mm agar discs (2 mm thick) containing Gamborg medium with glucose. After 24 h incubation to allow germination, these discs were inverted (germinated conidia facing downward) onto tobacco leaves. All infection assays were maintained at 21–22 °C in continuous low light under 100 % relative humidity in sealed containers. Infection tests on living bean plants were performed in closed boxes at 25 °C, 100 % relative humidity, with a 12 h light cycle.

2.4.5. Gamborg semi-solid inoculation medium for *Botrytis*

A semi-solid inoculation medium was prepared according to the composition and percentages indicated in Table 4, which includes Gamborg GB5 basal salts, KH_2PO_4, glucose, and Bacto Agar. After cooling to approximately 37°C, 10 ml portions were transferred into 15 ml Falcon tubes, and spores were added to a final concentration of 1 × 10^5 conidia/ml. The tubes were incubated on a rotating shaker at 24–25°C for 6–18 h to ensure uniform germination, which was verified microscopically (to reduce infection intensity, the incubation time in the semi-solid medium can be limited to six h). A 5–10 µl aliquot of the germinated spore suspension was then applied to either attached or detached leaves (e.g., Arabidopsis or maize). For mutant strains, a higher spore density (2 × 10^5 conidia/ml) may be used. Temperature control during incubation is critical to prevent premature agar solidification below 24°C or delayed germination above 27°C.

2.5. Production of secretomes (On-planta)

B. cinerea WT and multi-knockout mutant strains were maintained on 1×HA/ME agar plates at 21–22 °C, and fresh conidia (spores) were harvested immediately before each experiment. Conidial suspensions were prepared as described above. Tomato (*S. lycopersicum*) plants were grown for 5–6 weeks, and detached leaves were used for infection assays and subsequent secretome analyses.

2.5.1. Inoculation and culture conditions

For *B. cinerea* infection of detached tomato leaves, the leaves were placed on trays lined with wet tissue paper. Conidial suspensions (2 × 10^5 conidia·mL^−1 for the BcWT strain and 4 × 10^5 conidia·mL^−1 for mutant strains) were prepared, and 30 µL droplets of these suspensions were applied onto the leaf surfaces. Inoculated leaves were then maintained in closed containers at 21–22 °C until visible lesion formation. The secretome fluid of inoculation droplets containing the fungal secretome was collected at early (~26 h) and late (~48 h) stages post-inoculation. At around 26 h, when initial lesions became visible, approximately 70 % of the original inoculum volume was recovered. After 48 h, a second collection typically yielded about 50 % of the initial volume. The secretome fluid was carefully aspirated or pipetted from the lesion areas. Immediately following harvesting, each secretome sample was centrifuged at 4,000 rpm for 20 min at 4 °C in a swing-out rotor to remove hyphal fragments and leaf debris. For carbohydrate precipitation, 1.5 mL aliquots of secretome were placed in 2 mL tubes, stored at −80 °C for 6 h, then centrifuged at 14,000 × g

for 20 min at 4 °C. The supernatant was then passed through a 0.22 µm cellulose acetate membrane to ensure sterility, aliquoted into sterile tubes, and stored at –80 °C until further use.

2.5.2. Protein purification and sample preparation for MS/MS

TCA–acetone precipitation: For both protein quantification and MS-based analyses, 400 µL of sterile-filtered secretome was combined with 800 µL of cold TCA–acetone, gently inverted, and incubated at −20 °C overnight to precipitate proteins. The mixture was then thawed and centrifuged at 13,000–14,000 × g for 60 min at 4 °C, after which the supernatant was discarded. The supernatant was discarded, and the pellet was sequentially washed with 100% acetone followed by 80% acetone, centrifuged again for 10 min under the same conditions, and briefly air-dried (e.g., under laminar flow for ~10 min). Pellets intended for MS/MS were stored at −80 °C until further processing.

Protein concentration assay: For protein quantification, the dried pellet was dissolved in approximately 10 µL of solubilization buffer (Table 10) and incubated at 50 °C for 60 min with intermittent mixing. An aliquot of the fully resuspended sample was then mixed with Pierce™ 660 nm Protein Assay Reagent (Thermo Fisher Scientific) at a 1:7.5 ratio, incubated at room temperature for 5 min, and measured at 660 nm using a NanoDrop spectrophotometer (e.g., NanoDrop 2000). Protein concentrations were determined by comparison to a bovine serum albumin (BSA) standard curve.

Table 10. Solutions for protein precipitation.

Solution	Component	Concentration/Amount
TCA/Acetone	Trichloroacetic acid (TCA)	20% (w/v)
	Acetone	80% (w/v)
Solubilization Solution	Urea	9 M
	Thiourea	2 M
	DTT	20 mM
	CHAPS	4.0% (w/v)
	Triton X-100	0.5% (w/v)

2.6. Molecular biological methods

2.6.1. Preparation of genomic DNA from *B. cinerea* for standard analyses

Genomic DNA was isolated from 5–10-day-old *B. cinerea* cultures for standard PCR analysis. For this purpose, approximately 1 cm² of mycelium (free of agar) was removed

using a sterile forceps and placed into a 2 mL reaction tube containing 500 µL glass beads (Ø 0.75–1 mm) and 200 µL water. Alternatively, 200 µL of a spore suspension could be used. After adding 400 µL of CTAB solution (see Table 11), the sample was subjected to mechanical disruption in a FastPrep-24™ Classic bead homogenizer (MP Biomedicals) for 45 s at setting 6.0. The tube was then centrifuged at 14,000 × *g* for 60 s. Next, 400 µL chloroform was added, followed by ~10 s of vortexing and another centrifugation at 14,000 × *g* for 2 min.

The aqueous phase was transferred to a 1.5 mL reaction tube, and an equal volume of isopropanol was added. The mixture was gently mixed, and the DNA was precipitated overnight at −20 °C. Afterwards, the sample was centrifuged at 14,000 × *g* for 15 min, the supernatant was discarded, and the DNA pellet was washed with 1 mL of 70 % ethanol. Following a further centrifugation for 1 min at 14,000 × *g*, the supernatant was carefully removed, and the pellet was allowed to dry. Depending on the pellet size, the DNA was resuspended in 20–500 µL water. If needed, the quality of the DNA was checked by loading 2 µL of the sample on a 1 % (w/v) TAE agarose gel.

Table 11. Solutions used for gDNA preparation.

Solution	**Components**	**Concentration**
CTAB solution (pH 8.0)	Sorbitol	2.5 % (w/v)
	N-Laurylsarcosine	1.0 % (w/v)
	NaCl	4.7 % (w/v)
	Na-EDTA	1.0 % (w/v)
	Polyvinylpyrrolidone (PVP)	1.0 % (w/v)
	CTAB	0.8 % (w/v)

2.6.2. Isolation of DNA quick method

DNA from transformant strains was isolated following the protocol developed by Amir Sharon (Tel Aviv University, Israel). The procedure involved pipetting 20 µl of Extraction Solution (Sigma-Aldrich) into individual PCR tubes for each sample, followed by carefully scraping a small amount of fungal material from a 7-day-old culture plate using a sterile toothpick and transferring it directly into the PCR tubes containing the Extraction Solution. The samples were then placed into a thermocycler and incubated first at 65°C for 10 min to facilitate cell lysis and DNA release, and subsequently at 95°C for an additional 10 min to denature proteins and further release DNA. After thermal treatment, 30 µl of Neutralization

Solution (Sigma-Aldrich) was added to each tube and gently mixed. The resulting DNA samples were used for PCR screening.

2.6.3. Preparation of high-molecular-weight genomic DNA from *B. cinerea* for genome sequencing

Genomic DNA was extracted from *B. cinerea* cultures using the Qiagen Blood & Cell Culture DNA Mini Kit with a protocol optimized for *B. cinerea*. A total of 2–5 × 10^7 spores were suspended in 500 µL of water, frozen in liquid nitrogen together with a small amount of sea sand, and ground thoroughly with a pestle in a mortar. The resulting powder was transferred in a frozen state with a spatula to a 15 mL tube and resuspended in 2 mL of G2 buffer containing 4 µL of RNase A (100 mg mL^−1). After vortexing to ensure complete homogenization, 45 µL of Proteinase K (Qiagen stock solution) was added, and the sample was incubated at 50 °C for 45 min. Subsequently, the sample was centrifuged at 3,000 × *g* for 10 min, and the supernatant was transferred to 1.5 mL reaction tubes and centrifuged again at 14,000 × *g* for 2 min. The clarified supernatant was then applied to a Qiagen column pre-equilibrated with QBT buffer and washed three times with 1 mL of wash buffer. DNA was eluted twice with 1 mL of QF buffer at 50 °C, and the combined eluate was mixed with 1.4 mL of isopropanol by inverting the tube approximately 20 times. After transfer to a 1.5 mL reaction tube, the mixture was centrifuged at 14,000 × *g* for 20 min to pellet the DNA. The pellet was then washed with 1 mL of −20 °C ethanol, centrifuged for 10 min at 14,000 × *g*, and dried. Finally, the pellet was dissolved overnight in an appropriate volume of TE buffer (pH 8).

2.6.4. Polymerase Chain Reaction (PCR)

DNA fragments were amplified via PCR. For routine analytical purposes, Taq polymerase was employed. To amplify DNA fragments intended for cloning, high fidelity Q5 polymerase (NEB) or Phusion polymerase (Thermo Scientific) were used according to the manufacturers' instructions. The annealing temperature and elongation time were adjusted based on the anticipated product length.

2.6.5. Oligonucleotides

All oligonucleotides used in this study were synthesized by Eurofins Genomics and are listed in Table 12. For standard applications, a working concentration of 10 pmol/µL was prepared.

Table 12. Oligonucleotides used in 5' -> 3' sequence.

Name	Sequence	Gene/ Purpose
TL353_Pg1_L_F	TCCATTCCGGCTTCCACTTCG	Pg1 outside primers
TL354_Pg1_L_R	ACCGGCAATCCTGGTAACCTT	
TL355_Pg1_R_F	ATAGTCGCCTGTCATCGAGGG	Pg1 inside primers
TL356_Pg1_R_R	ATGACACAGGGTCGTGGGAT	
Chr1_S_for	AAGGTTTGTTTGACCACGCC	Chr1 outside primers
Chr1_S_rev	TGAGCATGGGAGTATTGCATC	
Chr1_wc_for	ATCCCCAAACCCCCATGTTG	Chr1 inside primers
Chr1_wc_rev	CGCCGTAGGTGTATTCGGTA	
CDI1_S_for	TATCCGTCTGTACCCTCCCC	CDI1 outside primers
CDI1_S_rev	AAGATAGAACCAAAGCCCGCA	
CDI1_wc_for	ATCCGCTCCATTTTCCCTCG	CDI1 inside primers
CDI1_wc_rev	TACCGTCGTTGTGGAAGTCG	
CFEM1_S_for	TCACTGCCACATATTGCCCT	CFEM1 outside primers
CFEM1_S_rev	GGCCTAGCGCAGTAATACCT	
CFEM1_wc_for	TCACCGTCGCTTTGAGTAAGT	CFEM1 inside primers
CFEM1_wc_rev	AGATGAAGAAGGAGCGGCAG	
PG2-OUT-FOR-1	AGTGGACGCTGAAAGAAAGGA	Pg2 outside primers
PG2-OUT-REV-1	AATGGATGCGGCTTGAAACTG	
BcPG2_RTfor	CTGGAGATGCTGGTAGCCTTG	Pg2 inside primers
BcPG2_RTrev	TCGCACGTCCTTGACATCG	
Ptp1_S_FOR	TAAGTTCAAGGTGGGGAGGCA	Ssp2 outside primers
Ptp1_S_REV	CAGAAACCACCAAAGGGGCA	
Ptp1_WC_FOR	AAAATGGTCCGCATCTCCTCC	Ssp2 inside primers
Ptp1_WC_REV	GGTTGCCAATTTCAGCATCCTAT	
CDI2_S_FOR	AGGTAGTGTGAGATTGGCAGTT	CDI2 outside primers
CDI2_S_REV	TGTGATGGTTGTGGTGGAGT	
CDI2_WC_FOR	TTCGCACTCGATGGTGCTC	CDI2 inside primers
CDI2_WC_REV	GTTTGCTCACTGGAGTTGGG	
SGP1-OUT-FOR	TGTCACGGCCAAGTGAAGTT	SGP1 outside primers
SGP1-OUT-REV	TTGGGTGTCGATGAAGGGGT	
SGP1-IN-FOR	AGCAGCAAAAAGACCACCCA	SGP1 inside primers
SGP1-IN-REV	CAAATACACTCAGCCTCCGTCA	
crh4-OUT-FOR	TTCCGCCCCCATTCATAACC	Crh4 outside primers
crh4-OUT-REV	CGACTCGCCGACGCTAATAA	
crh4-IN-FOR	GACCAAACGACCTGCTCTGA	Crh4 inside primers
crh4-IN-REV	CAGTGGCTTGCTTCGTTTCC	
XYG3-OUT-FOR	AGTCGAGACCGGGTACATGA	Xyg3 outside primers
XYG3-OUT-REV	CAACTAGACTTTTCCTTTCCCACA	
XYG3-IN-FOR	CACTGGATCCTCCATCGTCG	Xyg3 inside primers
XYG3-IN-REV	TGAATGTGAGGTTGGGGAGA	
NS16-gltr1-O-FOR	AGTCGATGCAAAATCTGAGGTACT	GAS5A outside primers
NS17-gltr1-O-REV	TTCTGCACCACACCATCCAT	
NS18-gltr1-I-FOR	AGGCTACCACATGTTAGTTGGG	GAS5A inside primers
NS19-gltr1-I-REV	AGATCACCGATCCGATTGCC	

NS20-CDI3-O-FOR	AAAGGCACGAGGAACCTAGC	CDI3 outside primers
NS21- CDI3-O-REV	GCTCAGCGAGTAACAGTGTG	
NS22- CDI3-I-FOR	CGAGCATCCTTAAACTCGCT	CDI3 inside primers
NS23- CDI3-I-REV	TGCGAGACTACCTGCACTGA	
NS36-RAE-O-FOR	TGACGAAGAAGCAACCGTCA	RAE1 outside primers
NS37-RAE-O-REV	AGCCGACGATCTCCCTATCT	
NS38-RAE-I-FOR	TTCGCAGTGTAGAGACCGTG	RAE1 inside primers
NS39-RAE-I-REV	TTTGTTCCTCAGCGAGTTTGG	
NS44-FAT-OUT-FOR	CGATGTGGGTTGTTTTCTGGG	FAT1 outside primers
NS45-FAT-OUT-REV	CGAAGTCCGGCAACATTCTCT	
NS42-FAT-I-FOR	TGTTGCTTGGCTACGAATGTG	FAT1 inside primers
NS43-FAT-I-REV	TAGCCAGCATCTCTGGACCT	
NS58-Xyl2-OUT-FOR	GATTTCGTTCGGGATGGCAC	Xyl2 outside primers
NS59-Xyl2-OUT-REV	TTACGGGCAATGGCAGAGTT	
NS60-Xyl2-IN-FOR	ACCACCAGTTCGCTTTGTCT	Xyl2 inside primers
NS61-Xyl2-IN-REV	TGTATCCATATTCCCCCGAGT	
NS86-IEB2-OUT-F	ATTGCACGGACCACTTCAGG	IEB2 outside primers
NS87-IEB2-OUT-R	GGTACCAAGCGCGCATATTG	
NS88-IEB2-IN-F	CCCCAAGCAGCATCCATCTA	IEB2 inside primers
NS89-IEB2-IN-R	GTACCTTCCCAACTGGAGCC	
NS96-CELP1-OUT-F	CCTTTGGAACAACTTCGGCG	CELP1 outside primers
NS97-CELP1-OUT-R	TGCTTCGACCTCAGAATCCC	
NS98-CELP1-IN-F	CCTCCCTTCTTTCCAGCCTC	CELP1 inside primers
NS99-CELP1-IN-R	CGGTGTATGTGTAGGCAGCA	
MH37-Spl2-Eco-F	GTCCGAATTCACCATCCAAGTAACCTACGACTCCG	Cloning into pCOLD-TF
MH38-Spl2-Pst-R	AACTGCAGCCAAATCTAAGCCTTACACGGTGATCCA	Cloning into pCOLD-TF
MH39-Xyl2-Nco-F	CTTCCATGGCCAACTCAAGTTTTGAGCTCGTCG	Cloning into pET28
MH40-Xyl2-Eco-F	GAGAGAATTCCTTGCTGCTGTCACGAGAGTC	Cloning into pCOLD-TF
MH41-Xyl2-Pst-R	TCCTGCAGGCCATATCTCACAAGCATTGAG	Cloning into pCOLD-TF
MH42-Xyl2-Xho-R	ACCTCGAGACACAAGCATTGAGAATAGTAAGAATTTGCA	Cloning into pET28
MH43-Xyl3-Nco-F	CATCCATGGCAATTTCTACCTCGCTCGC	Cloning into pET28
MH44-Xyl3-Eco-F	GTGTGAATTCTCGGCAATTTCTACCTCGCTC	Cloning into pCOLD-TF
MH45-Xyl3-Xho-R	CTCTCTCGAGGTAACTAACCGTCTGCGTAGCAGC	Cloning into pET28
MH46-Xyl3-Pst-R	CACTGCAGCTAACTAACCGTCTGCGTAGCAGC	Cloning into pCOLD-TF
MH47-IEB2-Eco-Nco-F	GTGTGAATTCTCCATGGCTAGCCCTATCGCCGCTAG	Cloning into pCOLD-TF
NS-IEB2-NcoI-F	TCTCCATGGCTAGCCCTATCGCCGCTAGCACATC	Cloning into pET28
MH48-IEB2-Xho-R	CTCTCGAGCTGTTGAGCAATCAATTGGATCTGCT	Cloning into pET28
MH49-IEB2-Xba-R	TCTCTAGACCAAGCAGCATCCATCTATTGAGC	Cloning into pCOLD-TF

MH50-RAE1-Nco-F	TTTCCATGGTGCCAACTTTGTATTTGGCTGGTGATTCCAGCATGG	Cloning into pET28
MH51-RAE1-Eco-F	GTTTGAATTCGTGCCAACTTTGTATTTGGCTGG	Cloning into pCOLD-TF
MH52-RAE1-Xho-R	CTCTCTCGAGGTAAGCACAGCTTCCGGCAATAC	Cloning into pET28
MH53-RAE1-Pst-R	CACTGCAGCCGAACTAAGCACAGCTTCCG	Cloning into pCOLD-TF
MH54-RAE2-Hind-Nco-F	AGAAAGCTTACCATGGGCTCTGCGGTCCCATTCAATCATG	Cloning into pCOLD-TF/pET28
MH55-RAE2-Xho-R	CTGTCTCGAGGTATATACAGGTACCGACAACACTATCAGT	Cloning into pET28
MH56-RAE2-Pst-R	CTCTGCAGCTCTCTTATATACAGGTACCGACAACAC	Cloning into pCOLD-TF
MH57-IEB2-BsaF	AGAAGTGAAGCTTG GTCTCAGGCTTTGC TAGCCCTATCGCCG CTAG	Green Gate Cloning
MH58-IEB2-BsaR	AGGGCGAGAATTCG GTCTCACTGAGTATT GAGCAATCAATTGGA TCTGCTCGCA	Green Gate Cloning
MH59-RAE2-BsaF	AGAAGTGAAGCTTG GTCTCAGGCTTCGT TGCCTCTAGCGCTG TC	Green Gate Cloning
MH60-RAE2-BsaR	AGGGCGAGAATTCG GTCTCACTGAGTATA TACAGGTACCGACA ACACTATCAGTGC	Green Gate Cloning
MH61-X11A-BsaF	AGAAGTGAAGCTTG GTCTCAGGCTCACC CGTCAGCGAGAACT TGA	Green Gate Cloning
MH62-X11A-BsaR	AGGGCGAGAATTCG GTCTCACTGAAAGAA ACAGTGATGGAAGC GGAAC	Green Gate Cloning
MH63-X11A-mutF	CACATACAAGATCCT CGAAACCACCCGTA CA	Green Gate Cloning
MH64-X11A-mutR	GTACGGGTGGTTTC GAGGATCTTGT	Green Gate Cloning
MH65-Xyl2-BsaF	AGAAGTGAAGCTTG GTCTCAGGCTCTCT TGCTGCTGTCACGA GAGTCTTAAC	Green Gate Cloning
MH66-Xyl2-BsaR	AGGGCGAGAATTCG GTCTCACTGAGCAC AAGCATTGAGAATAG TAAGAATTTGC	Green Gate Cloning
MH67-Xyl3-BsaF	AGAAGTGAAGCTTG GTCTCAGGCTTCGG CAATTTCTACCTCG CTCG	Green Gate Cloning
MH68-Xyl3-BsaR	AGGGCGAGAATTCG GTCTCACTGAGTAA CTAACCGTCTGCGT AGCAGCC	Green Gate Cloning
MH69-pColdF	CTGGCGAAAGCGAA AGTGAC	pCOLD-TF
MH70-pColdR	GCAGGGATCTTAGA TTCTGTGCTT	pCOLD-TF
MH71-X11A-Eco-F	gtgtgaattcGTCAGCGAGAACTTGAATGTCTTG	Cloning into pET28
MH72-X11A-Xba-R	tctctagaCCCAGATTTAAGAAACAGTGATGGAAG	Cloning into pET28
MH73-IEB1-Eco-F	tctcgaattctCTGCAACCCCCATTGTCTCTG	Cloning into pET28
MH74-IEB1-Xba-R	tctctagaCCATTCTTGATTTAAGCGTACTCCCAAG	Cloning into pET28
MH75-CDI2-Eco-F	gagagaattctTGGATCAGTTCATGGTTCCTACTCCATG	Cloning into pET28
MH76-CDI2-Xba-R	gatctagaCTCAACAGAACTCGCACTTCTCG	Cloning into pET28
MH77-Hip2-Eco-F	gttggaattcCTCAGCGTTGCCACTGCATCA	Cloning into pET28
MH78-Hip2-Xba-R	catctagaAGGCTAGGACAAAGCGAAAGTAGTAGG	Cloning into pET28
MH79-XYG3-Hind-F	accaagcttctAGCAGCCGACAAAACCTTGAAG	Cloning into pCOLD-TF

MH80-XYG3-Xba-R	cttctagatcaAGAGATTGAGACACTGTAGGC	Cloning into pCOLD-TF
IEB1_fwd_NDE1	CAA CAT ATG ACC CCC ATT GTC TCT GC	IEB1
IEB1_rev_EcoR1	TGT GAA TTC TTA AGC GTA CTC CCA AGC GGA	IEB1
CDI2_fwd_NDE1	CAA CAT ATG GAT CAG TTC ATG GTT CCT ACT CCA TG	CDI2
CDI2_rev_EcoR1	TGT GAA TTC TCA ACA GAA CTC GCA CTT CTC G	CDI2
XYG3_fwd_NDE1	CAA CAT ATG TCT ACT CAA ATC TGT GGT CAA TAT GAC AGT GT	XYG3
XYG3_rev_Sal1	TGT GTC GAC TTA AGC AGC AAC ACA CTG GGA GTA	XYG3
MH93-BcCDI7-Nco-F	CGTCCATGGTCTCCCAAACAACAATGGTGGTAGC	Cloning into pET28
MH94-BcCDI7-Xho-R	CAACCTCGAGGTATAGAGTGATTGGCAAGAAGATAACAAGAC	Cloning into pET28
MH95-BcCDI7-Eco-F	TTCCGAATTCCTCCCAAACAACAATGGTGGTAG	Cloning into pCOLD-TF
MH96-BcCDI7-Xba-R	CCATCTAGATTATAGAGTGATTGGCAAGAAGATAACAAGAC	Cloning into pCOLD-TF
MH97-BcCDI7-Bsa-F	agaagtgaagcttGGTCTCAGCCGCTCTCCCAAACAACAATGGTGGTAG	Green Gate Cloning
MH98-BcCDI7-Bsa-R	agggcgagaattcGGTCTCACTGAGTATAGAGTGATTGGCAAGAAGATAACAAGAC	Green Gate Cloning
MH87-pGGCO-F	AGCCTGAGACCAAGCTTCACTTCT	pGGCO-F
MH88-pGGCO-R	TCAGTGAGACCGAATTCTCGCCCT	pGGCO-R
MH89-RAE1-BsaF	AGAAGTGAAGCTTGGTCTCAGGCTTGCCAACTTTGTATTTGGCTGG	Green Gate Cloning
MH90-RAE1-BsaR	AGGGCGAGAATTCGGTCTCACTGAGTAAGCACAGCTTCCGGCAATAC	Green Gate Cloning
MH91-IEB1-BsaF	AGAAGTGAAGCTTGGTCTCAGGCTTTGCAACCCCCATTGTCTCTGCAC	Green Gate Cloning
MH92-IEB1-BsaR	AGGGCGAGAATTCGGTCTCACTGAGTAAGCGTACTCCCAAGCGGAAGG	Green Gate Cloning

2.6.6. Agarose gel electrophoresis

Agarose gel electrophoresis was used to separate DNA fragments to determine their size and/or quality. Fragments smaller than 1,500 bp were resolved on 1.5-2 % TBE–agarose gels, whereas fragments larger than 1,500 bp were separated on 1 % TAE–agarose gels. The buffers used are listed in Table 9. DNA bands were visualized by staining the gels in an ethidium bromide solution (0.5 µg/mL) for approximately 15 min, followed by a brief (about 5 min) wash in water. The results were recorded using a UV transilluminator ($\lambda = 312$ nm) and photographed.

Table 13. Buffers used for agarose gel electrophoresis.

Buffer	Components	Quantity
50× TAE Buffer (pH 8)	Tris	2 M
	Acetic acid (v/v)	5.71 %
	EDTA-Na_2	0.05 mM
10× TBE Buffer (pH 8–8.9)	Tris (v/v)	10.8 %
	Boric acid (v/v)	5.5 %
	EDTA-Na_2 (w/v)	0.93 %

2.7. Protein expression

2.7.1. Heterologous expression in *E. coli*

2.7.1.1. cDNA Preparation and PCR Amplification

The PCR reactions were set up using Q5 High-Fidelity DNA Polymerase (NEB), which is optimized for high fidelity and robust amplification. The reaction mix composition is provided in Table 14, and the PCR cycling conditions are detailed in Table 15.

Table 14. Q5 Polymerase reaction mix composition (per 50 µl reaction).

Component	Volume (µl)	Final Concentration/Remarks
5× Q5 Reaction Buffer	10	Provided with Q5 Polymerase
dNTP Mix (10 mM each)	1	Final concentration 200 µM each
Forward Primer (10 µM)	1	
Reverse Primer (10 µM)	1	
Q5 High-Fidelity DNA Polymerase	0.5	Typically, 1 U/50 µl reaction
Template cDNA	2–5	~50–100 ng
Nuclease-Free Water	To 50 µl	

Table 15. Q5 Polymerase PCR Program Parameters.

Step	Temperature	Time
Initial Denaturation	98 °C	30 seconds
Denaturation	98 °C	10 seconds
Annealing	Tm – 3 °C*	30 seconds
Extension	72 °C	30 sec per kb
Final Extension	72 °C	2 min
Hold	4 °C	Indefinite

*Annealing temperature optimized for each primer pair.

2.7.1.2. DNA Purification

Following amplification, PCR products were verified by agarose gel electrophoresis. Bands corresponding to the expected sizes were excised and purified using the NucleoSpin® Gel and PCR CleanUp Kit (Macherey-Nagel) according to the manufacturer's protocol.

2.7.1.3. Initial plasmid isolation

For cloning, plasmid backbones (pCold-TF and pET-28) were isolated from previously transformed *E. coli* DH5α cultures. Single colonies were inoculated into 4 ml LB broth containing 100 µg/mL ampicillin (for pCold-TF) or 100 µg/mL kanamycin (for pET-28) and incubated overnight at 37°C with shaking. Plasmid isolation was then performed using the NucleoSpin® Plasmid Kit (low-copy protocol), and concentrations were determined using a NanoDrop

2.7.1.4. Restriction digestion

Both the purified PCR products (inserts) and plasmid backbones were digested to create compatible ends for directional cloning.
Digestion reactions were incubated at 37°C for 1 h. Subsequently, 2.5 µl of QuickCIP (NEB) was added to the digested plasmids and incubated at 37°C for 10 min for dephosphorylation. Heat inactivation was then performed (80°C for 20 min for the insert and 80°C for 2 min for the plasmid) before ligation.

2.7.1.5. Ligation

The digested inserts were ligated into the appropriately digested and dephosphorylated plasmid backbones using T4 DNA ligase (NEB) (Table 16). In each 20 µl reaction, approximately 100 ng of vector was used with the insert at a 3:1 molar ratio.

Table 16. Ligation reaction components (20 µl total).

Component	**Volume/Amount**
Digested vector	100 ng (volume as required)
Digested insert	Adjusted for 3:1 molar ratio
10× T4 Ligase Buffer	2 µl
T4 DNA Ligase	1 µl
Nuclease-free Water	To bring the total volume to 20 µl

Ligation reactions were incubated at room temperature (22–25°C) for 10–30 min or overnight at 4°C.

2.7.1.6. Transformation into *E. coli* DH5α

For initial cloning, chemically competent *E. coli* DH5α cells were used: Thaw 50 µl aliquots of DH5α cells on ice for 20 min. Add 5 µl of the ligation mix (for pCold-TF and pET-28 plasmids) to the cells. Incubate on ice for 30 min. Heat shock at 42°C for 45 s, then immediately return to ice for 2 min. Add 500 µl LB medium and incubate at 37°C for 45 min with shaking at 200 rpm. Plate on LB agar containing ampicillin and incubate overnight at 37°C.

2.7.1.8. Screening by colony PCR and restriction analysis

Transformed colonies were screened by colony PCR using primers flanking the insert site. A portion of each colony was used for PCR, and the remaining was re-streaked for isolation. Colonies showing the expected insert size were inoculated into LB broth with antibiotic and grown overnight. Plasmids were then isolated (miniprep) and subjected to restriction digestion to confirm the correct insert before sequencing.

2.7.1.8. Sequencing Confirmation

Plasmid DNA from positive clones was prepared for sequencing. A typical 10 µl sequencing reaction contained: 5 µl plasmid DNA (100 ng/µl), 2.5 µl sequencing primer (10 pmol/µl) and 2.5 µl nuclease-free water. Sequence data were analyzed using SnapGene® to confirm insert integrity and orientation.

2.7.1.9. Transformation into *E. coli* Rosetta

After sequence confirmation, the recombinant plasmids were transformed into *E. coli* Rosetta strains for protein expression using the same transformation procedure as described above.

2.7.1.10. Culture conditions and induction

For protein expression, *E. coli* Rosetta cells harboring either pCold-TF or pET-28-based constructs were used. Cells were grown in LB medium (composition in Table 1) supplemented with the appropriate antibiotic.

For all constructs, an overnight preculture was grown at 37°C. The following day, the culture was diluted 1:100 into large flasks (500–2000 ml) and incubated at 37°C until the optical density at 600 nm (OD_{600}) reached approximately 0.5. The cultures were then cooled for 10 min to either 16°C (for pCold-TF) or 21.5°C (for pET-28), followed by induction with

0.4 mM IPTG. Induction was performed overnight with shaking at the corresponding temperatures (16°C for pCold-TF, 21.5°C for pET-28).

2.7.1.11. Screening and expression analysis

Testing for expression (Induced vs. Uninduced)

For each culture, 1.5 ml samples were taken both before and after IPTG induction. Cell pellets were resuspended in 75–150 µl of 1× SDS-PAGE sample buffer (see Table 17), boiled for 10 min at 95°C, cooled, and centrifuged. Aliquots (20 µl) were loaded onto SDS-PAGE to assess expression.

Table 17. Gel loading buffer for SDS-PAGE.

Component	Concentration
SDS	8% (w/v)
Glycerol	40% (v/v)
Tris-HCl (pH 6.8)	200 mM
DTT	400 mM
Bromophenol Blue	0.4% (w/v)

Testing for solubility

Induced cells were lysed using B-PER (Bacterial Protein Extraction Reagent). Approximately 100 µl of B-PER was added (adjusted for pellet size) and incubated at room temperature for 10 min. Lysates were centrifuged at maximum speed for 10 min at 4°C. The supernatant (soluble fraction) was mixed with 75 µl of 2× SDS-PAGE buffer, while the pellet (insoluble fraction) was resuspended in 150 µl of 1× SDS-PAGE buffer. Both fractions were heated to 95°C for 5 min, cooled, and analyzed by SDS-PAGE

2.7.1.12. SDS-PAGE analysis

Gel Preparation

Protein samples were separated using SDS-PAGE. Two different gel systems were prepared as follows:

Table 18. SDS-PAGE gel composition for two gels.

Gel Type	% Acrylamide	Composition (for 2 gels)
Separating Gel	12%	4.5 ml H_2O, 5.3 ml Rotiphorese Gel 30, 3.3 ml 1.5 M Tris (pH 8.8), 133 µl 10% SDS, 100 µl 10% APS, 10 µl TEMED
Stacking Gel	3%	4.1 ml H_2O, 0.7 ml Rotiphorese Gel 30, 1.7 ml 1.5 M Tris (pH 8.8), 66.7 µl 10% SDS, 66.7 µl 10% APS, 6.7 µl TEMED

Table 19. SDS-PAGE running buffer composition.

Buffer	Composition
10× Running Buffer	1.00% (w/v) SDS, 0.25 M Tris, 1.92 M Glycerol
1× Running Buffer	10× Running Buffer diluted 1:10 with nuclease-free water

After electrophoresis (typically run at 120 V for ~1 h), gels were fixed by incubating in a solution of 40% ethanol and 10% acetic acid for 30 min. Gels were then stained using Brilliant Blue G – Colloidal Concentrate (Sigma) for 2 h with gentle shaking. Finally, the gels were destained over 1 hour, with the destaining solution (40% methanol, 10% acetic acid) being changed several times.

2.7.1.13. Protein extraction and purification

A total of 300 mL of induced culture was collected and centrifuged at 2800 × g for 20 min at 4 °C in 50 mL Falcon tubes. The resulting cell pellets were resuspended in 10–20 mL of HSB30 buffer (Table 20) (per pellet, adjusting the volume to match the pellet size). Lysozyme was then added to reach a final concentration of 1 mg/mL. To disrupt the cells, the suspension was sonicated on ice using an MS72 sonicator set to 90–97% power in two rounds of 5 min each. Each 5 min round consisted of five 10 s pulses, ensuring efficient lysis while minimizing heat buildup. Afterward, the lysate was transferred to Nalgene tubes and centrifuged at maximum speed (approximately 18,500 rpm) for 20 min at 4 °C using a fixed-angle rotor. Finally, the clarified supernatant was collected for further purification steps.

10 mL of the cleared lysate was incubated with ~1.5 ml ROTI ® GAROSE His/Ni-Beads in a 25 ml Erlenmeyer flask for 3 h at 4°C with gentle shaking to allow binding of the His_{6x}-tagged protein. Columns were pre-equilibrated by sequentially washing with 15 ml pure ethanol, ultrapure water (Milli-Q), and 15 ml HSB30 buffer. After the lysate–bead mixture was added and allowed to settle (with the column valve closed), the column was washed twice with 15 ml HSW60 buffer. The beads were then incubated on-column for 15 min with 3 ml HSE500 buffer, and the eluted protein was collected in a 15 ml Falcon tube, keeping a 20 µl aliquot for SDS gel analysis.

Table 20. Buffers for protein purification (HSB/HSW/HSE).

Buffer Name	Components	Final Volume/ Notes
Sodium-Phosphate Buffer (50 mM)	For 2.4 L: 32 ml 0.2 M NaH_2PO_4, 568 ml 0.2 M Na_2HPO_4, 1.8 L distilled water	Prepared in bulk
Binding Buffer (HSB30)	2.04 g Imidazole (30 mM), 17.5 g NaCl (300 mM) in 1 L of 50 mM Sodium-Phosphate buffer (pH 8)	1 L
Wash Buffer (HSW60)	4.1 g Imidazole (60 mM), 17.5 g NaCl (300 mM) in 1 L of 50 mM Sodium-Phosphate buffer (pH 8)	1 L
Elution Buffer (HSE500)	8.51 g Imidazole (500 mM), 4.38 g NaCl (300 mM) in 250 ml of 50 mM Sodium-Phosphate buffer (pH 8)	250 ml

2.7.1.14. Dialysis and protein quantification

The eluted protein was dialyzed using a SnakeSkin® dialysis tube (3.5 kDa MWCO) against 1 L of 50 mM Sodium-Phosphate buffer with 100 mM NaCl, pH 6. The dialysis buffer was changed three times at 1 h intervals (see Table 21). Protein concentration was measured by absorbance at 280 nm (A280) using a NanoDrop and the Pierce™ 660 nm Protein Assay.

Table 21. Composition and preparation of dialysis buffer.

Component	Concentration	Amount for 3 L Total Volume
Sodium Dihydrogen Phosphate (NaH_2PO_4)	0.2 M	28.4 g per liter; 660 ml of 0.2 M solution used
Disodium Hydrogen Phosphate (Na_2HPO_4)	0.2 M	27 g per liter; 93 ml of 0.2 M solution used
Sodium Chloride (NaCl)	50 mM	17.5 g total
Milli-Q Water	–	Adjust to a total of 3 L

2.7.1.15. Functional analysis: Phytotoxicity assay

Following purification, the protein concentration was measured by A280. For the phytotoxicity assay, the protein was diluted in dialysis buffer to a final concentration of 15 between 5 µM and 30 µM. Approximately 20 µl of each protein dilution was infiltrated into the abaxial side of leaves of 5- to 7-week-old *N. benthamiana* plants using a needle-less syringe. Infiltrated sites were marked, and plants were maintained under controlled conditions. After 5 days, the treated areas were assessed for signs of chlorosis or necrosis. Lesion areas were determined by ImageJ to determine relative lesion sizes. Statistical analysis was performed using one-way ANOVA, with a significance threshold of $P < 0.05$.

2.7.2. Transient expression in *N. benthamiana* via Agroinfiltration

This protocol details the transient expression of CDIPs candidate genes from *B. cinerea* in *N. benthamiana* leaves. The workflow includes: (1) Cloning and assembly of the expression cassette via Golden Gate; (2) Transformation into *Agrobacterium tumefaciens* GV3101; (3) Co-infiltration with the plasmid pCB301-p19 (encoding the silencing suppressor P19) to enhance transgene expression; (4) Preparation of bacterial suspensions and agroinfiltration; and (5) Protein extraction and analysis.

2.7.2.1. Cloning and assembly of the expression cassette

Target genes were amplified from *B. cinerea* cDNA using Q5 High-Fidelity DNA Polymerase. PCR products were gel-purified and cloned into the donor vector (pGGC000) using a BsaI-based digestion/ligation strategy. The complete expression cassette was then assembled via the GreenGate system using standardized modules. The modules employed were as follows:

- **pGGA004 (Module A–B):** 35S promoter
- **pGGB006 (Module B–C):** Signal peptide (or alternatively pGGB003 as a dummy module)
- **pGGC000 (Module C–D):** Gene of interest
- **pGGD-HA or pGGD011 (Module D–E):** Epitope tag (3×HA or mGFP)
- **pGGE001 (Module E–F):** Terminator (rbcS)
- **pGGF011 (Module F–G):** Fluorescent marker (e.g., PM-mCherry)
- **pGGZ003 (Module A–G):** Destination vector

The Golden Gate assembly reaction was set up as described in Table 22.

Table 22. Golden Gate assembly reaction setup (20 µL Total).

Component	**Amount/Volume**	**Remarks/Notes**
Destination vector (pGGZ003)	100 ng	Typically, 0.5–1 µL; adjust per stock concentration
Each insert module (pGGA004, pGGB006, pGGD-HA, pGGE001, pGGF011)	150 ng each	Adjust volume according to concentration
10× T4 Ligase Buffer	2 µL	Provided with the enzyme
BsaI-HF v2 (10 U/µL)	2 µL	High-fidelity restriction enzyme
T4 DNA Ligase (400 U/µL)	1 µL	
Nuclease-free Water	To adjust total volume to 20 µL	Molecular biology–grade water

Table 23. Golden Gate assembly reaction cycling conditions.

Step	Temperature	Time	Purpose
Digestion	37°C	5 min	BsaI restriction digest
Ligation	16°C	10 min	T4 DNA ligase activity
Repeat	-	25–30 cycles	Alternate digestion/ligation
Final digestion	50°C	5 min	Remove incomplete constructs
Inactivation	80°C	10 min	Enzyme inactivation

After completing the thermal cycling, add an additional 0.5 µL of BsaI-HF v2 and incubate the reaction at 37 °C for 30 min, followed by incubation at 65 °C for 20 min. For transformation into *E. coli* DH5α, 10 µL of the reaction mix was used to transform 50 µL of chemically competent *E. coli* cells. Subsequently, 100 µL of the recovered culture was plated on LB agar containing spectinomycin (100 µg/ml; for selection of the pGGZ003 destination vector), while LB plates with ampicillin (100µg/mL) were used for intermediate verification if necessary. The assembled constructs were verified by colony PCR and Sanger sequencing before proceeding to plant experiments.

2.7.2.2. Transformation into *A. tumefaciens* GV3101

The verified expression cassette was introduced into *A. tumefaciens* GV3101 cells via electroporation. As shown in Table 24, briefly, 50 µL aliquots of electrocompetent cells were thawed on ice for 15 min. Plasmid DNA (500 ng to 2 µg, depending on experimental requirements) was gently mixed with the cells. The mixture was transferred to a pre-chilled 1 mm electroporation cuvette and pulsed at 2.5 kV. Immediately after electroporation, 1 mL of chilled LB medium was added, and the cells were transferred to a sterile microfuge tube. The transformed cells were allowed to recover at 28 °C with shaking at 200 rpm for 2 h before plating on LB agar supplemented with rifampicin (50 µg/mL), gentamycin (20 µg/mL), and spectinomycin (100 µg/mL) (see Table 25). Plates were incubated at 28 °C for 2–3 days.

Table 24. Electroporation conditions for Agrobacterium GV3101.

Parameter	Value	Remarks
Cell Volume	50 µL	Electrocompetent GV3101 cells
Plasmid DNA	500 ng–2 µg	Amount adjusted based on needs
Electroporation Voltage	2.5 kV	In a 1 mm gap cuvette
Recovery Medium	1 mL LB	Chilled LB added immediately
Recovery Conditions	28 °C, 200 rpm, 2 h	Post-electroporation shaking
Plate Incubation	28 °C for 2–3 days	

Table 25. LB agar antibiotic conditions for Agrobacterium.

Antibiotic	Final Concentration	Remarks
Rifampicin	50 µg/mL	-
Gentamycin	20 µg/mL	-
Spectinomycin	100 µg/mL	For selection of the expression construct

2.7.2.3. Co-infiltration with pCB301-p19

To improve transient expression by countering post-transcriptional gene silencing, we co-infiltrated two *A. tumefaciens* strains: one carrying our gene-of-interest construct and one carrying the binary vector pCB301-p19, which expresses the P19 silencing suppressor. Each strain was grown independently to the appropriate density, pelleted by centrifugation, and resuspended in infiltration buffer. Immediately before use, the two suspensions were mixed in a 1:1 ratio to create the final infiltration mix. This combined culture was then infiltrated into the abaxial side of *N. benthamiana* leaves using a needle-free syringe, resulting in enhanced transient expression of the transgene.

2.7.2.4. Preparation of Agrobacterium suspension for infiltration

A single colony from each transformation (expression construct and pCB301-p19) was inoculated into 5 mL LB medium with the appropriate antibiotics and grown overnight at 28 °C with shaking (200 rpm). For infiltration, 1–2 mL of each overnight culture (typically OD_{600} ~0.8–1.0) was harvested by centrifugation at 2500×g for 10 min. Pellets were resuspended separately in 1 mL of infiltration buffer (see Table 26), washed once, and then adjusted to an OD_{600} of 0.3–0.6. Equal volumes of the expression construct suspension and the pCB301-p19 suspension were mixed and incubated at room temperature for 2 h with gentle agitation to induce virulence genes.

Table 26. Infiltration buffer composition.

Component	Final Concentration	Preparation/Remarks
MES (pH 5.6)	10 mM	Adjust pH with NaOH
$MgCl_2$	10 mM	-
Acetosyringone	0.1 mM	Add freshly prepared from stock
Nuclease-free Water	–	To adjust final volume

2.7.2.5. Agroinfiltration of *N. benthamiana* leaves

Healthy *N. benthamiana* plants (4–6 weeks old) were used for infiltration. Using a 1 mL needleless syringe, the mixed Agrobacterium suspension (expression construct + pCB301-

p19) was gently applied to the abaxial surface of a fully expanded leaf. The infiltration was performed slowly until the targeted region appeared uniformly water-soaked and darker. The infiltrated areas were marked with a permanent marker. Post-infiltration, plants were returned to a growth chamber maintained at 22–25 °C with a 16-hour light/8-hour dark photoperiod and incubated for 3–5 days to allow transient protein expression.

2.7.2.6. Protein extraction and analysis

At 3–5 days post-infiltration, infiltrated leaf discs (approximately 0.5–1 cm in diameter) were excised from the marked regions. Samples were immediately flash-frozen in liquid nitrogen and stored at –80 °C until processing. For protein extraction, frozen tissue was ground to a fine powder in pre-chilled 1.5 mL tubes using sea sand as an abrasive. Extraction buffer (see Table 27) was added, and the homogenate was incubated on ice for 10 min. The extract was then centrifuged at 14,000 rpm (~16,000×g) for 10 min at 4 °C to remove debris. The clarified supernatant was collected and used for SDS-PAGE and Western blot analysis.

Table 27. Extraction buffer for transiently expressed proteins.

Component	Amount	Final Concentration
KCl	744.5 mg	100 mM
HEPES (pH 7.5)	476.6 mg	20 mM
EDTA	3.72 mg	0.1 mM
DTT	30.86 mg	2 mM
PMSF	17.42 mg	1 mM
Protease Inhibitor Cocktail	10 µL	0.1% (v/v)
Milli-Q Water	To 100 mL	–

*Note: PMSF is typically prepared as a 100 mM stock in isopropanol.

Protein extracts were separated by SDS-PAGE. For additional validation, Western blotting was carried out using specific antibodies (e.g., anti-HA, anti-GFP).

Table 28. Semi-Dry blotting buffer.

Component	Amount
Tris	5.82 g
Glycine	2.93 g
Methanol	200 mL
H_2O	Up to 1 L

Table 29. PBS Solutions.

Reagent	**10× PBS (1 L)**
NaCl	80 g
KCl	2 g
Na_2HPO_4	14.6 g
KH_2PO_4	2 g
Tween-20	-
H_2O	Up to 1 L

2.8. Data processing, statistical analysis, and bioinformatics software

All calculations, statistical analyses, and the creation of diagrams, graphs, and tables were performed using Microsoft Excel 2021 and GraphPad Prism 5. Lesion areas were measured with ImageJ. Image editing was conducted using CorelDRAW X7 and Microsoft PowerPoint 2019. The design and planning of DNA constructs were carried out with SnapGene 3.3.4. In addition, images were designed using BioRender.

3. Results

3.1. Generation and characterization of multi-knockout strains with up to 29x gene deletions of *B. cinerea* using an optimized marker-free CRISPR/Cas9 system

Leisen et al. (2022) investigated the role of multiple gene knockouts in *B. cinerea*, targeting 14 putative virulence factors. The authors employed a marker-free CRISPR/Cas9 approach for successive rounds of deletion, yielding up to 12-gene (Bc12x) mutants. Below is an adapted table from Leisen et al. (2022), summarizing how the gene knockouts were added in sequence.

Table 30. Overview of genes deleted in the 12-gene knockout mutants (Bc12x).

Transf. round	Name	Genotype	Gene(s) targeted for knockout
1	**WT**	WT	*spl1*
2	**spl1**	*spl1*	*nep1, nep2*
3	**3x**	*spl1 nep1 nep2*	*xyn11A, ieb1*
4	**4x**	*spl1 nep1 nep2 xyn11A*	*hip1, xyg1*
5	**6x**	*spl1 nep1 nep2 xyn11A hip1 xyg1*	*plp1, ieb1*
6	**8x**	*spl1 nep1 nep2 xyn11A hip1 xyg1 plp1 ieb1*	*xyll, gs1*
7a	**10x**	*spl1 nep1 nep2 xyn11A hip1 xyg1 plp1 ieb1 xyll gs1*	*pg1, pg2*
7b		*spl1 nep1 nep2 xyn11A hip1 xyg1 plp1 ieb1 xyll gs1*	*bot2, boa6*
8a	**11x**	*spl1 nep1 nep2 xyn11A hip1 xyg1 plp1 ieb1 xyll gs1 pg1*	*pg1*
8b	**12xpg**	*spl1 nep1 nep2 xyn11A hip1 xyg1 plp1 ieb1 xyll gs1 pg1 pg2*	*pg1, pg2*
8c	**12xbb**	*spl1 nep1 nep2 xyn11A hip1 xyg1 plp1 ieb1 xyll gs1 bot2 boa6*	*bot2, boa6*

According to Leisen et al. (2022), infection tests with the mutants demonstrated a progressive reduction in virulence as the number of mutated genes increased, along with varied impacts of the knockouts on different host plants. Two particularly important gene sets in this knockout series were (i) the polygalacturonases *pg1* and *pg2*, and (ii) the toxin biosynthesis genes *bot2* and *boa6*. The *pg1* and *pg2* genes encode major endopolygalacturonases responsible for pectin degradation in plant cell walls. Single knockouts of *pg1* or *pg2* conferred moderate or host-dependent reductions in virulence, suggesting partial functional overlap (ten Have et al., 1998; Kars et al., 2005). Double knockout *pg1 pg2* mutants exhibit substantially diminished lesion development across various plant hosts, demonstrating a synergistic role in pathogenicity (Leisen et al., 2022). When these two deletions are stacked with ten additional PG knockouts (the Bc12xpg mutant), virulence is further reduced on

bean, tomato, and apple, yet significant residual pathogenicity remains, indicating that multiple effectors besides PGs are involved (Leisen et al., 2022). The *bot2* and *boa6* genes encode key enzymes in biosynthesis of botrydial (a sesquiterpenoid) and botcinins (polyketides), respectively. Single knockouts of either gene typically show no obvious virulence defects (Dalmais et al., 2012). In contrast, the double knockout *bot2 boa6* causes a pronounced reduction in pathogenicity, underscoring the importance of these toxins (Dalmais et al., 2012; Leisen et al., 2022). Further deletion of ten additional genes in the Bc12xbb mutant leads to markedly impaired lesion expansion and diminished secretome-mediated phytotoxicity (Leisen et al., 2022). These findings indicate that although most known phytotoxic compounds were lost, the in planta secretomes of the multiple mutants still exhibited considerable phytotoxic activity. This suggests that additional, yet unidentified, CDIPs contribute to necrosis and virulence (Leisen et al., 2022).

Experimental constraints prevented the simultaneous elimination of *pg1*, *pg2*, *bot2*, and *boa6* in a single strain in the study by Leisen et al. (2022). In our extended study, we built on the Bc12xbb background and subsequently deleted *pg1* and *pg2*, along with 15 additional genes related to cell-death induction. This expansion yielded a 29-gene knockout mutant (Bc29x) the most comprehensive genetic disruption of any fungal virulence-associated factors to date.

In the following sections, we provide a detailed description of the additional genes deleted beyond those in Bc12xbb and their impact on *B. cinerea* pathogenicity.

3.2. Iterative marker-free CRISPR/Cas9 transformations from Bc12xbb to Bc29x mutants

Starting with the Bc12xbb strain, we utilized a marker-free CRISPR/Cas9 system, applying one or two guide RNA (gRNA) pairs to achieve successive deletions of further genes (Leisen et al., 2020). Each round was designed to target one or two additional genes, with sequencing and PCR screening confirming the successful knockout of the respective loci. By the completion of the final transformation round, we obtained the Bc29x mutant, which incorporated a total of 29 deletions. In Figure 5, an overview is provided of the two phytotoxic metabolites and all 27 CDIPs targeted in the 29-gene knockout strain (Bc29x) developed in Leisen et al. (2022) and this PhD thesis. The selected genes span multiple functional categories, including phytotoxic metabolites, cell wall-degrading enzymes, necrosis-inducing proteins, plant cell death–inducing enzymes, and plant cell death–

inducing proteins, all of which collectively drive host tissue colonization and disease progression. In certain genes, such as PGs (D'Ovidio et.,2004) and Nep1-like proteins (Schouten et al., 2008; Lenarčič et al., 2017), the phytotoxic mechanism is well characterized. However, for many other CDIPs, the precise phytotoxic activity remains incompletely understood, despite accumulating evidence that they can induce plant cell death.

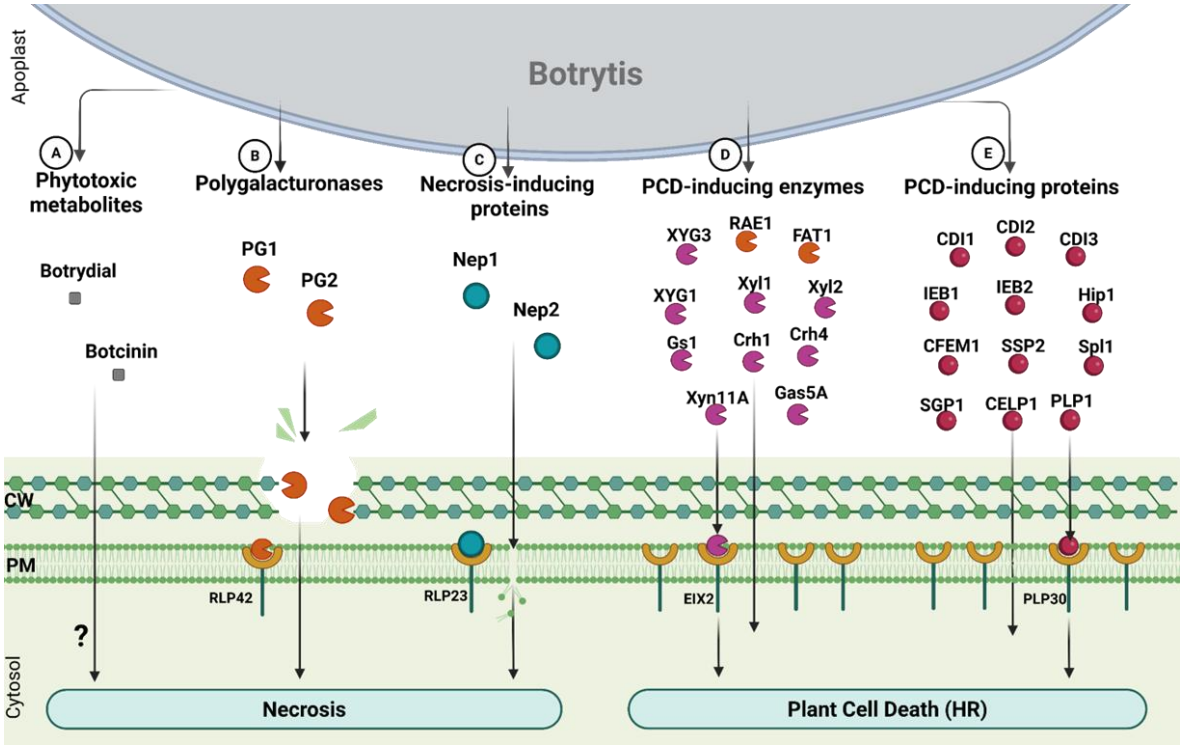

Figure 5. Schematic representation of the Bc29x multi-gene knockout strategy targeting *B. cinerea* phytotoxic metabolites and cell death–inducing proteins. This figure illustrates the targeted 27 proteins and two phytotoxins, highlighting five categories of CDIPs in *B. cinerea*. PAMP receptors in the plant plasma membrane known to interact with Nep1/Nep2 (Albert et al., 2015), Xyn11A (Alvarez et al., 2024), Plp1 (Zhang et al., 2013) and PGs (Zhang et al., 2021), and the assumed mechanism of host killing are indicated.

3.3. Knockout order and functional characterization of deleted cell-death-inducing proteins in *B. cinerea*

The search for new cell-death-inducing proteins (CDIPs) in *B. cinerea* (as depicted in the figure) was guided by recent publications on *B. cinerea* or closely related fungi such as *S. sclerotiorum*. Whenever published CDIPs had close homologs in *B. cinerea* and were found to be significantly expressed during plant infection either at the RNA level or detected in secretomes from infected tomato leaves those genes were prioritized for deletion.

Table 31 provides an overview of 27 *B. cinerea* CDIPs and two phytotoxic metabolites targeted for knockout in the Bc29x strain. These entries highlight a broad arsenal of secreted

proteins spanning necrosis-inducing proteins (NEPs), cell wall–modifying enzymes, and other toxic effectors underscoring their roles in pathogenicity as well as the diverse experimental approaches used to characterize them. The table also reveals gaps in our understanding (e.g., untested plant receptor interactions or unclear knockout phenotypes), suggesting areas that warrant further investigation.

Table 31. Knockout order and functional characterization of deleted virulence-associated proteins and phytotoxic metabolites in *B. cinerea* (Bc29x): proposed phytotoxic activities, expression profiles, secretome involvement, plant receptor interactions, and knockout phenotypes. Bot2 and Boa6 are key enzymes for biosynthesis of botrydial and botcinic acid, respectively.

KO order	Protein	In planta expression	Present in secretome	Protein expression system	Plant coreceptor involvement		KO phenotype	References
					BAK1	SOBIR1		
1	**Spl1 ceratoplatanin**	+++	Yes	Pichia	Predicted	No	Yes	Frias et al., 2011, 2014
2	**Nep1 necrosis-inducing protein**	+/+++	Yes, at 26 h secretome	Pichia	BAK1 in *A. thaliana*	SOBIR in *A. thaliana*	No	Albert et al., 2015; Fradin et al., 2011; Cuesta-Arenas et al., 2010; Schouten et al., 2007; Pirc et al., 2022
3	**Nep2 necrosis-inducing protein**	++	Yes	Pichia	BAK1 in *A. thaliana*	SOBIR in *A. thaliana*	No	Albert et al., 2015; Fradin et al., 2011; Cuesta-Arenas et al., 2010
4	**XYN11A ß-1,4 xylanase**	++/+++	Yes	Pichia	BAK1 (with EIX1 only) in *S. lycopersicum*	?	Yes	Ron and Avni, 2004; Frías et al., 2016; Brito et al., 2006; Alvarez et al., 2024
5	**Hip1**	+++	Yes	*E. coli* & *N. benthamiana*	Unknown	Unknown	No	Jeblick et al., 2023
6	**XYG1 xyloglucanase**	++	Yes	*E. coli*	BAK1 in *N. benthamiana*	SOBIR in *N. benthamiana*	No	Zhu et al., 2017
7	**PLP1**	+	No		BAK1 in *A. thaliana*	SOBIR in *A. thaliana*	No	Zhang et al., 2013; Nie et al., 2021
8	**IEB1**	+++	Yes	Pichia	No	Not Tested	No	Frias et al., 2016
9	**Xyl1 xylanase 1**	+	No	Pichia	BAK1 in *N. benthamiana*	SOBIR in *N. benthamiana*	yes	Yang et al., 2018a
10	**GS1 glucan 1,4 α-glucosidase**	++	Yes		Not Tested	Not Tested	Not Tested	Zhang et al., 2015; Yang et al., 2018b
11	**Bot2 (Botrydial)**	++	-	-	-	-	Yes (double KO)	Van Kan et al., 2017; Dalmais et al., 2012; Vignatti et al., 2020; Pinedo et al., 2008
12	**Boa6 (Botcinic acid)**	++	-	-	-	-	Yes (double KO)	Van Kan et al., 2017; Dalmais et al., 2012; Vignatti et al., 2020; Pinedo et al., 2008
13	**PG1 polygalacturonase 1**	+++	Yes	Pichia (poor)	No	Predicted	Yes	ten Have et al., 1998; Kars et al., 2005; Zhang et al., 2014
14	**Crh1 transglycosidase**	++	Yes	*N. benthamiana*	Not Tested	Not Tested	No	Bi et al., 2021
15	**CDI1**	+++	No	*N. benthamiana*	Predicted in Sclerotinia	Predicted in Sclerotinia	No	Franco-Orozco et al., 2017; Zhu et al., 2023
16	**CFEM1**	+++	Yes	*N. benthamiana*	Not Tested	Not Tested	Yes	Zhu et al., 2017

17	**PG2 polygalacturonase 2**	+++	Yes	Pichia	No	Predicted	Yes	ten Have et al., 1998; Kars et al., 2005; Zhang et al., 2014
18	**SSP2**	++	No	*N. benthamiana*	No	No	No	Denton-Giles et al., 2020; Zhu et al.,2022
19	**CDI2**	+++	Yes	*E. coli* & *N. benthamiana*	Predicted in Sclerotinia	Predicted in Sclerotinia	N.t.	Seifbarghi et al., 2020
20	**SGP1**	+++	No	*N. benthamiana*	Predicted	Not Tested	N.t.(?)	Song et al.,2021
21	**Crh4 transglycosidase**	+	Yes	*N. benthamiana*	Not Tested	Not Tested	Yes	Liang et al., 2024
22	**XYG3 xyloglucanase**	++	Yes	*E. coli* (PET28) & (pCold–TF) & *N. benthamiana*	Not Tested	Not Tested	Not Tested	Own data
23	**GAS5A ß-1,3 glucanosyltransferase**	+++	Yes	*N. benthamiana*	Not Tested	Not Tested	Not Tested	T. Müller and D. Scheuring, unpublished
24	**CDI3**	+	No	*N. benthamiana*	Not Tested	Not Tested	Not Tested	Seifbarghi et al., 2020
25	**RAE1 rhamnogalacturonan acetyltransferase**	++	Yes	*E. coli* (pCold–TF)	Not Tested	Not Tested	No	Zhang et al., 2024
26	**FAT1 fatty acyltransferase**	++	Yes	*E. coli* (pCold–TF)	Not Tested	Not Tested	No	Zhang et al., 2024
27	**Xyl2 Xylanase**	+	Yes	*E. coli* & *N. benthamiana*	Not Tested	Not Tested	Yes in *S. sclerotiorum*	Wang et al., 2024
28	**IEB2**	+++	Yes	*E. coli* (pCold–TF) & *N. benthamiana*	Not Tested	Not Tested	Not Tested	Own data
29	**CELP1**	++	Yes, at 26 h	*N. benthamiana*	Not Tested	Not Tested	Yes	Sharon et al. (2024)

In planta expression data are based on RNA sequencing (RPKM values) from infected tomato leaves (24–48 hpi), classified as +++ (RPKM >1000), ++ (100–1000), and + (<100). RNA sequencing data were provided by Jan van Kan (University of Wageningen).

3.4. Beyond Bc12xbb: evaluating Bc13x to Bc29x deletions and their impact on *B. cinerea* pathogenicity

Recipient: Bc12xbb

Knocked-out gene: *pg1*, resulting in Bc13x mutant

Bcpg1 encodes a highly expressed endopolygalacturonase, PG1. Knockout mutants were found to be reduced in virulence (ten Have et al., 1998). The phytotoxic activity of PG1, as well as PG2 (see below), was found to be dependent on its cell wall degrading activity (Kars et al., 2005). Moreover, fragments of *B. cinerea* endopolygalacturonases, including PG1,

when expressed in *Pichia pastoris*, have been shown to be recognized by the *Arabidopsis* receptor RBP1, triggering necrosis (Zhang et al., 2014). Polygalacturonases also display high genetic variability across *B. cinerea* isolates (Rowe et al., 2007), suggesting a co-evolutionary dynamics.

Preliminary in vitro and on planta phenotype of 13x mutant: Compared to BcWT and the Bc12xbb mutant, the 13x mutant showed no changes in its in vitro growth and differentiation behavior. Compared to the Bc12xbb mutant, the Bc13x mutant showed no significantly reduced infection on different host tissues.

Recipient: Bc13x

Knocked-out gene: *Crh1* and *CDI1*, resulting in Bc15x mutant

BcCrh1 is a transglycosylase involved in cell wall remodeling that also functions as a cytoplasmic effector. It accumulates in infection cushions and triggers hypersensitive-like responses in host tissue. The protein's phytotoxicity was characterized using Agrobacterium-mediated transient expression in *N. benthamiana* leaves, which allowed for detailed analysis of its effector activity and subcellular localization. Moreover, its necrosis-inducing capacity persists when the enzyme is rendered inactive, and Arabidopsis lines expressing BcCrh1 exhibit reduced susceptibility to *B. cinerea* (Bi et al., 2023).

BcCDI1, a secreted necrosis-inducing protein homologous to CDI1 and highly conserved among Ascomycete fungi, activates PTI and elicits reactive oxygen species (ROS) bursts in host plants. Transient expression of BcCDI1 in *N. benthamiana* leaves rapidly induces cell death, confirming its role as a novel PAMP that triggers innate immune responses (Franco-Orozco et al., 2017; Zhu, 2023).

Preliminary in vitro and on planta phenotype of Bc15x mutant (compared to 13x): Compared to BcWT and the Bc13x mutant, the Bc15x mutant showed no changes in its in vitro growth and differentiation behavior. Although Crh1 homologs in other fungi (e.g., *Candida albicans* and *Saccharomyces cerevisiae*) are crucial for cell wall assembly (Fang et al., 2019), our data indicate that Crh1 deletion in *B. cinerea* has no significant impact on colony radius, sclerotia & infection cushions formation or conidiation capacity. Compared to the Bc13x mutant, the Bc15x mutant showed no significantly reduced infection on different host tissues.

Recipient: Bc15x

Knocked-out gene: *CFEM1*, resulting in Bc16x mutant

CFEM proteins are recognized virulence factors in diverse fungi, mediating host–pathogen interactions, fungal adhesion, and stress tolerance. In *B. cinerea*, BcCFEM1 is a CFEM domain-containing protein with a predicted GPI-anchored site. Its expression is significantly induced during the early stages of infection on bean leaves, and transient expression in *N. benthamiana* triggers chlorosis suggesting that BcCFEM1 functions as an elicitor that weakens host defences and facilitates nutrient reallocation. Deletion of BcCFEM1 was reported to result in reduced virulence, impaired conidial production, and heightened sensitivity to osmotic and cell wall stress (Zhu et al., 2017).

Preliminary in vitro and on planta phenotype of Bc16x mutant (compared to Bc15x): Compared to BcWT and the Bc15x mutant, the Bc16x mutant showed no changes in its in vitro growth and differentiation behavior. Compared to the Bc15x mutant, the Bc16x mutant showed no significantly reduced infection on different host tissues.

Recipient: Bc16x

Knocked-out gene: *pg2* and *SSP2*, resulting in Bc18x mutant

PG2 has been already described above. Ssp2 is a small secreted protein, consisting of only 70 amino acids after removal of its signal peptide. It was first described by Denton-Giles et al. (2020) in three Sclerotiniaceae species including *B. cinerea*, and it was shown to induce necrotic lesions when injected into *Camellia* flower petals. Later, Zhu et al. (2022) and Newman et al. (2023) confirmed that *B. cinerea* and *S. sclerotiorum* SSP2 homologs, respectively, similarly induced necrosis when transiently expressed in *N. benthamiana* leaves.

Preliminary in vitro and on planta phenotype of Bc18x mutant (compared to Bc16x): Compared to BcWT and the Bc16x mutant, the Bc18x mutant showed no changes in its in vitro growth and differentiation behavior.

Compared to the Bc16x mutant, the Bc18x mutant showed significantly reduced infection on different host tissues. In addition to the Bc18x mutant, a single-deletion strain (Bc17x: Δpg2) was constructed for comparative purposes. Notably, when comparing the (Bc18x: Δpg2–ΔSSP2) mutant to the (Bc17x: Δpg2) strain, no further attenuation in infection was observed, suggesting that the additional deletion of *ssp2* does not confer extra reduction in virulence, consistent with normal infection behaviour observed for a *B. cinerea ssp2* mutant

(Zhu et al., 2022). These results imply that PG2 exerts a dominant effect on disease progression, whereas SSP2 plays no significant role.

Recipient: Bc18x

Knocked-out gene: *CDI2*, resulting in Bc19x mutant

BcCDI2 shares a high degree of sequence identity with its homolog SsNE1 in *S. sclerotiorum* (Seifbarghi et al., 2020). Transient expression assays in *N. benthamiana* demonstrated that this newly characterized group of *S. sclerotiorum* necrosis-inducing effectors, namely SsNE1, SsNE2, SsNE3, SsNE4, and SsNE5 requires co-receptors BAK1 and SOBIR1 to trigger robust cell-death symptoms.

Preliminary in vitro and on planta phenotype of Bc19x mutant (compared to Bc18x): Compared to BcWT and the Bc18x mutant, the Bc19x mutant showed no changes in its in vitro growth and differentiation behavior. Compared to the Bc18x mutant, the Bc19x mutant showed no significantly reduced infection on different host tissues.

Recipient: Bc19x

Knocked-out gene: SGP1, resulting in Bc20x mutant

BcSGP1 is a homolog of SGP1, a serine/threonine-rich, glycosylphosphatidylinositol (GPI)-anchored protein identified in *Ustilaginoidea virens*, the rice false smut pathogen (Song et al. 2021). This protein is widely conserved among fungi and functions as a thermostable, proteinaceous elicitor that activates BAK1-dependent defence responses in *N. benthamiana*. Notably, plants specifically recognize a 22 amino acid epitope located at the N terminus of SGP1, termed SNP22, which is sufficient to trigger cell death along with other immune responses (Song et al., 2021).

Preliminary in vitro and on planta phenotype of Bc20x mutant (compared to Bc19x): Compared to BcWT and the Bc19x mutant, the Bc20x mutant showed no changes in its in vitro growth and differentiation behavior. Compared to the Bc19x mutant, the Bc20x mutant showed no significantly reduced infection on different host tissues.

Recipient: Bc20x

Knocked-out gene: Crh4, resulting in Bc21x mutant

BcCrh4 is a homologue of BcCrh1 and also encodes a glycosyl hydrolase family 16 transglycosylase. During plant infection, BcCrh4 is accumulating first in infection cushions and then delivered to the apoplast. Its CDIP activity was detected by transient expression in

N. benthamiana and was found to be independent of its transglycosylase enzymatic function, as mutations that abolish the catalytic activity do not affect its ability to induce cell death (Liang et al., 2024). Furthermore, Liang et al. (2024) demonstrated that deletion of the BcCrh4 gene results in reduced vegetative growth, impaired infection cushion formation, and diminished virulence.

Preliminary in vitro and on planta phenotype of Bc21x mutant (compared to Bc20x): Compared to BcWT and the Bc20x mutant, the Bc21x mutant showed a moderate reduction in colony expansion and conidiation, a finding corroborated by Liang et al. (2024). Compared to the Bc20x mutant, the Bc21x mutant showed minor, statistically non-significant reductions in lesion size for the Bc21x: ΔCrh4 strain relative to Bc20x on different host tissues.

Recipient: Bc21x

Knocked-out gene: XYG3, resulting in Bc22x mutant

We found that XYG3 shares 53% sequence identity with the GH12 xyloglucanase BcXYG1, a well-characterized necrosis-inducing apoplastic protein from *B. cinerea* that elicits cell death via the SOBIR1/BAK1 pathway (Zhu et al., 2017). Using transient expression in *N. benthamiana*, the authors demonstrated that BcXYG1 is capable of triggering strong necrosis and activating plant immune responses in dicot hosts. In our study, XYG3 exhibited high in planta expression (see Table 31) and was detected in the pathogen's secretome. Further characterization of XYG3 is provided in chapter 4.

Preliminary in vitro and on planta phenotype of Bc22x mutant (compared to Bc21x): Compared to BcWT and the Bc21x mutant, the Bc22x mutant showed no changes in its in vitro growth and differentiation behavior. Compared to the Bc21x mutant, the Bc22x mutant showed no significantly reduced infection on different host tissues.

Recipient: Bc22x

Knocked-out gene: GAS5A, resulting in Bc23x mutant

GAS5A was recently identified in our group as a phytotoxic protein (T. Müller, unpublished data). It encodes a predicted β-1,3-glucanosyltransferase that is implicated in fungal cell wall remodeling. GAS5A might function similarly to other cell wall-associated enzymes in *B.*

cinerea such as BcCrh1 (Bi et al., 2021) and BcCrh4 (Liang et al., 2024), which are transglycosylases that cross-link chitin and glucan.

Preliminary in vitro and on planta phenotype of Bc23x mutant (compared to Bc22x): Compared to BcWT and the Bc22x mutant, the Bc23x mutant showed no significant changes in its in vitro growth and differentiation behavior.

Compared to the Bc22x mutant, the Bc23x mutant showed no significantly reduced infection on different host tissues.

Recipient: Bc23x

Knocked-out gene: CDI3, resulting in Bc24x mutant

CDI3 in *B. cinerea* is a homolog of the *S. sclerotiorum* effector SsNE3. As previously noted in the context of Bc19x: CDI2, Seifbarghi et al. (2020) demonstrated that SsNE2 and SsNE3 rely on the co-receptors BAK1 and SOBIR1 to induce full necrosis.

Preliminary in vitro and on planta phenotype of Bc24x mutant (compared to Bc23x): Compared to BcWT and the Bc23x mutant, the Bc24x mutant showed no significant changes in its in vitro growth and differentiation behavior. Compared to the Bc23x mutant, the Bc24x mutant showed no significantly reduced infection on different host tissues.

Recipient: Bc24x

Knocked-out gene: RAE1–FAT1, resulting in Bc26x mutant

RAE1 and FAT1 are two SGNH family CDIPs identified in *B. cinerea* that have been characterized together by Zhang et al. (2024). Using an optimized prokaryotic expression system based on the pCold-TF vector, the authors achieved robust expression of these proteins in soluble form in *E. coli*, enabling a detailed investigation of their necrosis-inducing functions. Their activity depends on conserved residues critical for enzymatic function, as site-directed mutagenesis of these residues abolished their ability to trigger cell death. Intriguingly, when transiently expressed in plants, RAE1 and FAT1 enhanced resistance to *B. cinerea* without causing overt necrosis (Zhang et al., 2024).

Preliminary in vitro and on planta phenotype of Bc26x mutant (compared to Bc24x): Compared to BcWT and the Bc24x mutant, the Bc26x mutant showed no significant changes in its in vitro growth and differentiation behavior. Compared to the Bc24x mutant, the Bc26x mutant showed no significantly reduced infection on different host tissues.

Recipient: Bc26x

Knocked-out gene: Xyl2, resulting in Bc27x mutant

Xyl2, identified as SsXyl2 in *S. sclerotiorum*, encodes a GH11 xylanase (Wang et al., 2024). Secreted during the late infection phase, SsXyl2 triggers hypersensitive-like cell death in the plant apoplast, a response confirmed through both transient expression in *N. benthamiana* and application of purified protein. SsXyl2 was shown to interact with NbHIR2 at the plasma membrane. SsXyl2 deletion mutants show reduced virulence, and complementation with a catalytically inactive variant restores pathogenicity, indicating that its virulence function relies on inducing host cell death rather than enzymatic activity (Wang et al., 2024).

Preliminary in vitro and on planta phenotype of Bc27x mutant (compared to Bc26x): Compared to BcWT and the Bc26x mutant, the Bc27x mutant showed no significant changes in its in vitro growth and differentiation behavior. Compared to the Bc26x mutant, the Bc27x mutant showed no significantly reduced infection on different host tissues.

Recipient: Bc27x

Knocked-out gene: IEB2 and CELP1, resulting in Bc29x mutant

IEB2 was identified by us as a novel CDIP based on its sequence homology to the previously characterized IEB1 effector, known for its phytotoxic activity and its interaction with the apoplastic pathogenesis-related protein 5 (PR5) (Frías et al., 2016; González et al., 2017). The characterization of IEB2 is described below (see 3.12.1)

BcCELP1 is an early, infection-specific effector secreted by *B. cinerea* that was shown to be required for full virulence. Sharon et al.,2024 employed agroinfiltration to demonstrate the phytotoxicity of BcCELP1and its role in facilitating colonization. The study revealed that BcCELP1 interacts with the host scaffold protein NbRACK1, which strengthens the association between NbRACK1 and the NADPH oxidase NbRBOHB. This enhanced interaction leads to an overproduction of reactive oxygen species (ROS), triggering localized cell death and forming necrotic foci that favor fungal invasion (Sharon et al., 2024).

Preliminary in vitro and on planta phenotype of Bc29x mutant (compared to Bc27x): Compared to BcWT and the Bc27x mutant, the Bc29x mutant exhibited significant differences in in vitro growth and spore production. Interestingly, while Sharon et al. (2024) reported a complete loss of sclerotia following CELP1 disruption, we still observed sclerotia formation in the Bc29x mutant. Moreover, in our *B. cinerea* background, sclerotia numbers were slightly elevated, though the increase was not statistically significant. Compared to the

Bc27x mutant, the Bc29x mutant showed slightly but not significantly reduced infection on different host tissues.

3.5. PCR and sequencing validation of targeted gene deletions in mutants

To verify the successful knockout of specific genomic loci in mutants, we employed a two-step validation strategy comprising PCR-based screening followed by sequencing. Here, the *cdi3* gene deleted in the Bc24x mutant was used as an example to illustrate the detection workflow.

Two distinct primer sets were designed for PCR analysis (Figure 6). First, outer primers flanking the region targeted for deletion yielded a shorter amplicon in the Bc24x mutant compared to the wild type, indicating a successful deletion event. Second, inner primers, which amplify a sequence fully contained within the deleted region, produced no detectable product in the Bc24x mutant, confirming the complete absence of the target sequence and supporting homokaryosis. A schematic overview of the primer design and the expected PCR products is presented in Figure 6, demonstrating how the two primer sets were positioned relative to the deletion site. Sanger sequencing of the resulting amplicons further validated the precise size and location of each deletion. These combined findings confirm the efficiency and specificity of the CRISPR/Cas9-mediated gene knockout strategy, as exemplified by the successful deletion of the *cdi3* locus in the Bc24x mutant. Primer sequences used in this study are listed in Table 12.

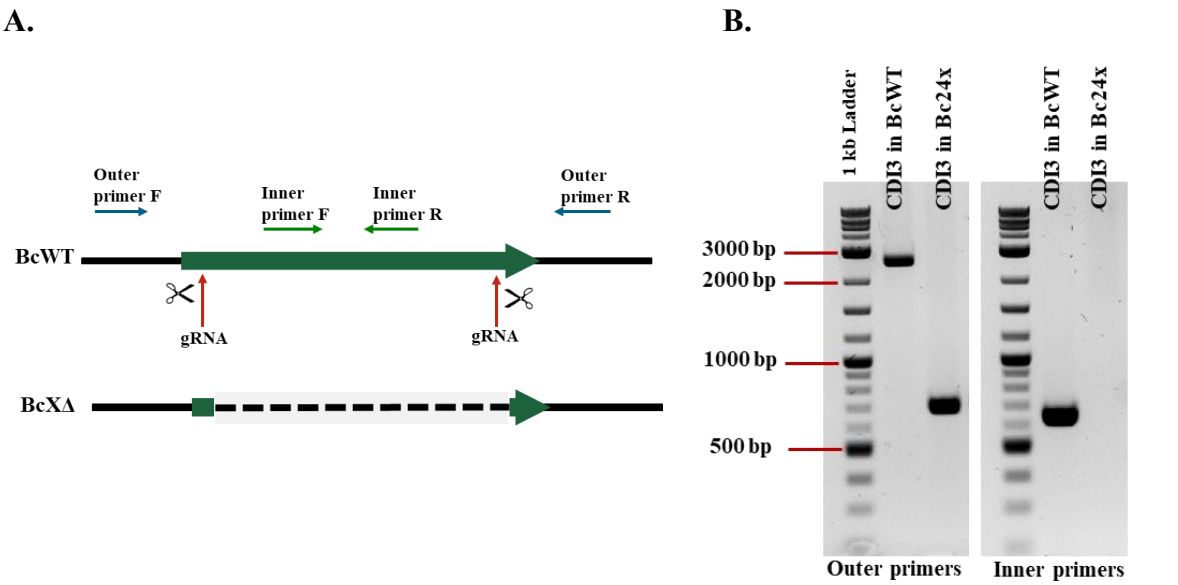

Figure 6. A: Schematic diagram illustrating the PCR-based confirmation of new deletion mutants, showing the outer (blue arrows) and inner (green arrows) primers relative to the targeted deletion site

(red arrows). **B**: Representative PCR products showing a reduced amplicon size when using outer primers (indicating successful deletion) and the absence of product when using inner primers (confirming homokaryosis). Validation of the exact size and location of the deletions was performed by sequencing (Table S1).

3.6. Genome sequencing reveals minimal off-target mutations in multi-knockout mutants

A previous study by Leisen et al. (2022) demonstrated that CRISPR/Cas9 ribonucleoprotein (RNP)-mediated genome editing in *B. cinerea* results in a remarkably low number of off-target mutations. To evaluate the extent of mutations introduced during the serial mutagenesis procedure in this study, whole-genome sequencing (via the Illumina platform) was performed on *B. cinerea* WT, the Bc18x mutant, and the Bc23x mutant (Figure 7).

All targeted gene deletions were successfully confirmed (Figure 7) except for BcSSP2**,** where a genomic rearrangement occurred instead of a clean deletion. To determine whether BcSSP2 was effectively disrupted, qRT-PCR analysis was conducted with the Bc22x mutant, revealing a loss of expression of *Bcssp2* transcript levels (Figure S1). In addition, proteomic analysis of the Bc22x secretome showed the absence of BcSSP2, strongly suggesting that *Bcssp2* was functionally inactivated (data not shown).

Consistent with the earlier findings, only a small number of off-target mutations were detected in the Bc18x and Bc23x mutants. Among these, two were classified as high impact:

1. Mutation in Bcin05g07980 (Chromosome 5:2807467-2808155): This gene encodes a putative α-1,6-mannosyltransferase (404 amino acids, non-secreted, not detected in the secretome). A nonsense mutation (TCA → TGA at codon 205) introduces a premature stop codon. However, functional comparison with its homolog Neurospora crassa OCH-1 suggests a limited impact on fungal growth, as OCH-1 mutants primarily exhibit a tight colony phenotype due to defective galactomannan synthesis (Maddi et al., 2010).
2. Mutation in Bcin12g06810 (Chromosome 12:2345441-2347039): This gene encodes a hypothetical protein (532 amino acids, non-secreted, not detected in the secretome). A point mutation (G → A at position 12:2346277) results in a premature stop codon. The biological significance of this mutation remains to be elucidated.

Table 32. Off-target mutations close to or within genes of BcWT, and Bc18x and Bc23x mutants.

Gene	Position	Ref	Alt	Location	Aa change	Impact	WT		18x		23x	
							Alt	Ref	Alt	Ref	Alt	Ref
Bcin01g04950	1:1785863	TA	T	3' UTR	no	no	1	47	41	1	47	1
Bcin05g01600	5:609368	G	A	upstream	no	no	0	3	73	0	71	0
Bcin05g07980	5:2807824	C	G	exon	S205stop	?	0	3	69	0	62	0
Bcin08g00960	8:392716	G	A	5' UTR	no	no	0	3	53	0	53	0
Bcin09g03260	9:1162811	G	A	5' UTR	no	no	0	5	44	0	75	0
Bcin12g06810	12:2346277	G	A	exon	Q255stop	?	0	4	71	0	61	0

Several additional mutations with predicted low impact or low probability were also identified and are currently under investigation.

These results reinforce the precision and reliability of the optimized marker-free CRISPR/Cas9 system for multi-gene knockouts in *B. cinerea*, with minimal off-target effects.

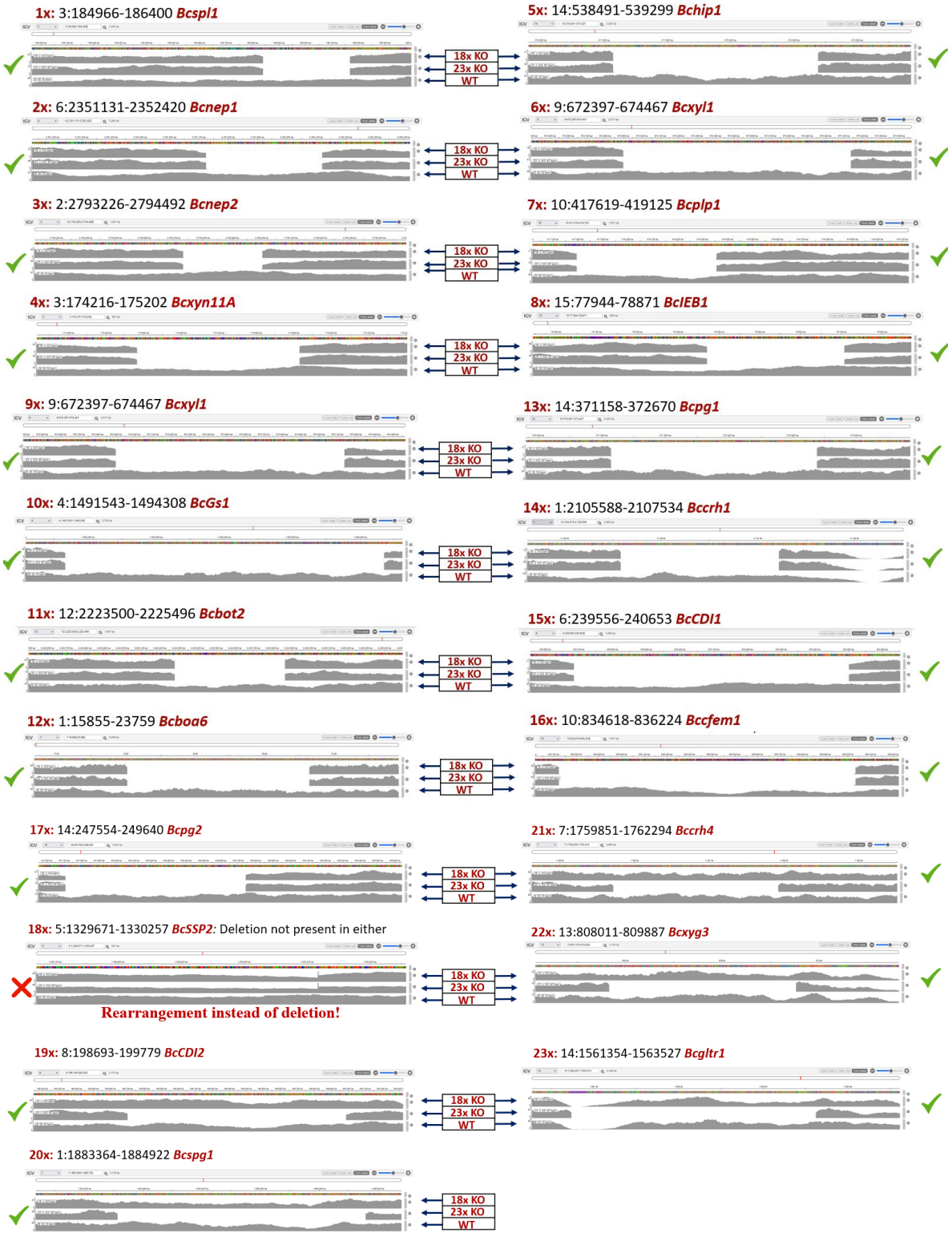

Figure 7. Overview of deletions in multi-gene knockouts confirmed by genome sequencing. Genomic coverage plots for each of the 23 target loci in the *B. cinerea* WT, Bc18x, and Bc23x strains (visualized in IGV). A green check mark indicates confirmed successful deletion, whereas the red "X" highlights the genomic rearrangement at BcSSP2. Horizontal coverage tracks for each strain are shown (BcWT at the bottom, Bc18x knockout in the middle, Bc23x knockout at the top). Despite the rearrangement at BcSSP2, transcript and proteome data (Supplementary Information Figure S1) confirm functional inactivation of this gene.

3.7. Phenotypic characterization of multi-gene knockout mutants in *B. cinerea*

3.7.1. In vitro phenotypic analysis: growth, conidiation, sclerotia formation, and infection cushion formation

Impact of gene deletions on radial growth and conidiation in *B. cinerea*

To investigate how cumulative gene deletions affect fungal development, we assessed radial growth and conidiation in wild-type *B. cinerea* and various mutant strains. Radial mycelial growth was measured on ME agar plates after five days, and conidiation was evaluated after ten days of continuous exposure to light (Figure 8. A-B). Mutants with up to 20 gene deletions showed radial growth and conidiation rates similar to the BcWT, suggesting that *B. cinerea* can compensate for the loss of multiple virulence-related genes without significantly affecting its growth or sporulation abilities. However, the Bc21x mutant exhibited a modest yet significant decrease in both radial growth and conidiation compared to the Bc20x mutant. More pronounced reductions were noted in the Bc28x-CELP1 and Bc29x strains. Specifically, the Bc29x mutant retained about 80% of the BcWT's radial growth capacity. Similarly, conidiation began to notably decrease after 21 gene deletions, with the Bc29x mutant displaying around 65% of BcWT conidiation levels, corresponding to approximately 85% of Bc21x levels ($p < 0.05$). In other words, mutants lacking the BcCrh4 gene (transition from Bc20x to Bc21x) and CELP1 gene (transition from Bc27x to Bc28x-CELP1) demonstrated significant reductions in conidiation. These results are consistent with previous findings by Sharon et al. (2024) and Liang et al. (2024), which identified the involvement of BcCrh4 and BcCELP1 in the developmental processes of *B. cinerea*.

Impact of gene deletions on sclerotia and infection cushion formation in *B. cinerea*

To investigate the effects of cumulative gene deletions on key developmental processes in *B. cinerea*, we examined both sclerotia and infection cushion formation.

Sclerotia formation: After 14 days of incubation in the dark (Figure 8. C), sclerotia production was assessed across the deletion panel. Overall, sclerotia numbers remained statistically similar, indicating that the genetic disruptions did not significantly affect this developmental process. While a few strains with more than 21 deletions showed a modest increase in sclerotia formation, these changes were not statistically significant. In contrast to Sharon et al. (2024), who reported a complete loss of sclerotia following CELP1 disruption, our results confirmed the presence of sclerotia in both the Bc28x-CELP1 and Bc29x strains.

Infection cushion formation: Infection cushion formation was evaluated after 48 h on glass slides (Figure 8. D). The wild-type strain developed large aggregates of appressoria-like structures known as infection cushions within two days on glass surfaces. These structures represent an alternative infection strategy that complements the formation of simple appressoria. Interestingly, our findings differ from those of Sharon et al. (2024), who implicated BcCrh4 in a role encompassing both growth and infection cushion formation. In our study, the deletion of the targeted gene sets did not prevent normal differentiation of infection cushions.

A

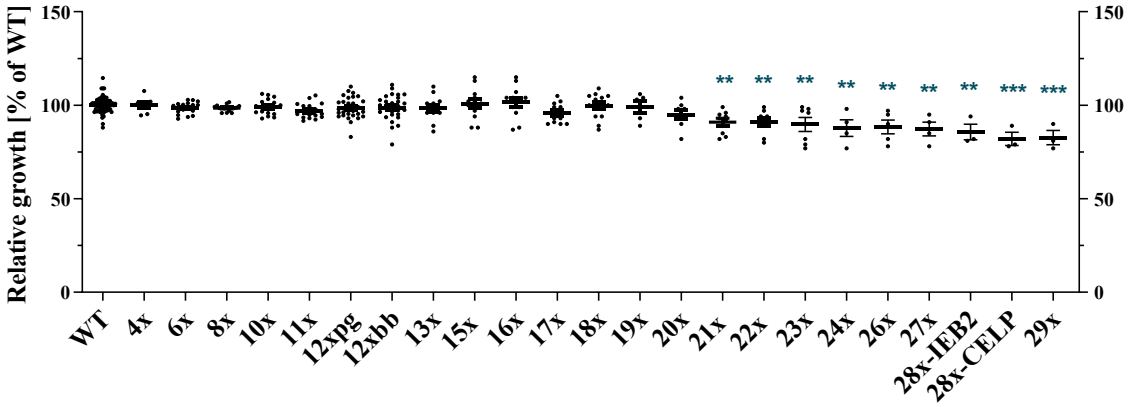

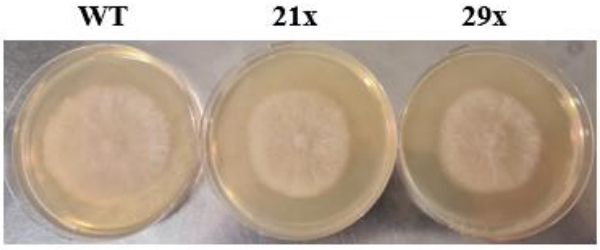

B

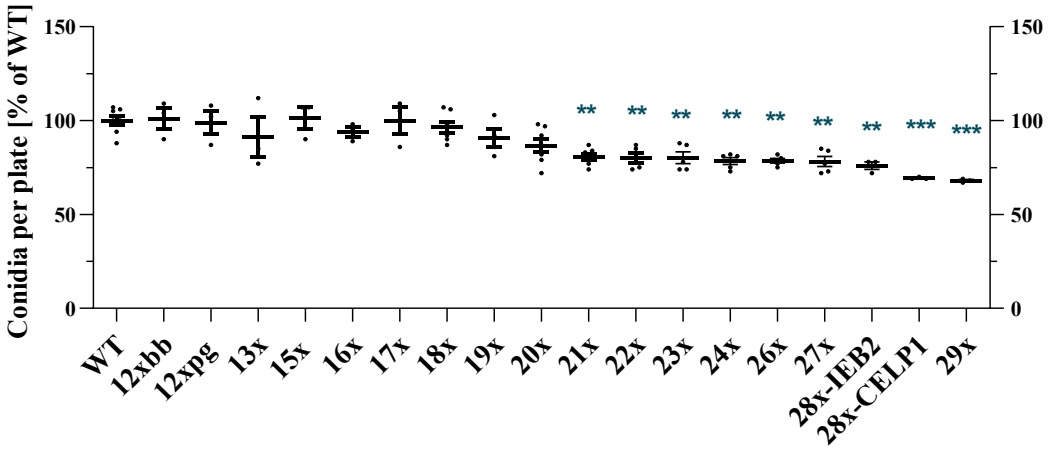

C

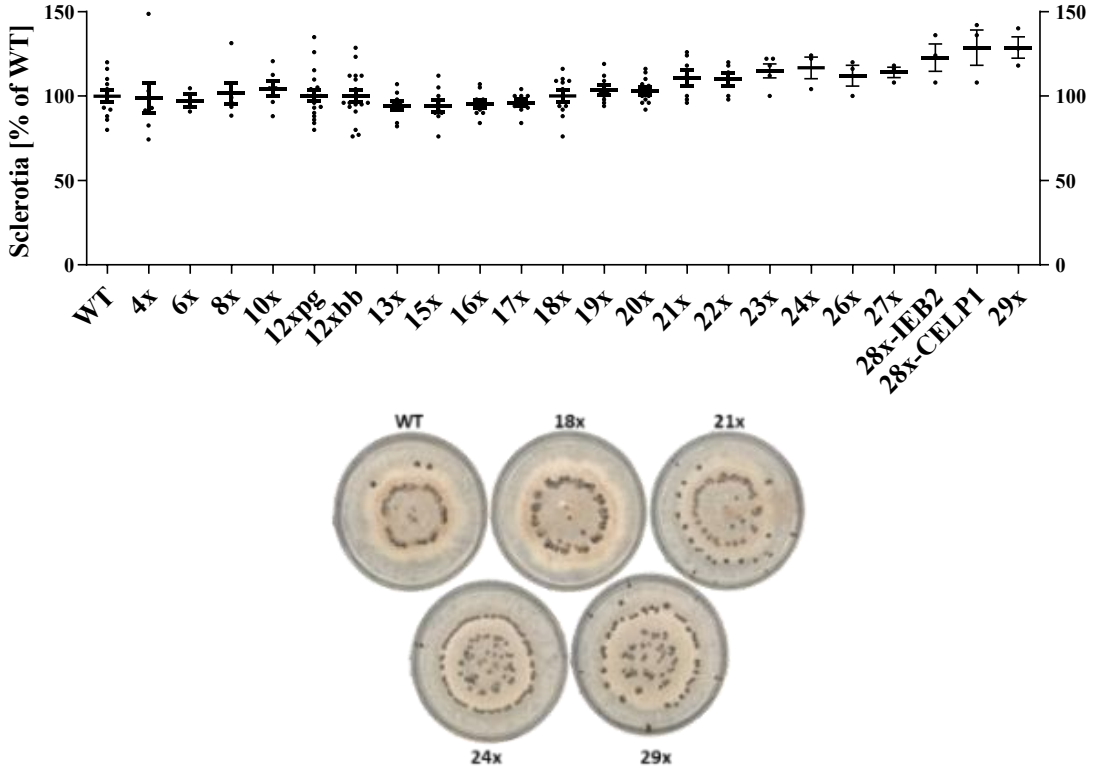

D

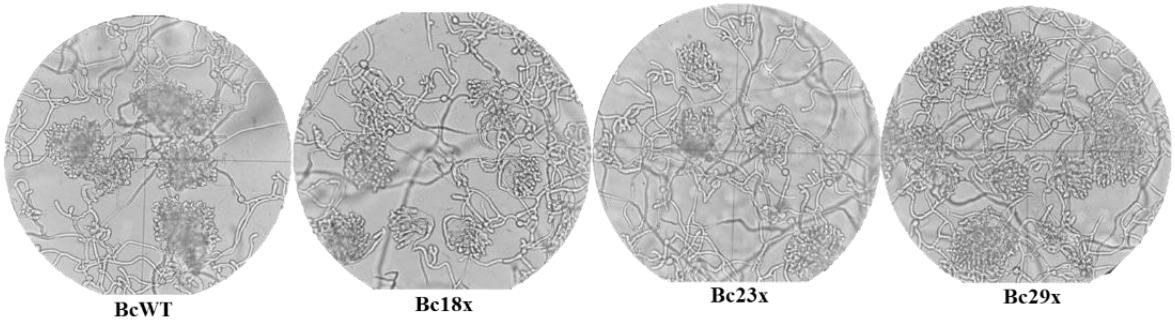

Figure 8. Growth and morphological differentiation of *B. cinerea* WT and multi-knockout mutants. (A) Radial mycelial growth on ME medium after 7 days, expressed as a percentage relative to the BcWT. **(B)** Conidiation assay performed after 10 days under continuous light, with sporulation quantified as a percentage of BcWT levels. **(C)** Sclerotia formation assessed after 14 days in the dark, expressed relative to BcWT. **(D)** Infection cushion formation observed on glass slides after 48 h, with upper scale bars representing 50 µm and lower scale bars 150 µm. Data in all panels represent the mean ± SD from at least three independent experiments. Statistical significance was determined using one-way ANOVA followed by Tukey's post hoc test, with asterisks indicating strains that differ significantly from BcWT ($p < 0.05$).

3.7.2. Infection behaviors of multi-knockout mutants

Virulence assessment on different plant tissues

In all tissues, progressive increases in the number of deleted virulence genes in *B. cinerea* generally resulted in diminishing lesion sizes and slower rates of disease progression. The same overall trends were observed across plant tissues (described further below).

***Phaseolus vulgaris* (Phaseolus bean) leaves**

Pathogenicity tests on Phaseolus bean primary leaves attached to the intact plant at 48 h post-inoculation (hpi) revealed a progressive decline in lesion development across the *B. cinerea* multi-gene knockout series (Figure 9. A). While lesion data for the Bc4x to Bc12xbb knockout strains were previously reported by Leisen et al. (2022), our study extends these findings by incorporating mutants from Bc13x to Bc29x.

Leisen et al. (2022) observed that early-stage deletion mutants (Bc4x, Bc8x) exhibited only a slight reduction in lesion size compared to the BcWT, and the most pronounced decrease in virulence was seen in the Bc12xPG and Bc12xbb strains. As illustrated in Figure 9, lesion size continued to shrink with increasing gene deletions, though some reductions reached statistical significance while others did not. Figure 9. A visually demonstrates of this stepwise decline in pathogenicity as gene deletions accumulated. These findings underscore the roles of specific genes in fungal virulence and indicate a cumulative effect of multiple gene deletions on pathogenicity.

When the assay was extended to 72 h, keeping the leaves on the plants for an extra 24 h sharpened the trend we had already seen (Figure 9. B). Lesions produced by the 18-gene knockout (Bc18x) were about 30-40 % larger than the wild-type spots scored at 48 h, but each additional round of deletions pared virulence back further. Importantly, none of the mutants became nonpathogenic and even Bc29x kept enlarging its lesions during the extra 24 h, forming lesions that still covered more than half the area produced by the BcWT at 48 h. In short, *B. cinerea* can still wound Phaseolus leaves after nearly thirty virulence factors have been taken out, but its capacity to do so is markedly reduced.

A

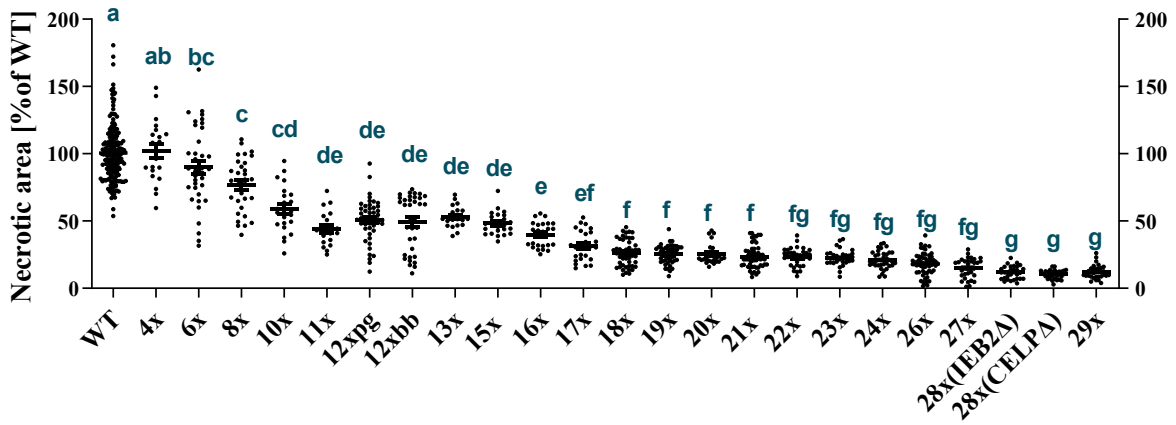

B

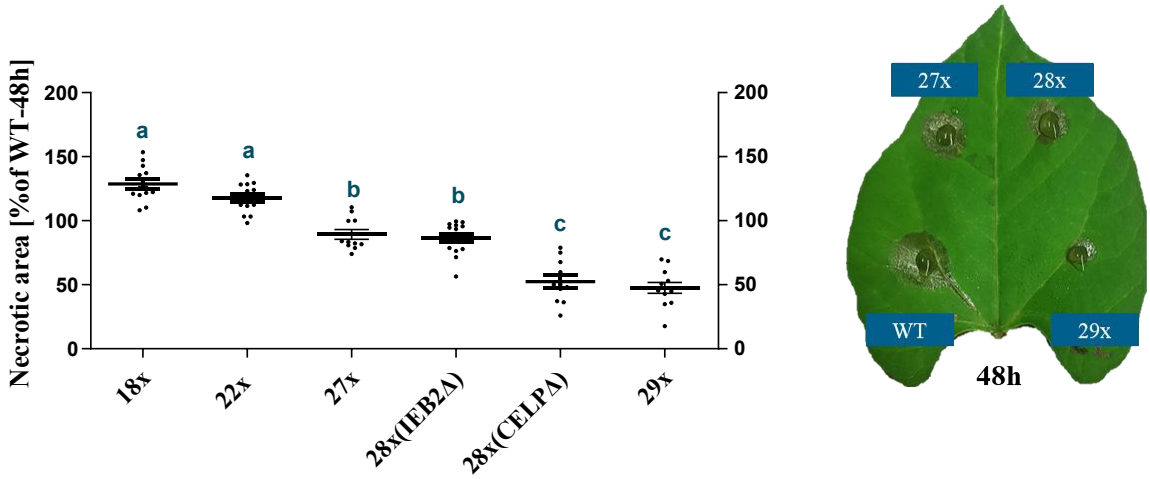

Figure 9. Pathogenicity assays of *B. cinerea* multi-gene knockout mutants on Phaseolus bean leaves at 48 h and 72 h post-inoculation (hpi). (A) demonstrate a progressive decrease in necrotic lesions, culminating in the Bc29x mutant, which causes only minor necrosis. **(B)** Lesion area measured 72 h post-inoculation for the late-generation mutants, expressed as a percentage of the BcWT lesion size at 48 h. The photograph on the right shows representative leaves 48 h after infection with the BcWT, Bc27x, Bc28x, and Bc29x strains, illustrating the visible reduction in necrotic area that accompanies successive deletions. Statistical differences ($p < 0.05$) are indicated by different letters (ANOVA, Tukey's test). Representative leaf images illustrate lesion reduction. Data are presented as mean ± SD ($n \geq 3$).

Solanum lycopersicum (Tomato) leaves

Similar to attached Phaseolus leaves, detached tomato leaves at 48 hpi revealed a progressive decline in virulence among *B. cinerea* knockout mutants, but following a less gradual pattern (Figure 10. A). According to Leisen et al. (2022), deletion mutants up to Bc10x showed no significant reduction in lesion size compared to the BcWT. The first noticeable decline in virulence was observed at Bc11x and Bc12x, associated with the sequential loss of PG1 and PG2 followed by a gradual reduction in subsequent mutants (Leisen et al., 2022). The higher

order deletion mutants beyond Bc12xbb generated in this thesis were found to result in the gradual decline of virulence in the Bc13x (loss of PG1), Bc15x (loss of CDI1 and Crh1), Bc16x (loss of CFEM1) and Bc17x (loss of PG2) mutants. We conclude from these data that these CDIPs play some role in virulence, as previously shown for PG2 and CFEM1 (Zhu et al., 2017). Similar to the results observed on Phaseolus bean leaves, the mutants Bc17x to Bc28x showed no statistically significant differences in lesion size compared to their parent strains, indicating no or only a small role of the deleted CDIPs for infection. A further decline was observed between the Bc27x and Bc29x mutants, indicating a role of CELP1 and IEB2. When the assay was extended to 72 h (Figure 10. B), the necrotic lesions continued to spread in the knock-out mutants. Although the 29-gene mutant (Bc29x) exhibited significantly slower lesion development compared to the wild-type at 48 h, the lesion growth did not stop entirely. In fact, over the next 24 h, lesions in the Bc29x mutant continued expanding until they covered nearly 80% of the area that the wild-type had colonized by the 48-hour mark. In practical terms, this indicates that even after the knockout of twenty-nine virulence-related genes, *B. cinerea* still retains some ability, albeit greatly reduced to damage tomato foliage. This residual pathogenic capability suggests that other unknown factors are likely involved, compensating for the loss of these genes, and enabling disease progression.

A

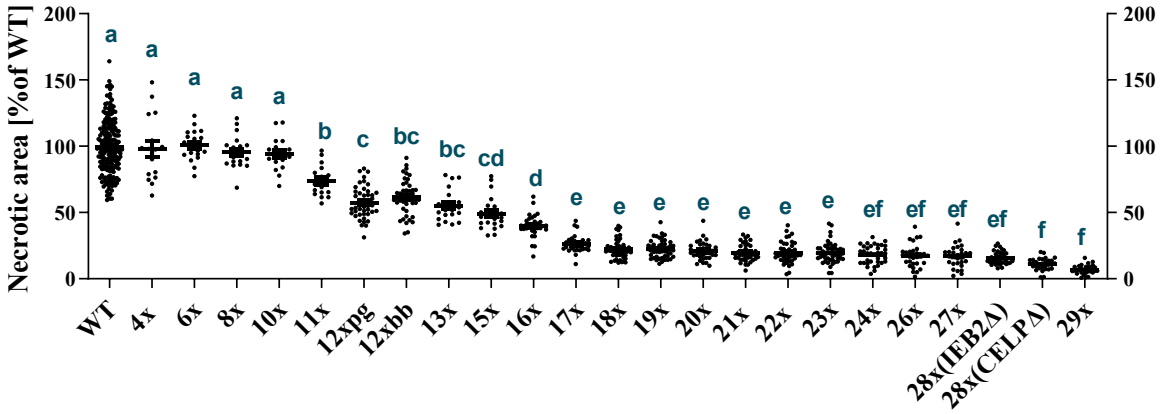

B

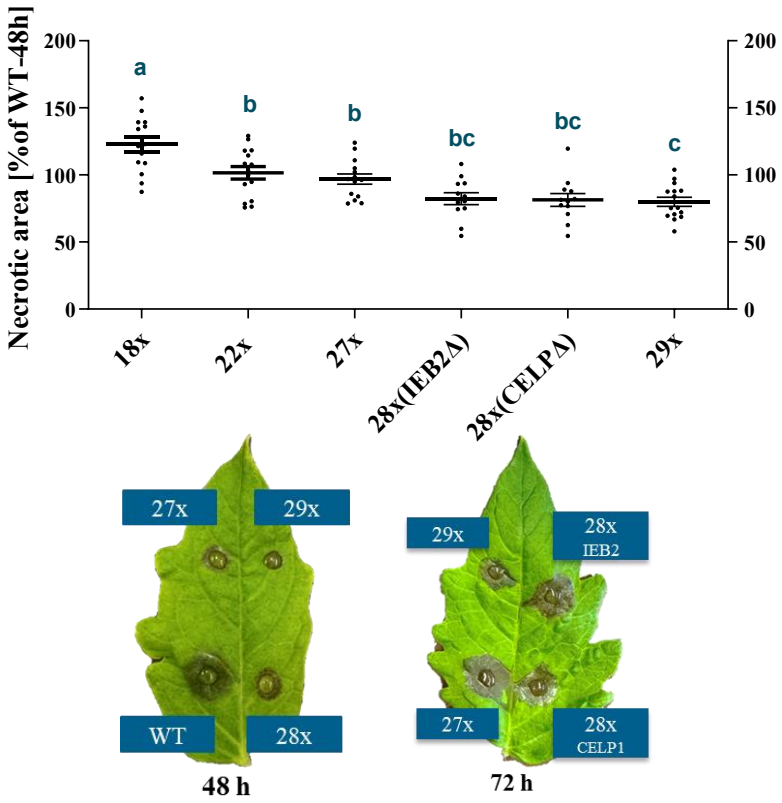

Figure 10. Pathogenicity assays of *B. cinerea* multi-gene knockout mutants on tomato leaves at 48 h and 72 h post-inoculation (hpi). (A) demonstrate that progressive increases in the number of deleted virulence genes in *B. cinerea* generally resulted in diminished lesion sizes. **(B)** Lesion expansion was monitored for selected late-generation knockouts (Bc18x, Bc22x, Bc27x, Bc28x, Bc29x) up to 72 hpi. Values are plotted relative to the BcWT lesion size at 48 hpi to emphasize continued growth. The same statistical treatment as in panel A was applied. Photograph panels to the right illustrate the marked reduction in necrotic tissue produced by high-order knockouts compared with the BcWT strain at 48 h and 72 h. Statistical differences ($p < 0.05$) are indicated by different letters (ANOVA, Tukey's test). Representative leaf images illustrate lesion reduction. Data are presented as mean ± SD ($n \geq 3$).

Malus domestica (Apple) fruit

Pathogenicity evaluations on apple fruit at 96 h post-inoculation (hpi) revealed an increased effect of gene deletions compared to the leaf assays (Figure 11). As reported by Leisen et al. (2022), the Bc12xbb and Bc12xpg mutants already showed more than a 50% reduction in lesion size compared to the BcWT. Introducing a PG2 deletion in the Bc17x mutant further diminished the necrotic area to approximately 10–15% of BcWT, underscoring the pivotal role of this polygalacturonase in pectin degradation. Beyond Bc17x–Bc26x, expanding lesions were nearly absent at 96 hpi under the chosen inoculation conditions.

Once lesion development was reduced in the Bc18x strains to 10% or lower, the effects of further gene deletions could not be detected anymore under the conditions used. Longer incubation times (e.g., up to two weeks) may help distinguish Bc18x from subsequent deletion mutants.

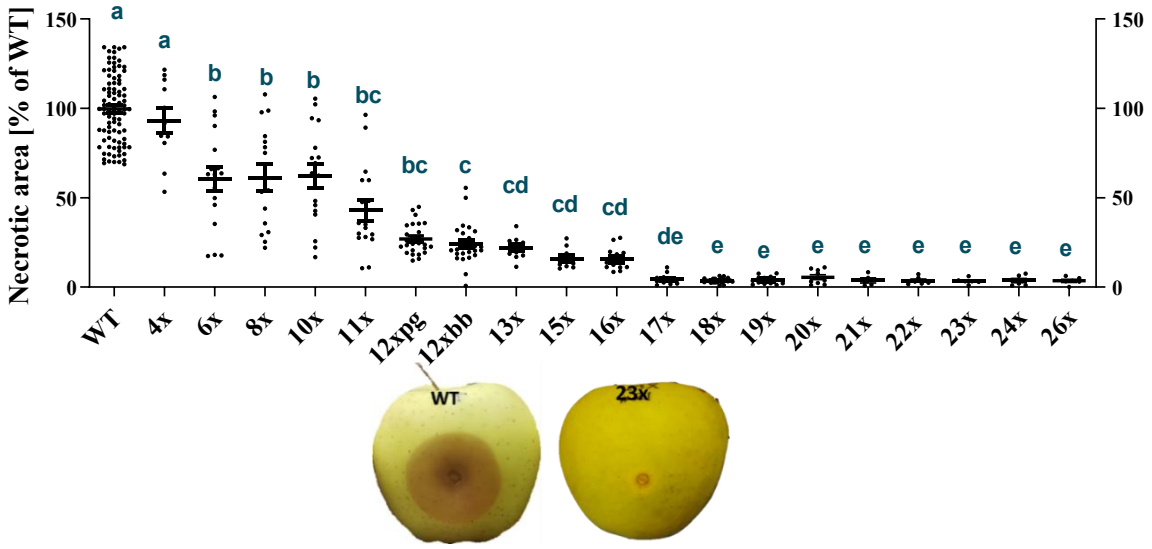

Figure 11. Pathogenicity test of *B. cinerea* multi-gene knockout mutants on apple fruit (96 hpi). Necrotic lesions progressively decreased with additional deletions up to Bc18x. Higher-order mutants showed minimal lesions, with no further reductions due to a masking effect. Statistical differences ($p < 0.05$) are indicated by letters (ANOVA, Tukey's test). Data are presented as mean ± SD ($n \geq 3$).

3.7.3. Host-dependent virulence patterns of the *B. cinerea* Bc18x multi-gene knockout mutant

A comparative analysis of the Bc18x multi-gene knockout mutant across diverse plant hosts was performed to compare the effects of a multi-CDIP knock-out on the virulence between leaf and fruit tissues (Figure 12). Despite the loss of multiple virulence-associated genes, the Bc18x mutant retained significant residual pathogenicity on most leaf tissues except for Arabidopsis. For instance, tomato leaves exhibited approximately 25% of the wild-type lesion, Phaseolus bean leaves around 30%, and maize leaves about 35% of BcWT necrosis. In stark contrast, the Bc18x mutant had lost most of its virulence on Arabidopsis leaves, showing only about 5% of BcWT lesion development.

On fruit tissues, the Bc18x mutant showed less infection than on leaves (except Arabidopsis). Infections on apple and tomato fruits produced merely 5–10% of the BcWT lesion area, while *Vitis vinifera* (grape) berries consistently showed around 5% necrosis with the Bc18x mutant compared to the BcWT. These tissue-specific responses indicate differences in the roles of at least some of the CDIPs for infection of different host tissues.

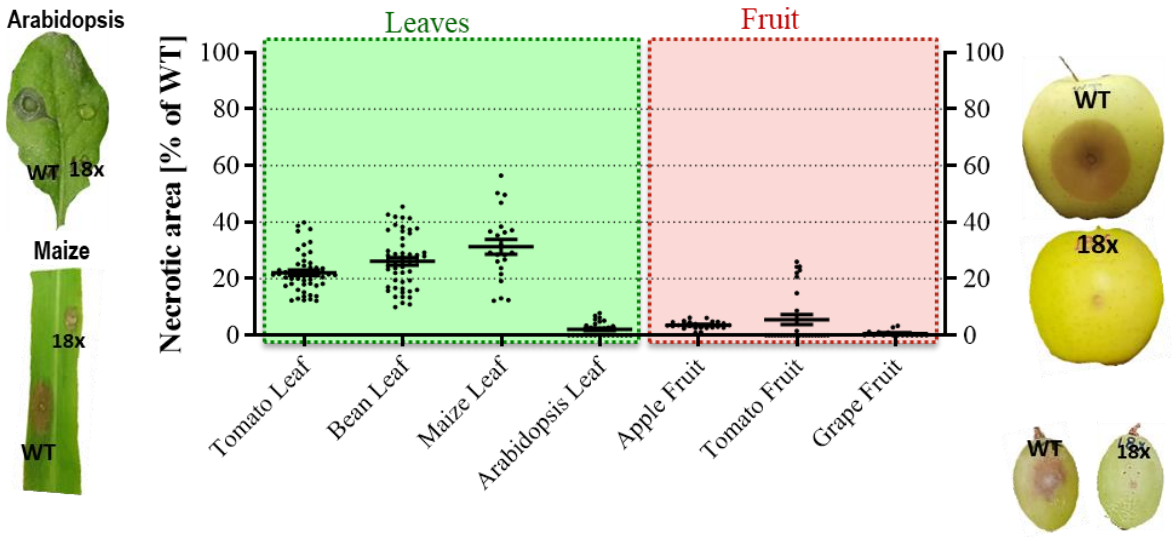

Figure 12. Pathogenicity of *B. cinerea* 18x vs. WT strain on different host tissues. Overview plot comparing necrotic areas caused by the *B. cinerea* strains on various leaf and fruit tissues. Statistical differences ($p < 0.05$) are indicated by different letters (ANOVA, Tukey's test). Data are presented as mean ± SD ($n \geq 3$).

3.10. Phytotoxic activity of secretomes from *B. cinerea* WT and multi-knockout mutants

Leisen et al. (2022) demonstrated that *B. cinerea* strains with multiple deletions of phytotoxic proteins (CDIPs) show a progressive reduction in their ability to induce necrosis in plant tissues. This underscores an important role of at least some of the deleted CDIPs in *B. cinerea*'s pathogenicity. Correspondingly, the phytotoxic activity of the on planta secretomes from infected tomato leaves of the 10x, the Bc12xbb and the Bc12xpg mutants was strongly reduced compared to BcWT, but these mutants retained significant phytotoxic activity.

In this study, dose-dependent phytotoxic activities of *B. cinerea* secretomes were assessed through infiltration assays using *N. benthamiana* leaves exposed to BcWT and three multi-gene knockout mutants (Bc18x, Bc22x, Bc29x). BcWT secretomes consistently caused necrosis when infiltrated between 0.5 to 2 µg/mL in a dose-dependent manner, with increasing lesion size, demonstrating strong phytotoxic activity even at low concentrations. Across the tested protein concentrations (BcWT 0.5, 1 and 2 µg; mutants 1, 2 and 4 µg), the multi-gene knockout secretomes produced markedly smaller lesions on *N. benthamiana* leaves than the BcWT preparation. Lesion size declined step-wise with successive CDIP deletions, Bc18x > Bc22x > Bc29x and, at the 1 µg dose, the mutants exhibited a four- to eight-fold reduction in phytotoxicity relative to BcWT (Figure 13).

These results support and expand the findings by Leisen et al. (2022), confirming the cumulative nature of phytotoxicity reduction following CDIP deletions. In agreement with the infection phenotypes, the remaining phytotoxicity of the mutant with the largest loss of CDIPs (Bc29x) clearly indicates the presence of additional, as yet unidentified CDIPs contributing to *B. cinerea* necrosis-inducing activity.

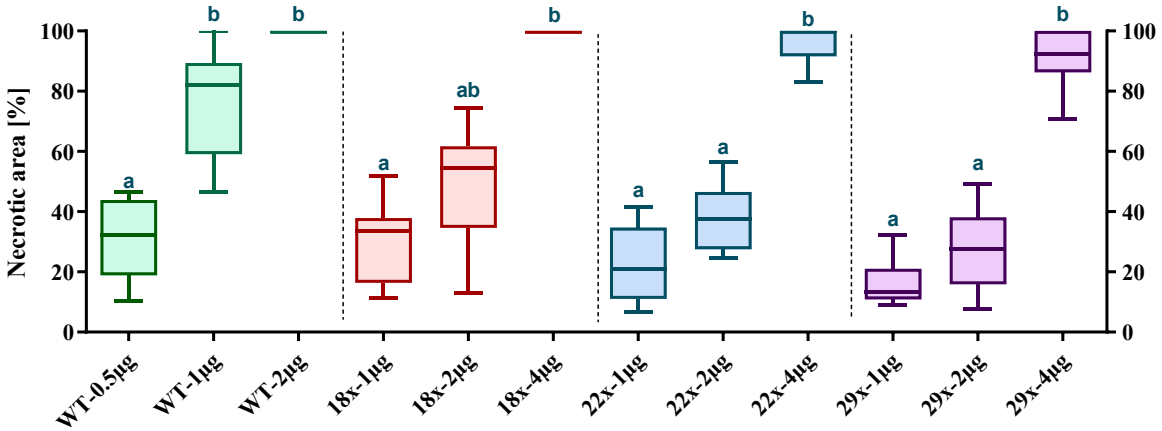

Figure 13. Dose-dependent phytotoxic effects of *B. cinerea* WT and multi-knockout mutant secretomes on *N. benthamiana* leaves. Secretomes were harvested 48 h post-inoculation and infiltrated at indicated protein concentrations (BcWT: 0.5, 1, 2 µg; mutants: 1, 2, 4 µg). Necrotic lesion areas were measured after 72 h. Letters above box plots indicate statistically significant differences (one-way ANOVA, Tukey's multiple comparisons test, $\alpha = 0.05$, $N = 6$).

3.11. Stage-dependent CDIPs secretion in the *B. cinerea* secretome

A label-free proteomic analysis of the *B. cinerea* wild-type secretome was performed at early (26 hpi) and late (48 hpi) timepoints to elucidate the stage-dependent secretion patterns of secreted proteins, with focus on CDIPs. Spectral data were acquired via tandem mass spectrometry (MS/MS), enabling identification and quantification of secreted proteins (see Table S2). Among the 27 candidate CDIPs targeted in the 29-gene knockout strain (Bc29x), 23 were detected in the BcWT at 26 hpi and again 23 at 48 hpi, but two CDIPs each were only found in one but not the other condition. Notably, Nep1, PLP1, and XYL1, which have not been observed in earlier studies (Leisen et al., 2022; Zhu et al., 2017; Müller et al., 2018), emerged in our secretome; Nep1, which has never been observed before in proteomic studies, appeared exclusively at 26 h in relatively high abundance, while CELP1 was also confined to 26 h but at low abundance, and CFEM1 and XYL1 were detected solely at 48 h. Three CDIPs (CDI1, SSP2, and CDI3) were not detected at either timepoint, whereas all others

were present at both 26 h and 48 h, although with varying abundance. (Table 33). Overall, sample-to-sample variability of the secretomes was very high for unknown reasons, precluding a detailed quantitative comparison.

Table 33. Relative abundance of the indicated *B. cinerea* WT secreted proteins at early (26 hpi) and late (48 hpi) infection stages, as determined by label-free LC–MS/MS.

KO order	Gene	Protein	*B. cinerea* (WT)	
			Early Stage (26h)	Late Stage (48h)
1	*Bcspl1*	**Spl1**	++	+++
2	*Bcnep1*	**Nep1**	++	-
3	*Bcnep2*	**Nep2**	++	++
4	*xyn11A*	**XYN11A**	++++	+++++
5	*BcHip1*	**Hip1**	++	++
6	*BcXYG1*	**XYG1**	++++	++++
7	*Bcplp1*	**PLP1**	++	++
8	*BcIEB1*	**IEB1**	+++	+++
9	*Bcxyl1*	**Xyl1**	-	+
10	*BcGs1*	**GS1**	++	++
11	*Bcbot2*	**-**	secondary metabolite	secondary metabolite
12	*Bcboa6*	**-**	secondary metabolite	secondary metabolite
13	*Bcpg1*	**PG1**	+++++	+++++
14	*Bccrh1*	**Crh1**	++	++
15	*BcCDI1*	**CDI1**	-	-
16	*Bccfem1*	**CFEM1**	-	+
17	*Bcpg2*	**PG2**	+++++	+++++
18	BcSSP2	**SSP2**	+	+
19	*BcCDI2*	**CDI2**	+	+
20	*Bcspg1*	**SGP1**	++	++
21	*Bccrh4*	**Crh4**	+	+
22	*Bcxyg3*	**XYG3**	++	+++
23	*BcGAS5A*	**GAS5A**	++	++
24	*Bccdi3*	**CDI3**	-	-
25	*Bcrrae1*	**RAE1**	+++	++++
26	*Bcfat1*	**FAT1**	++	++
27	*Bcxyl2*	**Xyl2**	+	++
28	*BcIEB2*	**IEB2**	++	++
29	*BcCELP1*	**CELP1**	+	-

Proteins not detected at a given timepoint are indicated by "–." The plus-sign notation (i.e., "+," "++," "+++," "++++," "+++++") reflects the following spectral intensity ranges: (+ = 1–10^6), (++ = 10^6–10^7), (+++ = 10^7–2×10^7), (++++ = 2×10^7–3×10^7), and (+++++ = > 3×10^7).

3.8. Nep1 overexpression in a multi-CDIP knockout mutant

To determine whether reintroduction of a phytotoxic protein into a multi-k.o mutant lacking many CDIPs can (partially) restore its strongly reduced virulence, a Bc22x mutant was transformed with an overexpression construct of Nep1, which is the most highly toxic CDIP

known from *B. cinerea*, causing cell damage in plant cells already at a concentration of 0.04 µM (Schouten et al., 2008). For Nep1 overexpression, two strong promoters were tested: **BcH2B** (Zhu et al., 2017; Histone 2B; 136 aa; coordinates 2:2369885–2370456; length 572 bp) and **BcHis3** (our own work; His3; 136 aa; coordinates 13:1592695–1593641; length 947 bp). Each promoter and the *nep1* coding sequence including the *nep1* terminator, were cloned into pBS-KS-Hyg. The resulting constructs were transformed into Bc22x and integrated by CRISPR–Cas9–mediated homology-directed integration into a non-essential locus containing highly expressed genes in chromosome 1 of *B. cinerea*, resulting in *B. cinerea* strains Bc22x-H2B-Nep1 (Fig. 14) and Bc22x-His3-Nep1.

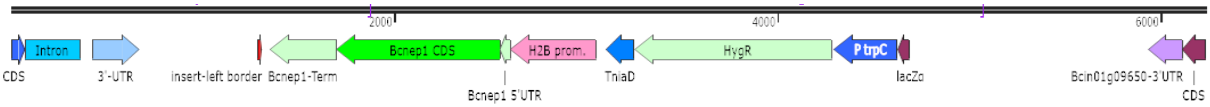

Figure 14. Scheme of the H2B-Nep1 overexpression cassette integrated into a non-essential locus in chromosome 1 of *B. cinerea*.

Nep1 overexpression was quantified and confirmed on the transcriptional level by RT-qPCR (Figure 15) and by detection of the protein in the secretome via LC–MS/MS (Figure 16). Despite robust Nep1 expression during plant infection, neither of the overexpressing strains (Bc22x-H2B-Nep1 and Bc22x-His3-Nep1) differed significantly in virulence from the Nep1-deficient parent strain Bc22x in plant infection assays (Figure 17). Based on these results, the increased phytotoxicity provided by overexpression of Nep1 was not sufficient to increase the low necrosis-inducing activity of the Bc22x mutant.

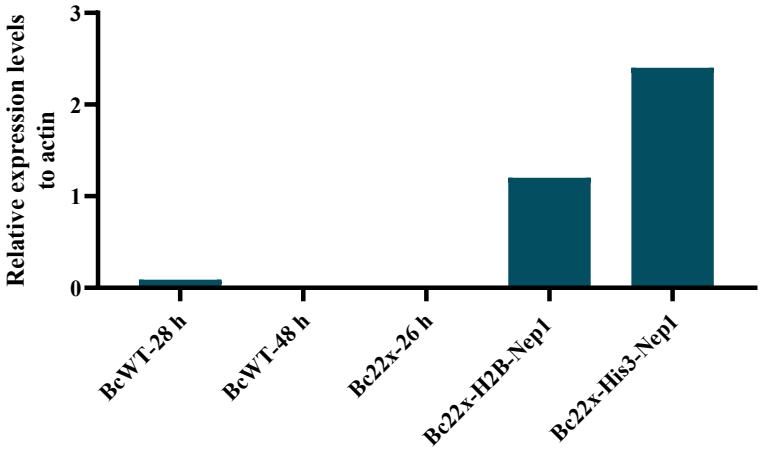

Figure 15: Expression analysis of *nep1* by qRT-PCR. Relative *nep1* transcript levels on infected tomato leaves at 24 and 48 h post-inoculation (hpi) of Nep1 overexpression strains were compared to those of the Bc22x mutant lacking *nep1* (BcΔnep1) and BcWT. Expression levels are displayed as fold changes relative to the actin gene. Data are from a single experiment (from Shekhar Chule, Master's Thesis).

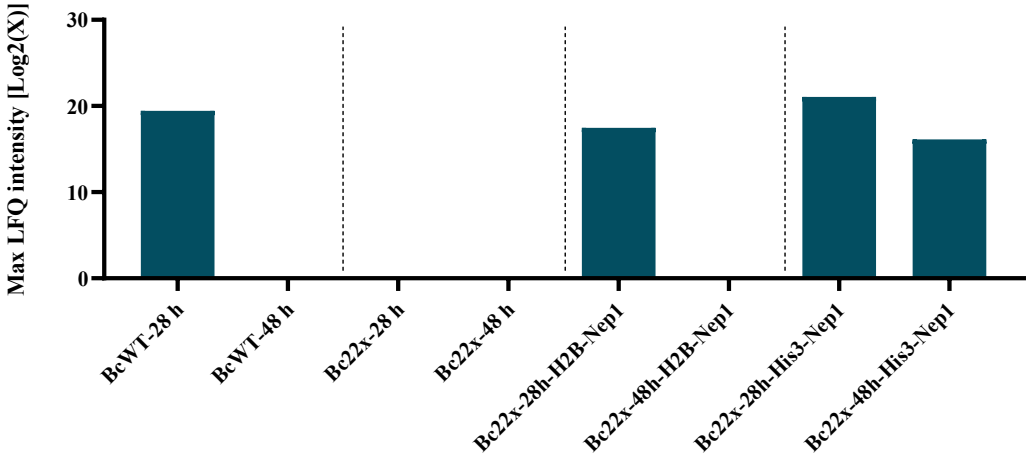

Figure 16: Nep1 accumulation in the secretomes of different *B. cinerea* strains at two time points after infection of tomato leaves. MaxLFQ intensities were $\log_2$-transformed prior to plotting. Data shown are from a single experiment.

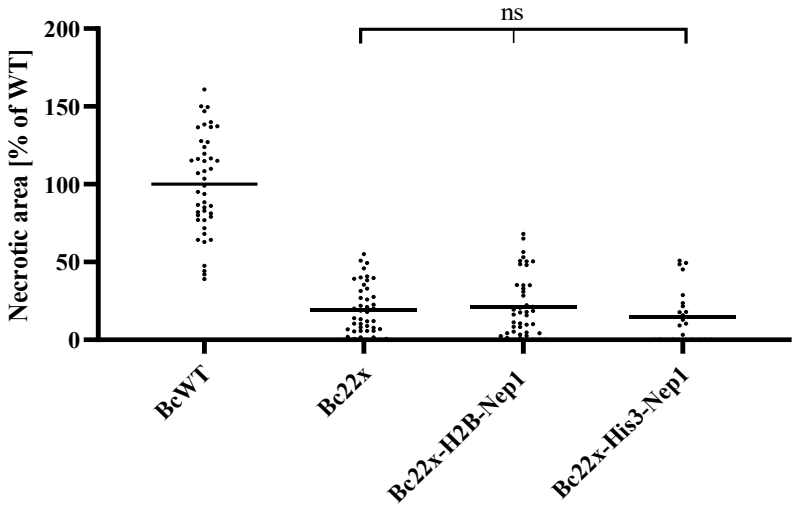

Figure 17. Results of infection assay of on tomato leaves (48 hpi). Data are mean ± SD ($n \geq 3$). Statistical significance was determined by one-way ANOVA followed by Tukey's multiple-comparisons test; $p < 0.05$, ns = not significant.

3.12. Identification and preliminary assessment of novel candidate CDIPs

In order to identify the missing CDIPs, five new candidates were tested for their phytotoxic activity, namely IEB2, RAE2, XYG3, Xyl3, and CDI4. These candidates were identified based on their homology to known CDIPs, and on their upregulation of gene expression during infection (Table 34). To investigate whether these proteins exhibit cytotoxic activity,

two expression systems were employed. First, recombinant forms of each CDIP were produced in *E. coli*, allowing for in vitro characterization of their cytotoxic potential. Second, transient expression in *N. benthamiana* via agroinfiltration was performed to examine the phytotoxic effects of in planta delivered proteins.

Table 34. Novel CDIP candidates and their characteristics.

Accession	Name	Homology	Sequence Identity (%)	RNA seq*		In the Secretome	References
				Mycelium	3d inf. Tissue		
Bcin13g00300	IEB2	IEB1	33.3	84.2	2237.4	++	Frias et al., 2016; Gonzalez et al., 2017; Gonzalez et al., 2018
Bcin01g06790	RAE2	RAE1	59.2	1.2	5.5	(+)	Zhang et al., 2024
Bcin13g02320	XYG3	BcXYG1	53	2.2	431.0	(+	Zhang et al., 2024; Frias et al., 2019
Bcin15g01600	Xyl3	Xyn11A & Xylanase 2	- (X-Y)	0.1	30.0	+++	Brito et al., 2006; Frias et al., 2019; Wang et al., 2023
Bcin11g05460	CDI4	*M. fructicola* MFRU_030g00190	67	775.7	18460.8	-	Lopez et al., 2024

*RNA sequencing data were provided by Jan van Kan.

IEB2 (Bcin13p00300)

IEB2 shows 33.3% sequence identity with IEB1, a previously characterized CDIP in *B. cinerea* (Frías et al., 2016; González et al., 2017). In addition to its phytotoxic activity, IEB1 has been shown to interacts with PR5-family proteins, particularly osmotin, which plays a role in antifungal defence (González et al., 2017). In contrast to the high constitutive expression of IEB1, IEB2 exhibits strong upregulation during infection and is present in the fungal secretome.

```
BcIEB1   1 MFSKTFIATLLASSAAATPIVSARAASDAFGLI---SIRSGTDLQNQAIV     47
           |||||.|||||||:.||:||  |.:.|||..::   ...:|:..:...|.
BcIEB2   1 MFSKTIIATLLASTIAASPI--AASTSDATYILRTFPTGAGSIFRGLEIT     48

BcIEB1  48 ANGGRLYIGKETSSYCPLATGCPAGTSTTFVAGESTISLNTEVPGGQQVY     97
           |:.|.|::||:|:         || ...:|..|    .:|||:  .||::|
BcIEB2  49 ADNGYLWVGKQTT---------PA-IHFSFNNG----YVNTQ--EGQELY     82

BcIEB1  98 IG---TDYSVSYTQPHSADTHGGVTSGWVYTA---GENGSLGSLSFPDYG    141
           |.   ..|:.|.|...:|       |||.:.|   |.|.|:|||::|.|.
BcIEB2  83 ISGNTVTYAASGTDAENA-------SGWEFVAPYSGPNISVGSLTYPGYD    125

BcIEB1 142 FIACRESDG-VYAVFITPGGSG-TGNCTGIAVATVPYTGESPSAWEYA     187
           ..||..|:. ||.:...|.|:| ||.|..|.:...
```

```
BcIEB2 126 IYACSGSEADVYTIAAVPTGTGATGKCEQIQLIAQ------------      160
```

Figure 18. Alignment of *B. cinerea* IEB1 and IEB2 (performed with EMBOSS Needle). Signal peptides are indicated with grey background. The 25 amino acid peptides of IEB1 which shows phytotoxic activity similar to IEB1 (Frias et al., 2016) is shown with bluish background.

RAE2 (Bcin01p06790)

RAE2 shares 59.2% sequence identity with RAE1, a putative rhamnogalacturonan acetyltransferase belonging to the SGNH hydrolase superfamily which showed phytotoxic activity when infiltrated as purified protein into *N, benthamiana* leaves (Zhang et al., 2024). Remarkably, phytotoxic activity was lost when an enzymatically inactive version of this enzyme was used for infiltration, indicating that the phytotoxic activity of RAE1 does not involve recognition by PRR receptors but might be due to an unknown cleavage product of RAE1 (Zhang et al., 2024).

```
RAE1              1 MKVKVSVKVLLSSLAAQVCAVP----------------------------     22
                    ||  .:..::|::|||.|.|||
RAE2              1 MK--TTSGLVLATLAASVSAVPFNHAYGSYNGGHVRPTWSPPSASSDAAP     48

RAE1             23 -----------------------------------------TLYLAGD     29
                                                             |:|:.||
RAE2             49 ENTASSTSASAVAATSVASSVVAASSVVVASSAVVLAASAASPTVYMCGD     98

RAE1             30 STMALGGGGTSTQGFGEYLKYSFTGINVVNNAVAGRSARSYYNEGRFTAL     79
                    ||||||||||.|||:|.||.||.| |.|||:|.||||||||.:|.||.|:
RAE2             99 STMALGGGGTGTQGWGVYLPYSLT-IPVVNDAKAGRSARSYTDENRFGAV    147

RAE1             80 ADKVVAGDYVLFEFGHNDGGSLSTTDNLRTDCYGGGTETCISPVTGETVY    129
                    .|.:.:||.|:.|||||||||||:|||||:||.|.|.|||.:.. |..|.
RAE2            148 IDTIKSGDIVIIEFGHNDGGSLTPTDNLRSDCVGAGNETCTTDA-GVVVQ    196

RAE1            130 TYVFYLLQAGRLITAKGAHLIIASPTPNNLWETGTFSYTAPRFTGYGRSV    179
                    ||..||..|..|:||||||:||:||||:|..||||.|||:|||||||..|
RAE2            197 TYPTYLTNATELMTAKGAHVIISSPTPDNTCETGTCSYTSPRFTGYGEIV    246

RAE1            180 VSSLGSLASFVDHGLYTANIYESLGATTVDAFYPIDHTHTSPAGANTVAA    229
                    |.::||:|||:|||.|.||.|..|||.|||.:||.|||||||..|:.||.
RAE2            247 VENVGSMASFIDHGTYLANQYAILGAATVDTYYPNDHTHTSPIAADLVAG    296

RAE1            230 AFMKGLMCGGSA--LSAYSKNTTSSIAGSCA    258
                    .|:||::|.||:  |.:|.||:|.|:.|:|.
RAE2            297 VFVKGVLCAGSSNPLYSYIKNSTDSVVGTCI    327
```

Figure 19. Alignment of *B. cinerea* RAE1 and RAE2. Signal peptides are indicated with grey background.

XYG3 (Bcin13p02320)

XYG3 is related to BcXYG1, a well-characterized necrosis-inducing protein in *B. cinerea*, with 53% sequence identity. BcXYG1 has been shown to trigger necrosis via the SOBIR1/BAK1 pathway, indicating that its function is mediated by host receptor complexes (Zhu et al., 2017).

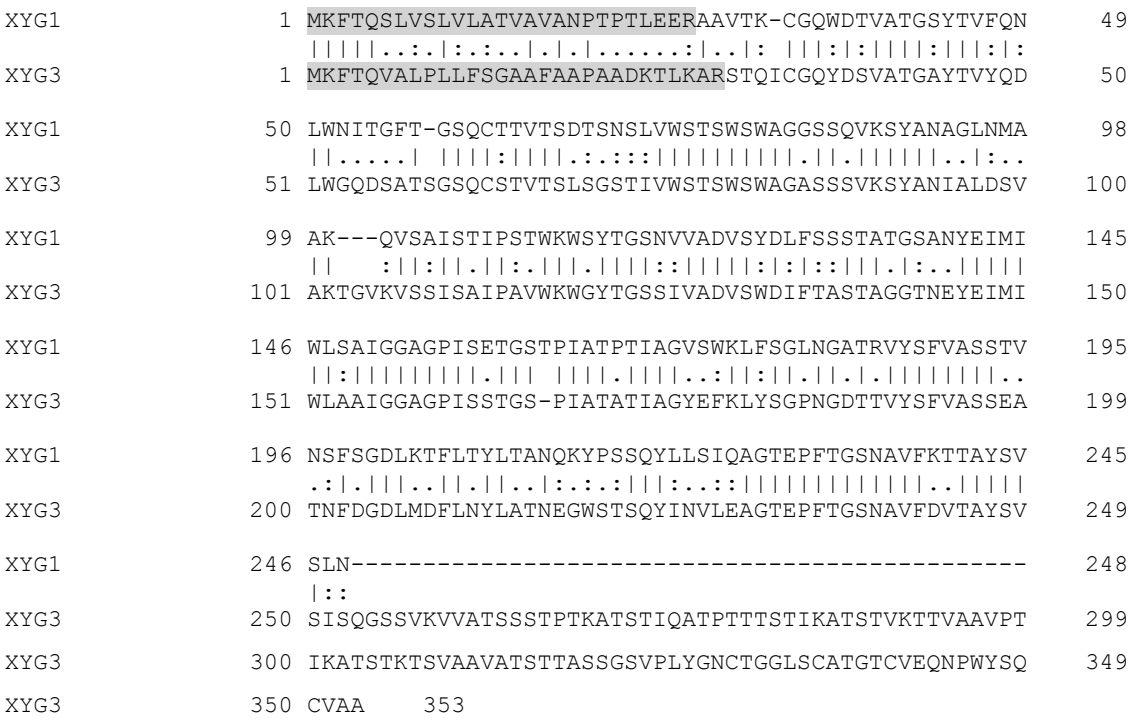

Figure 20. Alignment of *B. cinerea* XYG1 and XYG3. Signal peptides are indicated with grey background.

Xyl3 (Bcin15p01600)

Xyl3 is homologous to the xylanase CDIPs *B. cinerea* Xyn11A and *S. sclerotiorum* Xyl2, and both have been described as fungal virulence factors (Brito et al., 2006; Frías et al., 2019; Wang et al., 2023). Xyn11A has been demonstrated to elicit plant defences independent of its enzymatic activity, with a 25-residue peptide fragment shown to be sufficient for immune activation and cell death induction (Frías et al., 2019).

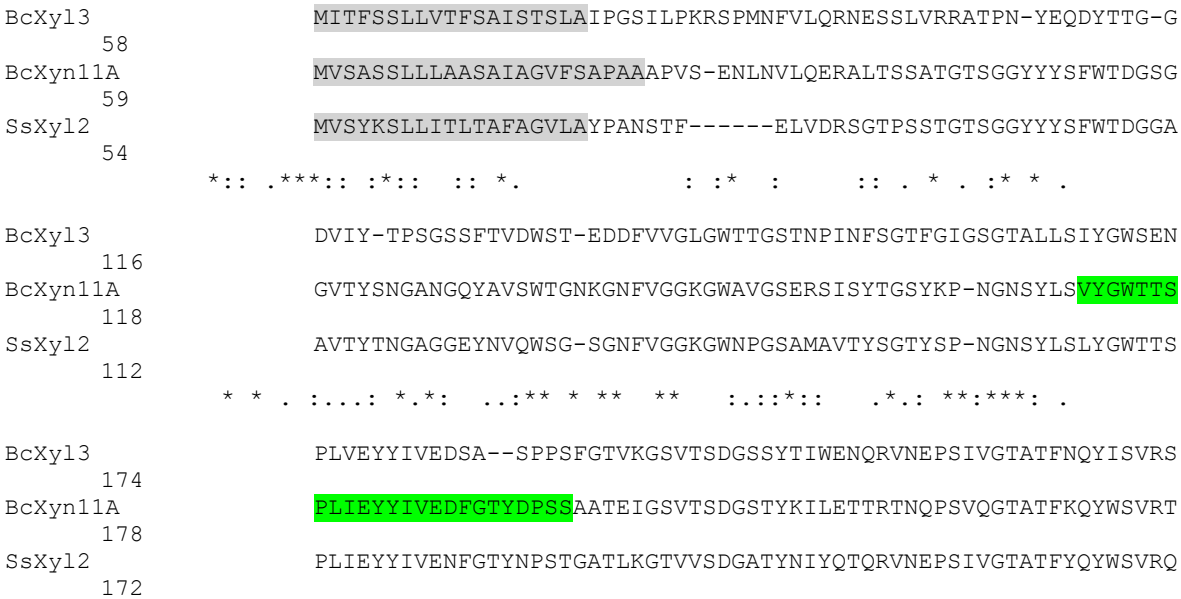

```
            **:******: .  .* : .*  *:*.***::*.* :. *.*:**: ***** ** ***

BcXyl3                SPRKSGTVTVENHFQAWAALGMNLG-TLNYQVLAVEGWGGEGAATQTVS-----------
      222
BcXyn11A              SKRTSGTVTTANHFAAWKKLGLTLGSTYNYQIVAVEGYQSSGSASITVS-----------
      227
SsXyl2                SKRTGGTVTTGNHFNAWKALGMDMG-TFNYMIVATEGYYSSGSSDITVGSSNGGGSTVPT
      231
            * *..****. *** **  **: :* * ** ::*.**: ..*::  **.

BcXyl3        --------------------------------------------------  222
BcXyn11A      --------------------------------------------------  227
SsXyl2        TSAPASSPTSSPGGTCGALYSQCGGTGFTGSSCCASGTCKYANSYYSQCL  281
```

Figure 21. Alignment of *B. cinerea* BcXyn11A, SsXyl2 and BcXyl3. The predicted signal peptides are shown with gray background, the phytotoxic Xyn25 peptide derived from Xyn11A is shown with green background.

CDI4 (Bcin11p05460)

CDI4 shares 67% sequence identity with a recently identified phytotoxic protein of the related brown rot fungus *Monilinia fructicola* (Lopez et al., 2024). The phytotoxic activity of the *M. fructicola* protein MFRU_030g00190 was detected after agroinfiltration of tomato leaves but not *N. benthamiana* leaves.

```
BcCDI4             1 MHASFSAVVTTLLAVSVAALPNNNGGSPTHTWGSTSPTGVPACSGSKYTC     50
                     |||||.||::..||::.||||.| ||:|| :|||:|||||.||||||||||
MfCDI4             1 MHASFIAVLSGFLALNAAALPTN-GGTPT-SWGSSSPTGTPACSGSKYTC     48

BcCDI4            51 ESNGLLTLLTCTNILNGVGISIPITLKNR--ALEERGIEART-SKDDGDY     97
                     .||||||:|||||:||.|||||||::..|  .:|||.||||. |..||||
MfCDI4            49 TSNGLLTILTCTNVLNDVGISIPISILKRDVQIEERDIEARGGSSKDGDY     98

BcCDI4            98 CCTSAGLLTLSCLNVANGLVIFLPIT-L    124
                     ||||.|||.|||:|||||:.:.||:. |
MfCDI4            99 CCTSNGLLALSCINVANGVGLSLPLNIL    126
```

Figure 22. Alignment of *B. cinerea* CDI4 (Bcin11g05460) with *M. fructicola* (MFRU_030g00190). Signal peptides are indicated with grey background.

3.12.1. Heterologous expression in *E. coli*

To evaluate the expression and solubility of the candidate CDIPs (IEB1as a control, IEB2, and XYG3), two expression vectors were employed in *E. coli* Rosetta: pET28 (induced at 21.5 °C) and pCold–TF (induced at 16 °C), which expresses the target protein as a C-terminal fusion with trigger factor (TF) chaperone under cold-shock conditions in order to increase its solubility.

IEB1 and IEB2 were both highly expressed and purified from the soluble fraction in both systems. In contrast, XYG3 expressed via pET28 was largely insoluble due to misfolding. However, when expressed with pCold–TF, XYG3 appeared also in the soluble fraction and was successfully purified via their His-tags by nickel-affinity chromatography (Figure 23),

highlighting the importance of TF co-expression in promoting correct folding. Further details on the expression conditions and yields are provided in Table 35.

Table 35. Summary of expression conditions and purification outcomes for the candidate CDIPs in *E. coli* Rosetta.

Samples	Protein size (KD)	Culture volume (ml)	IPTG (mM)	Incubation temperature (°C)	OD600	Yeild of protein (mg)
IEB1 in pET28	21.3	200	0.4	21.5	5.1	2.6
IEB2 in pET28	17.1	200	0.4	21.5	5	4.7
XYG3 in pET28	34.2	200	0.4	21.5	5	0.78
XYG3 in pColdTF	78.8	200	0.4	16	4.8	3.12
pColdTF	53.9	200	0.4	16	4.8	2.48

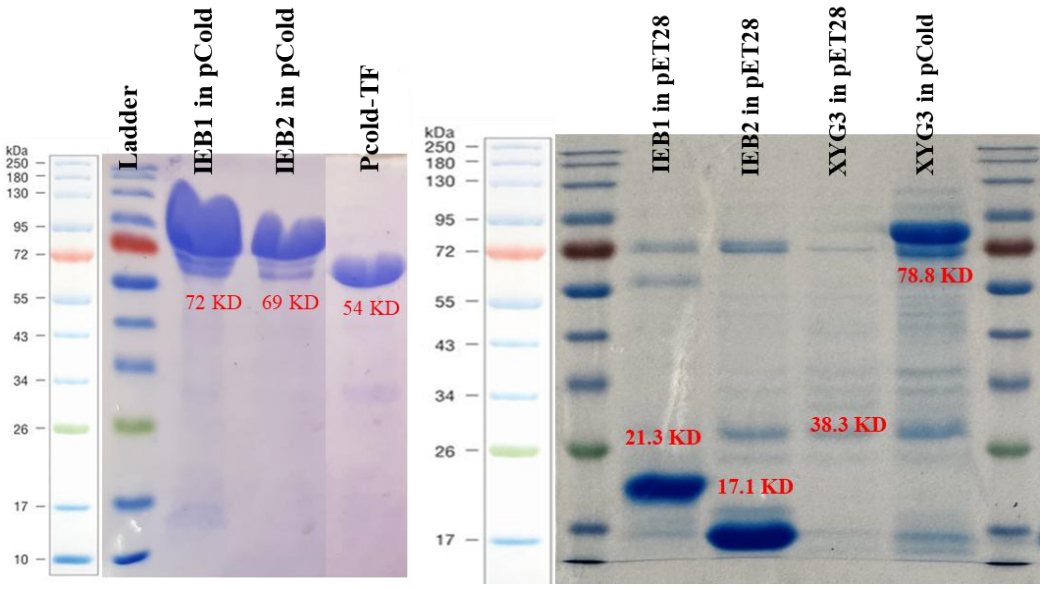

Figure 23. SDS-PAGE analysis of recombinant expression and purification of IEB1, IEB2, and XYG3 in *E. coli* Rosetta using two expression plasmids (pET28 and pCold–TF). Protein bands were observed at the expected sizes, confirming successful expression and purification of these proteins.

3.12.2. Infiltration of purified proteins and assessment of phytotoxicity

To evaluate the phytotoxic activity of the purified candidate CDIPs, *N. benthamiana* leaves were infiltrated with each protein, and necrotic lesions were measured 72 h post-infiltration (Figure 24). Nep2 (5 µM) served as a positive control and induced near-complete necrosis, while IEB1 caused significant leaf damage (60–80% necrosis) at 15µM. IEB2 (tested at 15 and 30 µmol) and XYG3 (15 µmol) were also toxic, but with lower activity. As a negative

control, TF protein alone (15 and 30 µmol) did not induce any necrosis. These findings demonstrate that both IEB2 and XYG3 possess moderate phytotoxic activity in *N. benthamiana*. They were therefore included into the multi-knockout mutagenesis program as described in 3.3 and 3.4.

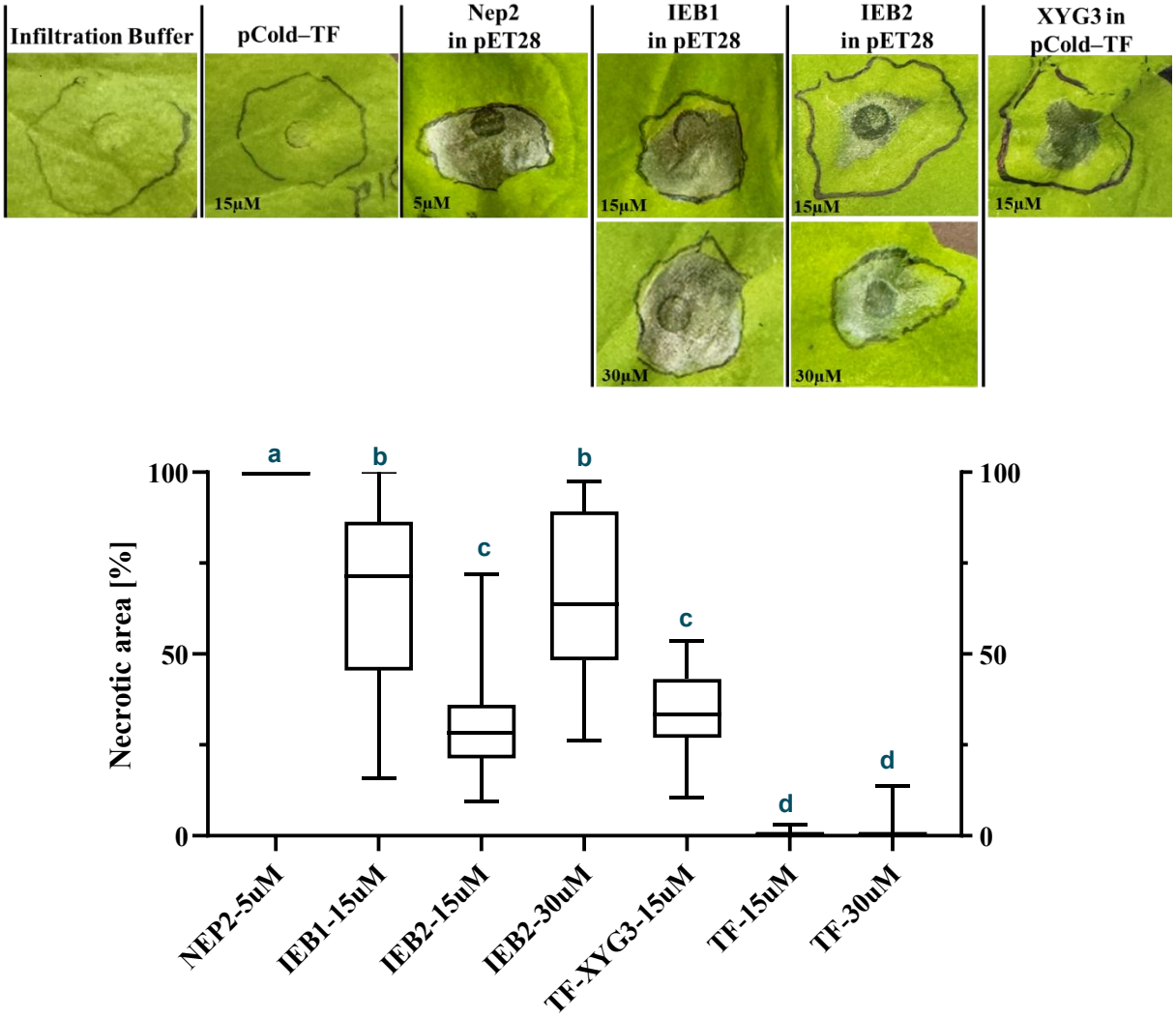

Figure 24. Phytotoxicity assay in *N. benthamiana* leaves at 72 h post-infiltration with purified candidate CDIPs expressed in *E. coli*. The upper panel shows representative leaf images for each treatment. The lower panel presents box plots indicating the percentage of necrotic leaf area. Letters above each box denote statistically significant differences ($p < 0.05$).

3.12.3. Transient expression in *N. benthamiana*

Alternatively, candidate CDIPs (IEB2, RAE2, Xyl3, and CDI4) were evaluated by agroinfiltration in *N. benthamiana* leaves. For this, they were cloned using the GreenGate cloning system as explained in the material and methods section. Necrotic lesions in *N. benthamiana* leaves were quantitatively assessed at 5 dpi (Figure 25). Again, the positive

control Nep2 induced necrotic lesions covering approximately 80–100% of the infiltrated leaf area. IEB2 and Xyl3 induced moderate necrosis, whereas RAE2 and CDI4 produced only very small necrotic lesions. The negative control (P19) exhibited no necrosis. These results indicate differential necrotic responses to the tested CDIP candidates. A consistent early symptom across all CDIPs was a glossy, water-soaked appearance on the abaxial leaf surface, emerging 48–72 h post-infiltration. This correlated with final lesion size and preceded necrosis. The symptom was absent in negative controls, confirming it as a specific response to CDIP expression (Figure S2).

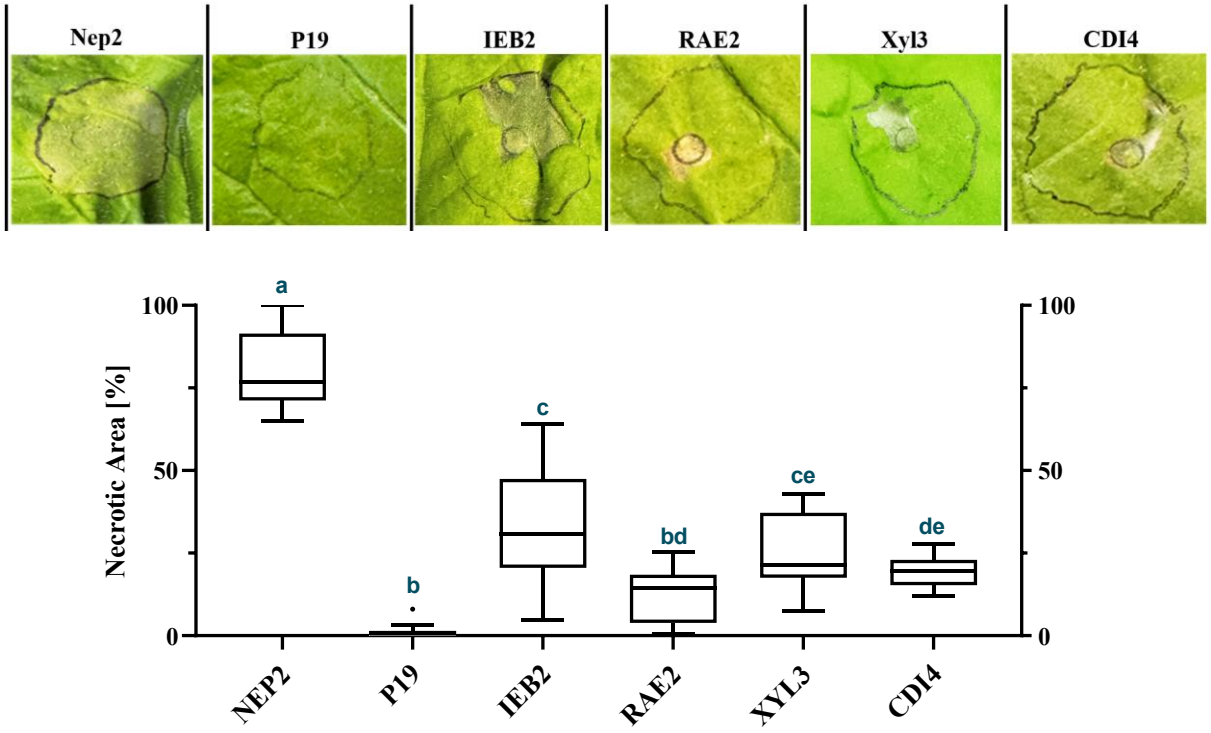

Figure 25. Phytotoxicity assay in *N. benthamiana* leaves at 5 days after agroinfiltration with pGreenGate constructs expressing the indicated CDIPs. The upper panel shows representative leaf images for each treatment, including Nep2 (positive control) and P19 (negative control). The lower panel shows the quantitative assessment of necrosis in a box and whisker plot. Different letters above the box-and-whisker plots indicate statistically significant differences among treatments ($p < 0.05$).

3.9. Role of PTI/ETI signaling in *B. cinerea* infection

Since most of the known CDIPs of *B. cinerea* are believed to function as PAMP-like molecules that activate plant PRRs, we explored whether the loss of host PTI/ETI defence signaling components would affect *B. cinerea* infection. Surprisingly, *N. benthamiana* leaves silenced for NbBAK1 or knocked out for NbSOBIR1 exhibited similar susceptibility to

either wild-type (BcWT) or Bc12xpg strains (Fig. 7; Leisen et al., 2022), indicating that these two coreceptors do not play a major role in defence against *B. cinerea*.

We next assessed whether infection by *B. cinerea* WT and a multiple CDIP deletion mutant (the Bc18x strain) are affected by key immune regulators in *N. benthamiana*. For this, an *N. benthamiana* wild-type and an *eds1 pad4 sag101a sag101b* (4x) mutant line were inoculated with either BcWT or Bc18x. As expected, the Bc18x strain induced significantly smaller lesions ($p < 0.01$) than BcWT in both plant genotypes after 72 h (Figure 26). Notably, lesion sizes induced by BcWT and Bc18x were similar on WT and 4x mutant leaves. These data indicate that EDS1/PAD1 (PTI) and EDS1/SAG101 (ETI) signaling, like BAK1 and SOBIR1, does not play a major role for infection of *N. benthamiana* by *B. cinerea* WT and a CDIP-depleted mutant.

A

B

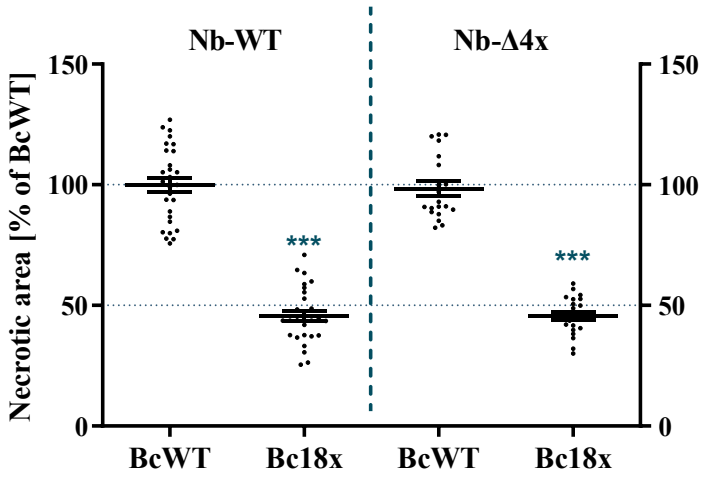

Figure 26. Lesion development in *N. benthamiana* WT and *eds1 pad4 sag101a sag101b* (4x) leaves inoculated with BcWT or Bc18x mutant *B. cinerea*. (A): Photographs of mycelium plug-inoculated leaves (48 hpi). **(B)**: Necrotic leaf areas (72 h.p.i.) Each data point in the scatter plots corresponds to a single infection site. Horizontal bars denote the mean lesion area relative to BcWT in wild-type plants (set at 100%). Asterisks (***) mark statistically significant differences between BcWT and Bc18x ($p < 0.001$). in A: write '*N.b.* WT' and '*N.b.* 4x mutant.'

In contrast, when Arabidopsis WT (Col-0) and defence mutants were inoculated with BcWT and Bc18x, lesion sizes of both strains were significantly diminished in the *eds1* mutant compared to the WT plant, and infection by the Bc18x mutant was strongly retarded compared to BcWT (Figure 27). In conclusion, the EDS1-mediated immune pathways appears to promote *B. cinerea* infection in Arabidopsis, but not in *N. benthamiana*.

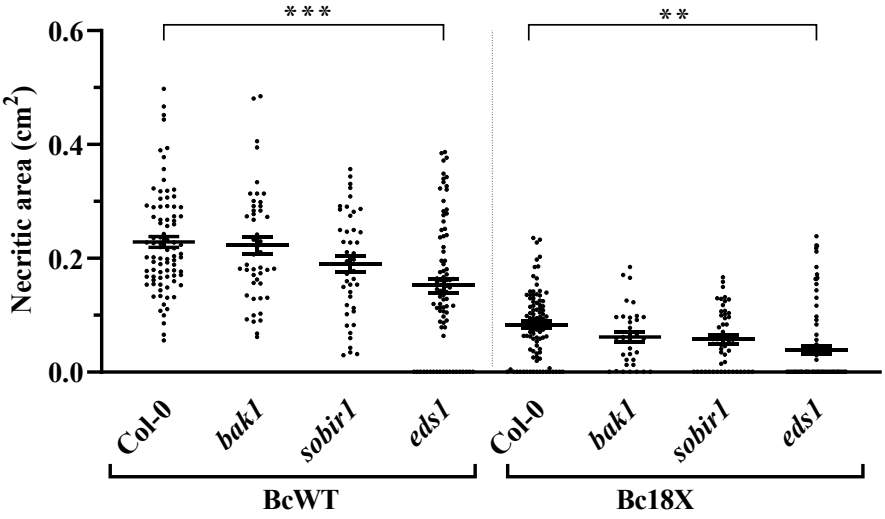

Figure 27. Lesion development in Arabidopsis WT and *bak1*, *sobir1* and *eds1* mutants inoculated with BcWT or multiple-knockout (Bc18x) *B. cinerea.* Each point in the scatter plots corresponds to a single infection site ($n \geq 15$). Horizontal bars indicate mean lesion areas. Asterisks mark statistically significant differences (**: $p < 0.01$: ***: $p < 0.001$). This experiment was conducted by Alejandra Vielba Fernandez.

4. Discussion

4.1. Marker-free mutagenesis resulting in a *B. cinerea* 29x knockout mutants

Using a marker-free CRISPR/Cas9 protocol based on ribonucleoprotein (RNP) complexes and starting with a previously generated Bc12xbb deletion strain by Leisen et al. (2022), we successfully deleted 27 CDIP and two phytotoxin genes in *B. cinerea* to create a Bc29x knockout strain. This represents the largest-scale effector knockout reported for this pathogen to date. Transformants were initially screened using PCR with gene-specific primers, confirming successful gene deletions in many cases following transient selection for fenhexamid resistance encoded by the unstable vector pTEL-fen, co-transformed alongside gene-specific RNP pairs. Sequencing typically confirmed precise excision of targeted DNA sequences. Additionally, whole-genome resequencing of selected multi-knockout mutants validated the accuracy of gene deletions, as detailed in chapter 3.6. Transformation efficiency varied significantly between different genes, as detailed in Table 36. For example, the fracions of edited mutants among the transiently fenhexamid-resistant transformants reached 94% for the *crh4* gene, whereas only 5% was achieved for *celp1*. When simultaneously targeting two genes, efficiency markedly decreased compared to single-gene knockouts and was not always achieved. Factors influencing knockout efficiency include chromatin accessibility, sgRNA sequence characteristics and GC content, epigenetic modifications, PAM site availability, genetic polymorphisms, transcriptional activity, biases in DNA repair mechanisms, and potential gene essentiality-related toxicity (Yarrington et al., 2018; Doench et al., 2016; Hsu et al., 2013; Hsu et al., 2014).

The marker-free approach avoids introducing selectable marker genes, allowing the resulting strain to serve as a valuable platform for subsequent reintroduction of individual or small groups of effectors, facilitating analysis of their specific roles in pathogenicity. However, complementation using intact genes to validate phenotypes was not feasible due to the extensive nature of the knockouts. Instead, multiple isogenic transformants were phenotypically assessed at each knockout step, and the best performing isolate in growth and infection assays was selected for subsequent rounds of transformation.

Table 36. Efficiency of targeted single and double-gene deletion transformations in *B. cinerea* mutants

Mutants used	Genotype	Gene(s) targeted for knockout	Total	Analysed by PCR	% Of Single deletion	% Of Double deletion
13x	spl1 nep1 nep2 xyn11A hip1 xyg1 plp1 ieb1 xyl1 gs1 bot2 boa6 pg1	pg1	>500	60	5%	-
15x	spl1 nep1 nep2 xyn11A hip1 xyg1 plp1 ieb1 xyl1 gs1 bot2 boa6 pg1 CDI1 Crh1	CDI1 Crh1	>1000	92	(ΔCDI)27%, (ΔCrh1)18%	4%
16x	spl1 nep1 nep2 xyn11A hip1 xyg1 plp1 ieb1 xyl1 gs1 bot2 boa6 pg1 CDI1 Crh1 CFEM1	CFEM1	>1000	60	10%	-
18x	spl1 nep1 nep2 xyn11A hip1 xyg1 plp1 ieb1 xyl1 gs1 bot2 boa6 pg1 CDI1 Crh1 CFEM1 pg2 SSP2	pg2, SSP2	>1000	48	(ΔSSP2)4%, (Δpg21)8%	2%
19x	spl1 nep1 nep2 xyn11A hip1 xyg1 plp1 ieb1 xyl1 gs1 bot2 boa6 pg1 CDI1 Crh1 CFEM1 pg2 SSP2 CDI2	CDI2	>1000	60	30%	-
20x	spl1 nep1 nep2 xyn11A hip1 xyg1 plp1 ieb1 xyl1 gs1 bot2 boa6 pg1 CDI1 Crh1 CFEM1 pg2 SSP2 CDI2 SGP1	SGP1	>1000	30	30%	-
21x	spl1 nep1 nep2 xyn11A hip1 xyg1 plp1 ieb1 xyl1 gs1 bot2 boa6 pg1 CDI1 Crh1 CFEM1 pg2 SSP2 CDI2 SGP1 Crh4	Crh4	>1000	50	94%	-
22x	spl1 nep1 nep2 xyn11A hip1 xyg1 plp1 ieb1 xyl1 gs1 bot2 boa6 pg1 CDI1 Crh1 CFEM1 pg2 SSP2 CDI2 SGP1 Crh4 XYG3	XYG3	>1000	30	20%	-
23x	spl1 nep1 nep2 xyn11A hip1 xyg1 plp1 ieb1 xyl1 gs1 bot2 boa6 pg1 CDI1 Crh1 CFEM1 pg2 SSP2 CDI2 SGP1 Crh4 XYG3 GAS5A	GAS5A	>1000	30	15%	-
24x	spl1 nep1 nep2 xyn11A hip1 xyg1 plp1 ieb1 xyl1 gs1 bot2 boa6 pg1 CDI1 Crh1 CFEM1 pg2 SSP2 CDI2 SGP1 Crh4 XYG3 GAS5A CDI3	CDI3	>1000	30	30%	-
26x	spl1 nep1 nep2 xyn11A hip1 xyg1 plp1 ieb1 xyl1 gs1 bot2 boa6 pg1 CDI1 Crh1 CFEM1 pg2 SSP2 CDI2 SGP1 Crh4 XYG3 GAS5A CDI3 RAE1 FAT1	RAE1, FAT1	>100	60	(ΔRAE1)60%, (ΔFAT1)40%	23%
27x	spl1 nep1 nep2 xyn11A hip1 xyg1 plp1 ieb1 xyl1 gs1 bot2 boa6 pg1 CDI1 Crh1 CFEM1 pg2 SSP2 CDI2 SGP1 Crh4 XYG3 GAS5A CDI3 RAE1 FAT1 Xyl2	Xyl2	>1000	30	30%	-
29x	spl1 nep1 nep2 xyn11A hip1 xyg1 plp1 ieb1 xyl1 gs1 bot2 boa6 pg1 CDI1 Crh1 CFEM1 pg2 SSP2 CDI2 SGP1 Crh4 XYG3 GAS5A CDI3 RAE1 FAT1 Xyl2 IEB2, CELP1	IEB2, CELP1	>100	30	(ΔIEB2)50%, (ΔCELP1)5%	5%

4.2. Effects of CDIP multi knockouts on in vitro growth and differentiation

Because most of the genes deleted in the multi-knockout strains, except for the two toxin biosynthesis genes, encoded secreted proteins with no essential functions for normal growth, it was hoped that even the multi-knockout mutant still showed normal growth and differentiation in vitro. However, this assumption might not hold true for the genes encoding enzymes involved in fungal cell wall remodeling such as Crh1, Crh4 and GAS5A, and their loss could also affect the growth of *B. cinerea* (Zhang et al., 2025).

Our findings confirmed potential roles for Crh4 and CELP1, which previous knockout studies identified as being involved in fungal growth and sporulation in addition to their phytotoxic activities. These genes likely participate in cell wall biosynthesis or effector-mediated interactions, with their deletion causing noticeable differences in radial growth and sporulation. Crh proteins typically dimerize, facilitating transglycosylase activities important for fungal development and structural integrity. When secreted into the apoplast, they modulate host cell death responses while maintaining fungal cell wall integrity (Bi et al., 2021). Consequently, the slower radial growth and decreased conidiation observed upon Crh4 deletion may stem from impaired chitin–β-glucan cross-linking and disrupted developmental signaling pathways (Bi et al., 2020; Liang et al., 2024). Liang et al. (2024) similarly reported that deleting BcCrh4 leads to slightly decreased colony expansion, conidia production, and sclerotia formation, and resulted in reduced virulence. In contrast, Bi et al. (2021) showed no effects from loss of BcCrh1 unless a catalytically inactive form is overexpressed, leading to reduced mycelial growth and abnormal conidiation but unchanged sclerotial formation. Our data further confirmed that although multi-knockout mutants lacking Crh4 exhibit reduced radial growth and conidiation, infection cushion and sclerotia formation remain largely unaffected. This supports the view that BcCrh4 primarily influences vegetative growth and indirectly affects disease progression through interactions with the host. The predicted structure of BcGAS5A resembles Crh-type transglycosylases, suggesting a similar function in cell wall rearrangement rather than a cumulative effect. CELP1, previously characterized as a secreted effector protein essential for infection establishment, reportedly has minimal influence on radial hyphal growth (Sharon et al., 2024). Nonetheless, Sharon et al. (2024) found decreased conidiation in *celp1* mutants, highlighting CELP1's role in asexual sporulation. Microscopic analyses also confirmed unaffected infection cushion formation, suggesting CELP1 is not essential during initial infection stages. However, Sharon et al. (2024) described notable impairment in sclerotia

development. Interestingly, our findings deviate somewhat from earlier studies, as mutants lacking CELP1 demonstrated reduced radial growth and sporulation. These discrepancies indicate that environmental conditions or strain-specific variations could substantially influence the phenotypic outcomes of CELP1 deletion. Taken together, although Bc29x exhibited moderate decreases in growth and sporulation, it retained the ability to form sclerotia, indicating that the loss of these 29 genes affects virulence more significantly than general fitness.

4.3. Effects of CDIP multi knockouts on infection of different plant hosts

Successive individual or pairwise deletions of CDIPs resulted in either no effect, weak effects, or significantly reduced virulence on at least one tested host tissue. The strongest reductions occurred when both phytotoxins or both *pg1* and *pg2* were removed, consistent with previous findings by Leisen et al. (2022). Conversely, the four-fold deletion of *spl1*, *nep1*, *nep2*, and *xyn11A* had no measurable impact on infection (Leisen et al., 2022). Similarly, deletion of most CDIPs from mutants Bc13x to Bc29x led to either negligible or weak reduction of infection, especially evident on tomato and Phaseolus bean leaves (Figure 9A and 10A).

Infection assay sensitivity was limited by the already reduced virulence of multi-knockout mutants, making further virulence reductions challenging to detect. This limitation was particularly notable in apple fruit infection assays, where virulence substantially decreased in Bc12x mutants and nearly ceased entirely in Bc18x mutants. Extending the incubation time (to 72 h for leaf infections (Figure 9-10. A) allowed a better resolution between different multi-knockout mutants. The persistent, albeit slow, lesion development after 72 h even in the Bc29x mutant indicates considerable functional redundancy within the *B. cinerea* pathogenic factors. It suggests that unknown factors can compensate for the absence of the already known CDIPs.

Overall, *B. cinerea* secretes a diverse set of toxins, CWDEs, and CDIPs whose importance varies based on the chemical and structural characteristics of the infected tissue (Leisen et al., 2022). Although successive deletion of CDIP clusters similarly reduced lesion sizes on tomato and bean leaves, these mutants became almost avirulent on apple and tomato fruits and exhibited weak aggressiveness on Arabidopsis leaves (Figure 12).

Mutants lacking 18 or more CDIPs were particularly impaired in their ability to degrade pectin-rich tissues, such as apple and tomato fruit, severely restricting their lesion

development. This underlines the necessity of coordinated pectin degradation and the generation of oligogalacturonides, potentially triggering host defence responses, including cell death (ten Have et al., 1998; Kars et al., 2005). In contrast, cellulose-rich leaves allowed limited fungal growth even after extensive gene deletions, suggesting other CWDEs or unknown factors might compensate when pectinases are unnecessary (Leisen et al., 2022). On the other hand, the analysis of *pg1 pg2* double mutants (Fig. S3 in Leisen et al., 2022) revealed a similar reduction in virulence on tomato leaves and on apple fruit, which does not support a very different role of pectin degradation in leaves and fruits.

Based on these findings, it is proposed that the role of CDIPs depends not only on their phytotoxic effects but also on their defence-inducing activity. This may result from differential recognition by plant surface receptors present only in specific host tissues. For instance, Hip1, recently characterized in our group, exhibited high toxicity only to tobacco leaves, moderate to low toxicity to Phaseolus beans and tomato, and no toxicity to Arabidopsis leaves (Jeblick et al., 2023).

One explanation for CDIP redundancy could be the broad host range of *B. cinerea*, which could be supported by a large diversity of phytotoxic factors that facilitate killing of a large range of different plant tissues (Leisen et al., 2022). However, recent comparative analyses of the genome, transcriptome, and secretome of *B. fabae*, a closely related but host-specific fungus, revealed similar complex secretome composition and toxicity profiles to *B. cinerea*, challenging this hypothesis (Klug et al., 2023). Additionally, many CDIPs are conserved across other fungi, including other Sclerotiniaceae and more distantly related groups, raising questions about their specific roles in *B. cinerea* pathogenesis.

Future studies utilizing tissue-specific RNA-seq analyses may help identify additional enzymatic or toxic activities and further clarify how *B. cinerea* infects diverse plant tissues.

4.4. Investigation of the secretome of *B. cinerea* WT and multi knockout mutants

In this study, we examined the phytotoxic potential and protein composition of secretomes from BcWT and three multigene knockout strains deficient in multiple CDIPs. Our results show a clear, dose-dependent phytotoxic effect of BcWT secretomes infiltrated into *N. benthamiana*, detectable even at low protein concentrations (0.5 µg mL^{-1}). As expected, secretomes from the knockout strains displayed reduced phytotoxicity, with the Bc29x strain, lacking 29 CDIPs, exhibiting approximately four-fold lower toxicity compared to the BcWT at a concentration of 1 µg mL^{-1} total protein.

Label-free LC-MS/MS profiling of BcWT secretomes at 26- and 48-h post-inoculation provided insight into the timing of CDIP secretion. Of the 27 targeted CDIPs, 23 were detected at both time points. Early secretomes prominently featured proteins such as BcNep1 and CELP1, while XYL1 and CFEM1 accumulated at later stages. The early presence of BcNep1 aligns with its known transient expression during initial infection stages (Cuesta Arenas et al., 2010), possibly indicating its instability or rapid degradation by host proteases. Cell wall-degrading enzymes (CWDEs), including XYN11A and polygalacturonases PG1 and PG2, remained abundant throughout infection, suggesting their ongoing roles in tissue colonization. These observations partly confirm existing understanding that secreted proteins, such as CWDEs, toxins, and necrosis-inducing factors, are critical for *B. cinerea* virulence (Williamson et al., 2007). Variation in secretome composition is likely an adaptive response. Espino et al. (2010) reported that *B. cinerea* secretes a core proteome alongside variable components influenced by environmental conditions. A clear temporal pattern was also observed. Necrosis- and ethylene-inducing proteins predominated early, likely preparing host tissues for subsequent CWDE activity that expands necrotic lesions. Even with extensive gene knockouts, residual toxicity in the Bc29x secretome indicates the presence of additional, unidentified or infection stage-specific CDIPs. Recent dual RNA-seq studies of the *B. cinerea*-Arabidopsis interaction have identified numerous candidate effectors with peak expression at distinct infection stages (Wei et al., 2024).

A comprehensive secretome analysis, perhaps combining proteomics with transcriptomics during early infection, could reveal additional CDIPs that remain active in multi-knockout strains. Future secretome research would benefit from targeted enrichment approaches. Lectin-affinity methods, such as Concanavalin-A (ConA) chromatography, can selectively isolate glycoproteins such as Spl1 and Crh4. If toxicity is primarily mediated by glycoproteins in *the B. cinerea* secretome, passing the secretome through a ConA affinity column, which binds specifically to α-d-mannosyl/α-d-glucosyl residues, could enrich glycoproteins and remove non-glycosylated proteins (Dahabiyeh et al., 2019). This approach, performed with the 29x knockout mutant, would generate a purified glycoprotein fraction suitable for further fractionation, followed by toxicity assays and LC-MS/MS analysis Consequently, this would reduce sample complexity, enhance detection of low-abundance toxic proteins, and facilitate identification of as yet unknown CDIPs of B. *cinerea*.

4.5 Functional redundancy of CDIPs in *B. cinerea*: Nep1 overexpression fails to restore virulence in a multi-gene knockout

Nep1 is among the most potent CDIPs in *B. cinerea*, capable of perforating dicot plasma membranes within minutes after treatment (Schouten et al., 2007). However, it also contains a conserved peptide motif recognized by the plant receptor RLP23, which triggers host immune responses (Seidl and Van den Ackerveken, 2019). Because Nep1 combines strong phytotoxicity with immune elicitation, we tested whether overexpressing Nep1 in a strain lacking 22 CDIPs could restore virulence. However, although Nep1 levels exceeded those in the parental mutant, plant assays showed no improvement in virulence.

This result indicates that Nep1 overexpression alone cannot compensate for the loss of multiple other CDIPs, highlighting extensive functional redundancy within the *B. cinerea* effector repertoire (Leisen et al., 2022). It was somewhat unexpected, given Nep1's high intrinsic toxicity. By comparison, overproducing another CDIP, Hip1, has been shown to produce a small but measurable increase in virulence of wild type *B. cinerea* (Jeblick et al., 2023).

Pathogenicity in *B. cinerea* appears to depend on both the total "toxic load" delivered to the host and a combination of effectors with complementary actions. Deleting up to 22 CDIP genes dramatically reduces virulence but reintroducing a single potent CDIP (Nep1) is insufficient to reach the toxicity threshold required for efficient colonization. The fact that Hip1 overproduction can modestly boost virulence suggests that each factor's mode of action and its perception by the host influence outcomes. Hip1 elicits a hypersensitive response in host plants and, when overexpressed, can tip the infection balance toward the fungus if it evades detection long enough (Jeblick et al., 2023). Hip1 may evade or suppress some defences more effectively than Nep1, whereas Nep1 is strongly detected by RLP23, activating immune responses (Seidl and Van den Ackerveken, 2019). Therefore, it might be the relative 'strengths' of the two key properties of CDIPs, namely their intrinsic toxicity and their visibility to the host immune system, which determine their role for fungal infection. Nep1's rapid membrane-perforating activity reflects high potency, but its conserved motif also serves as a microbe-associated molecular pattern recognized by RLP23, leading to reactive oxygen species production and other defences (Seidl and Van den Ackerveken, 2019). In this way, Nep1's toxic effect may be counterbalanced by a strong immune response. Future studies of Nep1 overexpression in plants lacking RLP23 will be essential to separate its purely toxic effects from its immune-eliciting consequences.

However, the situation is more complex in the case of several other CDIPs, e.g., Xyn11A for which toxicity (induction of the hypersensitive response) and plant defence induction cannot be separated.

The residual pathogenicity of the Bc22x mutant, and of Bc29x, which lacks even more CDIPs, leads to the conclusion that additional, unidentified molecules contribute to the fungus's ability to induce plant cell death. Our results emphasize that no single CDIP is essential for necrotrophy, and that *B. cinerea* employs a broad, multi-layered attack strategy. Each CDIP contributes incrementally, and together they form a "toxic cocktail" that exceeds the host's threshold for defence.

4.6. Moderate cell-death activity of newly identified *B. cinerea* CDIPs underscores effector redundancy in necrotrophic infection

In this study, five newly identified candidate CDIPs from *B. cinerea*, IEB2, RAE2, XYG3, Xyl3, and CDI4, were characterized. Recombinant proteins IEB1, IEB2, and XYG3 were produced in *E. coli* using expression vectors pET28 and pCold-TF. Both IEB1 and IEB2 accumulated successfully in soluble form under either condition, whereas XYG3 could be expressed in a soluble form only when fused with TF1. In phytotoxicity assays involving infiltration into *N. benthamiana* leaves, these proteins showed a toxicity hierarchy of BcNep2 > IEB1 ≫ IEB2 ≈ XYG3. Agrobacterium-mediated transient expression assays of IEB2, RAE2, Xyl3, and CDI4 revealed a toxicity hierarchy of Nep2 > IEB2 > Xyl3 > CDI4 ≈ RAE2. IEB2 induced moderate necrotic lesions, Xyl3 elicited weak responses, and RAE2 and CDI4 caused only marginal necrosis. IEB2 emerged as the most promising novel CDIP, but showed lower toxicity compared to its paralogue IEB1. Interestingly, IEB2 turned out to be the most specific CDIP identified for *B. cinerea* up to now: Whereas all other CDIPs are conserved at least in most sequenced members of the Sclerotiniaceae, IEB2 is largely restricted to *Botrytis* spp., and strongly induced during infection. Previously characterized IEB1 interacts with PR5-type osmotins, protecting *B. cinerea* against their antifungal activity (González et al., 2017). Given the 33% amino acid identity shared between IEB2 and IEB1, it was hypothesized that IEB2 might similarly induce phytotoxicity and might also interact with PR5. However, the phytotoxicity of IEB1 could be confined to a 35 aa peptide within the protein, but IEB2 does not contain a similar sequence and therefore might induce cell death by a different mechanism. XYG3, a homologue of the xyloglucanase BcXYG1 belonging to glycohydrolase family 12, and Xyl3, a glycohydrolase family 11 xylanase,

induced only weak damage. For BcXYG1, cell-death induction is uncoupled from catalytic activity and depends on recognition by the receptor-like kinases SOBIR1 and BAK1 (Zhu et al., 2017); whether XYG3 follows the same route remains unresolved. Likewise, the modest lesions caused by Xyl3 may reflect limited similarity to the 25-residue surface peptide that is essential for the causing necrosis in Xyn11A and Xyl2 (Frías et al., 2019). RAE2, an SGNH-hydrolase related to RAE1 (Zhang et al., 2024), and CDI4 were virtually inactive. Notably, the *M. fructicola* orthologue of CDI4 induces marked necrosis in *Prunus* spp., pointing to strict host specificity that may explain the near absence of a response observed in Solanaceae (Lopez et al., 2024). Further investigation of CDI4, RAE2 and Xyl3 is necessary before their phytotoxicity can be confirmed or not.

4.7. Interplay between Botrytis and plant PTI/ETI pathways

Plants defend against pathogens using a multilayered immune system. PTI begins when plasma-membrane PRRs bind conserved microbial patterns (PAMPs) and recruit coreceptors such as BAK1 or SOBIR1 to launch downstream defence signalling (Chinchilla et al. 2007; Liebrand et al. 2013; Ngou et al. 2022). PTI induces the oxidative burst, strengthens cell walls, and activates antimicrobial outputs without causing large-scale cell death. ETI, in contrast, is mediated by intracellular NLRs and often ends in a HR that is effective against biotrophs, but it can inadvertently aid necrotrophs by providing a dead, nutrient-rich substrate (Govrin and Levine 2000; Wang et al. 2014).

Among PTI coreceptors, BAK1 and SOBIR1 interact with various RLPs to recognize diverse PAMPs and necrosis- and ethylene-inducing peptide 1-like proteins (NLPs) secreted by pathogens (Liebrand et al., 2013; Albert et al., 2015). In particular, the RLP23–BAK1–SOBIR1 complex in Arabidopsis detects NLPs from *B. cinerea* and triggers typical PTI responses (Albert et al., 2015). Because NLPs produced by *B. cinerea* are recognized by RLP23 in conjunction with BAK1 and SOBIR1, one might expect that disrupting either coreceptor would increase plant susceptibility to this necrotroph. In our group's previous work, we tested whether silencing NbBAK1 or knocking out NbSOBIR1 in *N. benthamiana* would affect susceptibility to the BcWT and a 12-CDIP-deficient mutant (Bc12xpg) (Leisen et al., 2022). Lesion sizes in both mutants were similar in the NbBAK1-silenced and the NbSOBIR1-mutated plants to those in control plants, suggesting that BAK1- or SOBIR1-mediated PTI does not play a critical role in resistance to *B. cinerea* in this host. One explanation is that *B. cinerea* deploys a complex suite of effectors and toxins that overwhelm

PTI, or that *N. benthamiana* relies on additional receptors or defence components to restrict fungal growth.

Because ETI usually leads to cell death, we also assessed whether disabling TIR-NLR–EDS1-dependent responses would affect susceptibility. EDS1 functions downstream of TIR-NLR receptors and is essential for HR (Wiermer et al., 2005). In *N. benthamiana*, the EDS1/PAD4/SAG101 module is critical for ETI (Gantner et al., 2019). We inoculated an *N. benthamiana eds1pad4 sag101a sag101b* quadruple mutant with BcWT and a Bc18x mutant and found that lesion sizes were similar to those on wild-type plants for both fungal strains (Figure 26). Thus, disabling EDS1-dependent ETI did not alter lesion formation by *B. cinerea* in tobacco, suggesting that this branch of ETI is not a critical barrier in *N. benthamiana*. Because EDS1 also modulates parts of PTI (Feys et al. 2001; Zönnchen et al. 2022), its loss might weaken early defences, but in this necrotrophic interaction the benefit of suppressing HR appears to outweigh that cost.

To determine whether these observations hold also in Arabidopsis, we inoculated Col-0 and mutants lacking BAK1, SOBIR1, or EDS1 with BcWT and Bc18x. In Col-0, Bc18x produced significantly smaller lesions than BcWT, confirming that CDIPs contribute to fungal virulence (Figure 27). Neither *bak1* nor *sobir1* mutants showed significant differences in lesion size compared with Col-0 for either strain, indicating that BAK1- and SOBIR1-dependent PTI are not essential for limiting *B. cinerea* under our experimental conditions. By contrast, the *eds1* mutant developed significantly smaller lesions with both BcWT and Bc18x than Col-0 (Figure 27). Loss of EDS1 likely reduces HR-mediated cell death, depriving the fungus of dead tissue necessary for its growth and thereby increasing plant resistance.

Overall, in both plant hosts, PTI mediated by BAK1 or SOBIR1 was not required to limit *B. cinerea* infection, whereas in Arabidopsis, EDS1-dependent ETI appeared to increase disease severity. These results are consistent with a model in which *B. cinerea* secretes a set of overlapping CDIPs that can shift the balance of host defences. However, the real-world interaction between Botrytis and the plant's immune system is complex, and we still cannot fully explain it. To understand precisely how each CDIP activates its corresponding PRR or NLR, and how the downstream signaling in the host plant finally leads to cell death, will require further molecular dissection and detailed functional analysis.

5. Summary

The grey mould fungus *Botrytis cinerea* is a plant pathogen that attacks a wide range of host plants, causing enormous pre- and postharves damage on a large number of economically important fruits, vegetables and ornamental flowers. As a necrotroph, it quickly kills host cells and colonizes dead tissue, supported by the secretion of CWDE, cell death inducing proteins (CDIPs) and metabolites, tissue acidification and detoxification of plant defence compounds. This thesis focused on the role of CDIPs and their contribution to necrotrophic infection and killing of plant cells. The majority of CDIPs is found in the apoplast and are likely to interact with defence-related pattern recognition receptors (PRRs) that upon activation induce programmed cell death, which supports infection by *B. cinerea*. Based on a highly efficient CRISPR/Cas9 editing protocol, a consecutive mutagenesis was performed to eliminate all known CDIPs in a single *B. cinerea* strain. This resulted in series of multiple mutants lacking up to 27 CDIPs and two phytotoxic metabolites. These mutants still showed almost normal growth and differentiation in vitro but decreased virulence with increasing numbers of deleted CDIPs. Similarly, the secretomes of these mutants showed a strongly reduced phytotoxic activity compared to the wild type secretome. Genome and secretome analysis confirmed the targeted elimination of the CDIPs from the secretome and the absence of CRISPR/Cas-induced off-target mutations. The Bc29x mutant caused strongly reduced lesion formation on leaves and almost no infection of fruits of different species. Besides of the two major polygalacturonases PG1 and PG2, none of the other CDIPs made a major contribution to necrotic lesion formation on most tissues. Overexpression of the highly phytotoxic CDIP Nep1 in a multi-knockout mutant did not increase its virulence, raising doubt on a central role of CDIPs in *B. cinerea* infection. The remaining virulence and phytotoxicity of the secretome of the Bc29x mutant further confirmed an extraordinary degree of redundancy of secreted phytotoxic proteins in *B. cinerea*, and the existence of even more as yet unknown CDIPs. The search for remaining CDIPs is ongoing, with the final goal to generate a non-necrotrophic *B. cinerea* mutant. Based on their homology to known CDIPs, new CDIPs with low to moderate phytotoxic activity were discovered that are currently under investigation. To get insights into the plant defence pathways that are triggered by CDIPs and fungal infection, the sensitivity of plant mutants defective in the PRR coreceptors BAK1 and SOBR1, and the signaling protein EDS1 was investigated. Whereas the loss of BAK1 and SOBIR1 had no effect on infection, Arabidopsis *eds1* mutants showed reduced sensitivity to *B. cinerea*, confirming a positive role of EDS1 in triggering the programmed cell death of the plant cells and supporting fungal infection. This is the first systematic, large-

scale mutagenesis approach to address the functional redundancy of virulence factors in a filamentous fungus.

6. Zusammenfassung

Der Grauschimmelpilz *Botrytis cinerea* ist ein pflanzenpathogener Erreger, der ein breites Spektrum von Wirtspflanzen befällt und große Ernteausfälle bei einer Vielzahl wirtschaftlich bedeutender Obst-, Gemüse- und Zierpflanzenarten verursacht. Als nekrotropher Organismus tötet er die Wirtszellen schnell ab und besiedelt das abgestorbene Gewebe, unterstützt durch die Sekretion von zellwandabbauenden Enzymen (CWDE), zelltodinduzierenden Proteinen (CDIPs) und Metaboliten, Gewebeansäuerung und die Entgiftung pflanzlicher Abwehrmoleküle. Diese Dissertation konzentrierte sich auf die Rolle der CDIPs und ihren Beitrag zur Infektion und Abtötung pflanzlicher Wirtszellen. Die meisten CDIPs werden in den Apoplasten sekretiert und interagieren wahrscheinlich mit Mustererkennungsrezeptoren (PRRs), die nach ihrer Aktivierung den programmierten Zelltod auslösen, wodurch die Infektion durch *B. cinerea* gefördert wird. Mithilfe eines hocheffizienten CRISPR/Cas9-basierten Transformationsprotokolls wurde eine sequenzielle Mutagenese durchgeführt, um sämtliche bekannten CDIPs in einem einzigen Stamm von *B. cinerea* auszuschalten. Dies führte zu einer Serie multipler Mutanten, denen bis zu 27 CDIPs sowie zwei phytotoxische Metaboliten fehlten. Diese Mutanten zeigten ein nahezu normales Verhalten bei Wachstum und Differenzierung in vitro, jedoch eine abnehmende Virulenz mit steigender Anzahl fehlender CDIPs. Die Sekretome dieser Mutanten zeigten entsprechend eine stark reduzierte phytotoxische Aktivität im Vergleich zum Wildtyp-Sekretom. Genom- und Sekretomanalysen bestätigten die gezielte Eliminierung der CDIPs aus dem Sekretom und das weitgehende Fehlen von unerwünschten CRISPR/Cas-induzierten ‚off-target' Mutationen. Die 29-fach-Mutante verursachte stark reduzierte Läsionsbildung auf Blättern und nahezu keine Infektion mehr auf Früchten verschiedener Pflanzenarten. Neben den zwei dominierenden Polygalacturonasen PG1 und PG2 trugen keine der weiteren CDIPs wesentlich zur Läsionsbildung auf den meisten Geweben bei. Die verbliebene Virulenz und Phytotoxizität des Sekretoms der 29-fach-Mutante offenbarte einen außergewöhnlichen Grad an Redundanz sekretierter phytotoxischer Proteine bei *B. cinerea* und das Vorhandensein einer bislang unbekannten Anzahl noch nicht identifizierter CDIPs. Die Suche nach den verbleibenden CDIPs wird fortgesetzt, mit dem endgültigen Ziel, eine nicht-nekrotrophe *B. cinerea*-Mutante zu erzeugen. Basierend auf ihrer Homologie zu bereits bekannten CDIPs wurden neue CDIPs mit geringer bis mäßiger phytotoxischer Aktivität entdeckt, die derzeit weiter untersucht werden. Um Einblicke in die pflanzlichen Abwehrmechanismen zu erhalten, die durch CDIPs und die Pilzinfektion ausgelöst werden,

wurde die Empfindlichkeit von Pflanzenmutanten mit Defekten in den PRR-Corezeptoren BAK1 und SOBR1 sowie das Signalprotein EDS1 untersucht. Während der Verlust von BAK1 und SOBIR1 keine Auswirkungen auf die Infektion hatte, zeigten Arabidopsis *eds1*-Mutanten eine geringere Empfindlichkeit gegenüber *B. cinerea*, was eine positive Rolle von EDS1 bei der Auslösung des programmierten Zelltods der Pflanzenzellen und der Unterstützung der Pilzinfektion bestätigt. Diese Studie stellt den ersten systematischen und umfassenden Mutagenese-Ansatz zur Untersuchung der funktionellen Redundanz von Virulenzfaktoren in einem filamentösen Pilz dar.

7. Supplementary Information

Table S1. Genes targeted for knockout in *B. cinerea*. Gene IDs, protein sizes, and sequencing-confirmed deletion sizes/locations are shown.

KO order	Protein	Gene	Accession	Protein size	Observed	Deletion start	Deletion end	Codons deleted
1	**Spl1 ceratoplatanin**	*Bcspl1*	Bcin03g00500	137 aa	330 bp	3:185839	3:186168	24-end[3]
2	**Nep1**	*Bcnep1*	Bcin06g06720	246 aa	398 bp	6:2351724	6:2352121	34-end[3]
3	**Nep2**	*Bcnep2*	Bcin02g07770	244 aa	271 bp	2:2793732	2:2794002	80-133
4	**XYN11A ß-1,4 xylanase**	*xyn11A*	Bcin03g00480	151 aa	742 bp	14:538686	14:539427	all
5	**Hip1**	*BcHip1*	Bcin14g01200	227 aa	434 bp	3:174482	3:174915	64-end[3]
6	**XYG1 xyloglucanase**	*BcXYG1*	Bcin03g03630	248 aa	1193 bp	3:1224165	3:1225357	all
7	**PLP1 (SCFE1-VmE02)**	*Bcplp1*	Bcin10g01020	147 aa	564 bp	10:417793	10:418356	all
8	**IEB1**	*BcIEB1*	Bcin15g00100	187 aa	341 bp	15:78367	15:78707	20-115
9	**Xyl1 xylanase 1**	*Bcxyl1*	Bcin09g01800	329 aa	1239 bp	9:672899	9:674137	all
10	**GS1 glucan 1,4 α-glucosidase**	*BcGs1*	Bcin04g04190	645 aa	2344 bp	4:1491832	4:1494175	all
11	**bot2 (Botrydial)**	*Bcbot2*	Bcin12g06390	399 aa	589 bp	12:2224280	12:2224868	157-end[3]
12	**boa6 (Botcinic acid)**	*Bcboa6*	Bcin01g00060	2460 aa	2626 bp	1:18020	1:20645	661-end[3]
13	**PG1 polygalacturonase 1**	*Bcpg1*	Bcin14g00850	382 aa	1625 bp	14:371071	14:372695	all
14	**Crh1 transglycosidase**	*Bccrh1*	Bcin01g06010	391 aa	1658 bp	1:2105575	1:2107234	all
15	**CDI1**	*BcCDI1*	Bcin06g00550	205 aa	840 bp	6:239683	6:240524	all
16	**CFEM1**	*Bccfem1*	Bcin10g02180	215 aa	1333bp	10:834719	10:836050	all
17	**PG2 polygalacturonase 2**	*Bcpg2*	Bcin14g00610	374 aa	1371 bp	14:247554	14:249640	all
18	**SSP2**	BcSSP2	Bcin05g03680	90 aa		5:1329604	5:1330122	Rearrangement instead of deletion!
19	**CDI2**	*BcCDI2*	Bcin08g00400	174 aa	1285 bp	8:198700	8:200004	all
20	**SGP1**	*Bcspg1*	Bcin01g05310	300 aa	2115 bp	1:1883265	1:1885400	all
21	**Crh4 transglycosidase**	*Bccrh4*	Bcin07g04870	376 aa	2207 bp	7:1759715	7:1761929	all
22	**XYG3 xyloglucanase**	*Bcxyg3*	Bcin13g02320	353 aa	2015 bp	13:807832	13:809781	all
23	**GAS5A ß-1,3 glucanosyltransferase**	*BcGAS5A*	Bcin14g03970	457 aa	2896 bp	14:1561089	14:1563811	all
24	**CDI3**	*Bccdi3*	Bcin14g01490	295 aa	1973 bp	14:656981	14:658953	all
25	**RAE1 rhamnogalacturonan acetyltransferase**	*Bcrrae1*	Bcin02g07100	258 aa	1166 bp	2:2511511	2:2512773	all
26	**FAT1 fatty acyltransferase**	*Bcfat1*	Bcin07g03280	402 aa	1890 bp	7:1180651	7:1182560	all
27	**Glycosyl hydrolase family 11 xylanase**	*Bcxyl2*	Bcin12g00090	281 aa	1661 bp	12: 54785	12: 56295	all
28	**IEB2**	*BcIEB2*	Bcin13g00300	138 aa	1072 bp	13:146218	13:147289	all
29	**Cerato-platanin protein family**	*BcCELP1*	Bcin09g02160	232 aa	1243 bp	9:801869	9:803111	all

Table S2. Proteins identified and quantified by mass spectrometry in the *B. cinerea* WT secretome at 26 hpi and 48 hpi

	26 hpi					48 hpi				
Protein	Sample 1	Sample 2	Sample 3	Sample 4	Sample 5	Sample 1	Sample 2	Sample 3	Sample 4	Sample 5
	WT-Early-1	**WT-Early-2**	**WT-Early-3**	**WT-Early-4**	**UF-Early-WT-1**	**WT-1**	**WT-2**	**UF-WT-1**	**UF-WT-1**	**UF-WT-3**
Spl1	3,749,240	3,320,561	4,601,643	3,283,927	4,598,022	18,200,000	20,900,000	18,800,000	16,800,000	25,100,000
Nep1	852,598	305,559		1,625,677	3,473,026	0	0	0	0	0
Nep2	10,100,000	7,080,638	7,860,759	7,790,739	11,500,000	5,153,396	8,184,066	8,799,861	8,224,392	12,400,000
XYN11A	27,500,000	22,500,000	32,000,000	29,700,000	24,600,000	46,500,000	50,700,000	52,000,000	52,900,000	48,900,000
Hip1	9,106,377	4,675,499	6,167,789		6,286,492		11,200,000	9,839,713	10,400,000	11,300,000
XYG1	29,400,000	26,700,000	32,700,000	30,100,000	28,700,000	23,200,000	28,900,000	24,600,000	24,800,000	15,000,000
PLP1		834,623	1,039,934		2,324,580		1,282,421	1,446,354	1,464,181	2,274,351
IEB1	13,000,000	5,416,618	11,500,000	4,531,288	6,534,885	9,491,777	13,200,000	12,000,000	11,600,000	24,400,000
Xyl1	58,157	0	0	0	0	128,538	148,664	76,188	86,064	214,513
GS1	12,800,000	5,683,446	9,113,438	7,606,730	7,428,265	5,083,551	8,781,346	8,180,930	7,862,405	9,913,153
bot2										
boa6										
PG1	53,500,000	52,100,000	50,300,000	46,900,000	57,900,000	33,400,000	40,600,000	49,100,000	50,000,000	53,700,000
Crh1	4,662,451	3,213,811	3,788,022	2,973,792	4,175,510	2,974,415	4,234,617	3,550,312	3,321,968	5,338,670
CDI1										
CFEM1	0	0	0	0	0		40,230	864,840	857,765	236,247
PG2	50,700,000	46,800,000	49,500,000	52,800,000	55,600,000	37,400,000	36,400,000	45,400,000	46,300,000	43,800,000
SSP2		154,053	130,900	159,387	139,777				33,284	51,697
CDI2	63,903	0	72,259			64,834	161,251			237,010
SGP1	2,672,493	483,496		660,551	1,504,250		1,232,311	1,787,974	1,030,575	2,157,259
Crh4	305,330	182,934	246,647	165,327	291,205	361,718	547,464	350,563	362,793	781,379
XYG3	13,100,000	5,587,950	9,404,970	6,403,512	5,955,890	17,400,000	19,400,000	24,400,000	23,600,000	16,800,000
GAS5A	5,352,604	3,162,668	3,427,232	2,848,431	3,744,665	2,985,767	3,024,536	3,770,732	3,999,610	4,434,174
CDI3										
RAE1	22,200,000	12,700,000	18,700,000	15,300,000	12,800,000	21,500,000	22,100,000	29,500,000	30,400,000	27,800,000
FAT1	3,905,739	1,059,573	2,380,932	1,752,126	1,666,177	1,657,821	2,767,759	8,302,283	7,985,619	3,904,087
Xyl2	176,508		381,541	211,092	129,553	717,752	1,826,821	2,091,985	2,160,163	2,050,622
IEB2	2,297,455	1,259,646	1,176,297	1,111,041	1,436,077	1,454,898	2,297,332	5,890,109	6,018,617	4,537,791
CELP1	83,740	137,925	59,661	185,678	581,815	0	0	0	0	0

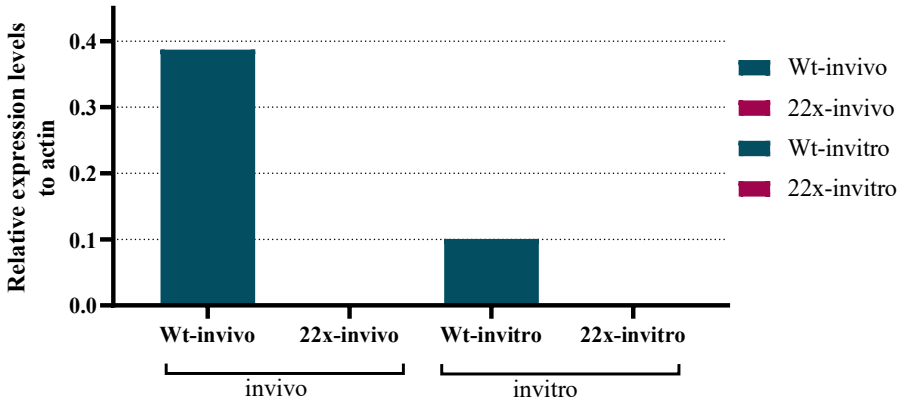

Figure S1. qRT-PCR analysis of *BcSSP2* disruption in *B. cinerea* Bc22x. Relative *BcSSP2* transcript levels were measured in BcWT and Bc22x cultures under *in vivo* (tomato leaf) and *in vitro* (Gamborg + pectin) conditions. Expression was normalized to *actin*. Significantly lower *BcSSP2* levels in Bc22x confirm its disruption.

Figure S2. "Shiny" phenotype on the abaxial leaf surface of *N. benthamiana* at 3 days post-Agrobacterium infiltration with CDIP candidates, but not in control leaves.

8. List of Abbreviations

Abbreviation	Meaning
CDIP	Cell death–inducing protein
CDPK	Calcium dependent protein kinase
CWDE	Cell wall degrading enzyme
dNTPs	Deoxyribonucleotide triphosphate
dpi	Days post infiltration / inoculation
DTT	Dithiothreitol
EDTA	Ethylenediaminetetraacetic acid
ETI	Effector triggered immunity
GFP	Green fluorescence protein
HR	Hypersensitive response
HSB	High Salt Buffer
HSE	High Salt Elution Buffer
HSW	High Salt Wash Buffer
IPTG	Isopropyl β-d-1-thiogalactopyranoside
LC MS/MS	Liquid Chromatography-Tandem Mass Spectrometry
LB	Luria broth
MAPK	Mitogen-activated protein kinase
NLR	Nucleotide-binding domain leucine-rich repeat containing receptor
NLPs	Necrosis- and Ethylene-Inducing Peptide 1-Like Lroteins
PAMP	Pathogen associated molecular pattern
PBS	Phosphate-buffered saline
PCD	Programmed cell death
PRR	Pattern recognition receptor
PTI	PAMP triggered immunity
qRT-PCR	Quantitative real-time polymerase chain reaction
RLCK	Receptor-like cytoplasmic kinase
RLK	Receptor like kinase
RLP	Receptor like protein
RNL	RPW8-like CC domain nucleotide-binding domain leucine-rich repeat containing receptor
ROS	Reactive oxygen species
RT	Room temperature
RT-qPCR	Real time quantitative polymerase chain reaction
SDS-PAGE	Sodium Dodecyl Sulfate Polyacrylamide Gel Electrophoresis
TAE	Tris Acetate EDTA
TF	Transcription factor
TIR	Toll/Interleukin-1 receptor/Resistance protein
TNL	Toll/Interleukin-1 receptor/Resistance protein nucleotide-binding domain leucine-rich repeat containing receptor
WT	Wild Type

9. References

Agrios, George N. (2005): Plant pathology. 5th ed., [3rd print]. Amsterdam: Elsevier Academic Press. http://www.loc.gov/catdir/description/els051/2004011924.html.

Albert, Isabell; Böhm, Hannah; Albert, Markus; Feiler, Christina E.; Imkampe, Julia; Wallmeroth, Niklas et al. (2015): An RLP23-SOBIR1-BAK1 complex mediates NLP-triggered immunity. *Nature plants* 1, S. 15140. DOI: 10.1038/nplants.2015.140.

Atwell, Susanna; Corwin, Jason A.; Soltis, Nicole E.; Subedy, Anushryia; Denby, Katherine J.; Kliebenstein, Daniel J. (2015): Whole genome resequencing of Botrytis cinerea isolates identifies high levels of standing diversity. *Frontiers in microbiology* 6, S. 996. DOI: 10.3389/fmicb.2015.00996.

Bi, Kai; Liang, Yong; Mengiste, Tesfaye; Sharon, Amir (2023): Killing softly: a roadmap of Botrytis cinerea pathogenicity. *Trends in plant science* 28 (2), S. 211–222. DOI: 10.1016/j.tplants.2022.08.024.

Bi, Kai; Scalschi, Loredana; Jaiswal, Namrata; Mengiste, Tesfaye; Fried, Renana; Sanz, Ana Belén et al. (2021): The Botrytis cinerea Crh1 transglycosylase is a cytoplasmic effector triggering plant cell death and defence response. *Nature communications* 12 (1), S. 2166. DOI: 10.1038/s41467-021-22436-1

Brito, Nélida; Espino, José Juan; González, Celedonio (2006): The endo-beta-1,4-xylanase xyn11A is required for virulence in Botrytis cinerea. *Molecular plant-microbe interactions* 19 (1), S. 25–32. DOI: 10.1094/MPMI-19-0025.

Cai, Qiang; He, Baoye; Kogel, Karl-Heinz; Jin, Hailing (2018): Cross-kingdom RNA trafficking and environmental RNAi-nature's blueprint for modern crop protection strategies. *Current opinion in microbiology* 46, S. 58–64. DOI: 10.1016/j.mib.2018.02.003.

Cheung, Nicholas; Tian, Lei; Liu, Xueru; Li, Xin (2020): The Destructive Fungal Pathogen Botrytis cinerea-Insights from Genes Studied with Mutant Analysis. *Pathogens (Basel, Switzerland)* 9 (11). DOI: 10.3390/pathogens9110923.

Chinchilla, Delphine; Zipfel, Cyril; Robatzek, Silke; Kemmerling, Birgit; Nürnberger, Thorsten; Jones, Jonathan D. G. et al. (2007): A flagellin-induced complex of the receptor FLS2 and BAK1 initiates plant defence. *Nature* 448 (7152), S. 497–500. DOI: 10.1038/nature05999.

Choquer, Mathias; Fournier, Elisabeth; Kunz, Caroline; Levis, Caroline; Pradier, Jean-Marc; Simon, Adeline; Viaud, Muriel (2007): Botrytis cinerea virulence factors: new insights into a necrotrophic and polyphageous pathogen. *FEMS microbiology letters* 277 (1), S. 1–10. DOI: 10.1111/j.1574-6968.2007.00930.x.

Choquer, Mathias; Rascle, Christine; Gonçalves, Isabelle R.; Vallée, Amélie de; Ribot, Cécile; Loisel, Elise et al. (2021): The infection cushion of Botrytis cinerea: a fungal 'weapon' of plant-biomass destruction. *Environmental microbiology* 23 (4), S. 2293–2314. DOI: 10.1111/1462-2920.15416.

Cuesta Arenas, Yaite; Kalkman, Eric R.I.C.; Schouten, Alexander; Dieho, Mirjam; Vredenbregt, P.; Uwumukiza, Beatrice et al. (2010): Functional analysis and mode of action of phytotoxic Nep1-like proteins of Botrytis cinerea. *Physiol. Mol. Plant Pathol.* (74), S. 376–386.

Dahabiyeh, Lina A.; Tooth, David; Barrett, David A. (2019): Profiling of 54 plasma glycoproteins by label-free targeted LC-MS/MS. *Analytical biochemistry* 567, S. 72–81. DOI: 10.1016/j.ab.2018.12.011.

Dalmais, Bérengère; Schumacher, Julia; Moraga, Javier; Le Pêcheur, Pascal; Tudzynski, Bettina; Collado, Isidro Gonzalez; Viaud, Muriel (2011): The Botrytis cinerea phytotoxin botcinic acid requires two polyketide synthases for production and has a redundant role in virulence with botrydial. *Molecular plant pathology* 12 (6), S. 564–579. DOI: 10.1111/j.1364-3703.2010.00692.x.

Deacon, Jim W. (2006): Fungal biology. 4th edition. Malden, MA: Blackwell Publishing. Online verfügbar unter http://www.loc.gov/catdir/enhancements/fy0802/2005004137-b.html.

Dean, Ralph; van Kan, Jan A. L.; Pretorius, Zacharias A.; Hammond-Kosack, Kim E.; Di Pietro, Antonio; Spanu, Pietro D. et al. (2012): The Top 10 fungal pathogens in molecular plant pathology. *Molecular plant pathology* 13 (4), S. 414–430. DOI: 10.1111/j.1364-3703.2011.00783.x.

Denton-Giles, Matthew; McCarthy, Hannah; Sehrish, Tina; Dijkwel, Yasmin; Mesarich, Carl H.; Bradshaw, Rosie E. et al. (2020): Conservation and expansion of a necrosis-inducing small secreted protein family from host-variable phytopathogens of the Sclerotiniaceae. *Molecular plant pathology* 21 (4), S. 512–526. DOI: 10.1111/mpp.12913.

Doench, John G.; Fusi, Nicolo; Sullender, Meagan; Hegde, Mudra; Vaimberg, Emma W.; Donovan, Katherine F. et al. (2016): Optimized sgRNA design to maximize activity and minimize off-target effects of CRISPR-Cas9. *Nature biotechnology* 34 (2), S. 184–191. DOI: 10.1038/nbt.3437.

Doss, R. P.; Potter, S. W.; Chastagner, G. A.; Christian, J. K. (1993): Adhesion of Nongerminated Botrytis cinerea Conidia to Several Substrata. *Applied and environmental microbiology* 59 (6), S. 1786–1791. DOI: 10.1128/aem.59.6.1786-1791.1993.

Doss, R. P.; Potter, S. W.; Soeldner, A. H.; Christian, J. K.; Fukunaga, L. E. (1995): Adhesion of germlings of Botrytis cinerea. *Applied and environmental microbiology* 61 (1), S. 260–265. DOI: 10.1128/aem.61.1.260-265.1995.

D'Ovidio, Renato; Mattei, Benedetta; Roberti, Serena; Bellincampi, Daniela (2004): Polygalacturonases, polygalacturonase-inhibiting proteins and pectic oligomers in plant-pathogen interactions. *Biochimica et biophysica acta* 1696 (2), S. 237–244. DOI: 10.1016/j.bbapap.2003.08.012.

Elad Y; Pertot I; Prado AMC; Stewart A (2016): Plant hosts of *Botrytis* spp. *Elad Y; Vivier M; Fillinger S (ed), Botrytis, the good, the bad*, S. 413–486.

Espino, José J.; Gutiérrez-Sánchez, Gerardo; Brito, Nélida; Shah, Punit; Orlando, Ron; González, Celedonio (2010): The Botrytis cinerea early secretome. *Proteomics* 10 (16), S. 3020–3034. DOI: 10.1002/pmic.201000037.

Fang, Wenxia; Sanz, Ana Belén; Bartual, Sergio Galan; Wang, Bin; Ferenbach, Andrew T.; Farkaš, Vladimír et al. (2019): Mechanisms of redundancy and specificity of the Aspergillus fumigatus Crh transglycosylases. *Nature communications* 10 (1), S. 1669. DOI: 10.1038/s41467-019-09674-0.

Feys, B. J.; Moisan, L. J.; Newman, M. A.; Parker, J. E. (2001): Direct interaction between the Arabidopsis disease resistance signaling proteins, EDS1 and PAD4. *The EMBO journal* 20 (19), S. 5400–5411. DOI: 10.1093/emboj/20.19.5400.

Fillinger, Sabine (Hg.) (2018): Botrytis – the Fungus, the Pathogen and its Management in Agricultural Systems. Springer International Publishing. Softcover reprint of the original 1st edition 2016. Cham: Springer International Publishing; Springer.

Franco-Orozco, Barbara; Berepiki, Adokiye; Ruiz, Olaya; Gamble, Louise; Griffe, Lucie L.; Wang, Shumei et al. (2017): A new proteinaceous pathogen-associated molecular pattern (PAMP) identified in Ascomycete fungi induces cell death in Solanaceae. *The New phytologist* 214 (4), S. 1657–1672. DOI: 10.1111/nph.14542.

Frías, Marcos; González, Celedonio; Brito, Nélida (2011): BcSpl1, a cerato-platanin family protein, contributes to Botrytis cinerea virulence and elicits the hypersensitive response in the host. *The New phytologist* 192 (2), S. 483–495. DOI: 10.1111/j.1469-8137.2011.03802.x.

Frías, Marcos; Brito, Nélida; González, Mario; González, Celedonio (2014): The phytotoxic activity of the cerato-platanin BcSpl1 resides in a two-peptide motif on the protein surface. *Molecular plant pathology* 15 (4), S. 342–351. DOI: 10.1111/mpp.12097.

Frías, Marcos; González, Mario; González, Celedonio; Brito, Nélida (2016): BcIEB1, a Botrytis cinerea secreted protein, elicits a defence response in plants. *Plant science: an international journal of experimental plant biology* 250, S. 115–124. DOI: 10.1016/j.plantsci.2016.06.009.

Frías, Marcos; González, Mario; González, Celedonio; Brito, Nélida (2019): A 25-Residue Peptide From Botrytis cinerea Xylanase BcXyn11A Elicits Plant Defences. *Frontiers in plant science* 10. DOI: 10.3389/fpls.2019.00474.

Gantner, Johannes; Ordon, Jana; Kretschmer, Carola; Guerois, Raphaël; Stuttmann, Johannes (2019): An EDS1-SAG101 Complex Is Essential for TNL-Mediated Immunity in Nicotiana benthamiana. *The Plant cell* 31 (10), S. 2456–2474. DOI: 10.1105/tpc.19.00099.

Gao, Yuhan; Li, Ze; Yang, Chenyu; Li, Guangyue; Zeng, Hongmei; Li, Zhonghai et al. (2022): Pseudomonas syringae activates ZAT18 to inhibit salicylic acid accumulation by repressing EDS1 transcription for bacterial infection. *The New phytologist* 233 (3), S. 1274–1288. DOI: 10.1111/nph.17870.

González, Mario; Brito, Nélida; González, Celedonio (2014): Identification of glycoproteins secreted by wild-type Botrytis cinerea and by protein O-mannosyltransferase mutants. *BMC microbiology* 14. DOI: 10.1186/s12866-014-0254-y.

González, Mario; Brito, Nélida; González, Celedonio (2017): The Botrytis cinerea elicitor protein BcIEB1 interacts with the tobacco PR5-family protein osmotin and protects the fungus against its antifungal activity. *The New phytologist* 215 (1), S. 397–410. DOI: 10.1111/nph.14588.

Gourgues, M.; Brunet-Simon, A.; Lebrun, M-H; Levis, C. (2004): The tetraspanin BcPls1 is required for appressorium-mediated penetration of Botrytis cinerea into host plant leaves. *Molecular microbiology* 51 (3), S. 619–629. DOI: 10.1046/j.1365-2958.2003.03866.x.

Govrin, E. M.; Levine, A. (2000): The hypersensitive response facilitates plant infection by the necrotrophic pathogen Botrytis cinerea. *Current biology: CB* 10 (13), S. 751–757. DOI: 10.1016/s0960-9822(00)00560-1.

Hahn, Matthias (2014): The rising threat of fungicide resistance in plant pathogenic fungi: Botrytis as a case study. *Journal of chemical biology* 7 (4), S. 133–141. DOI: 10.1007/s12154-014-0113-1.

Have, A. ten; Mulder, W.; Visser, J.; van Kan, J. A. (1998): The endopolygalacturonase gene Bcpg1 is required for full virulence of Botrytis cinerea. *Molecular plant-microbe interactions: MPMI* 11 (10), S. 1009–1016. DOI: 10.1094/MPMI.1998.11.10.1009.

Hsu, Patrick D.; Lander, Eric S.; Zhang, Feng (2014): Development and applications of CRISPR-Cas9 for genome engineering. *Cell* 157 (6), S. 1262–1278. DOI: 10.1016/j.cell.2014.05.010.

Hsu, Patrick D.; Scott, David A.; Weinstein, Joshua A.; Ran, F. Ann; Konermann, Silvana; Agarwala, Vineeta et al. (2013): DNA targeting specificity of RNA-guided Cas9 nucleases. *Nature biotechnology* 31 (9), S. 827–832. DOI: 10.1038/nbt.2647.

Jarvis, William R. (1977): Botryotinia and botrytis species. Taxonomy, physiology and pathogenicity; a guide to the literature. Ottawa: Canada Department of Agriculture Research Branch (Monograph / Canada Departement of Agriculture, 15).

Jeblick, Tanja; Leisen, Thomas; Steidele, Christina E.; Albert, Isabell; Müller, Jonas; Kaiser, Sabrina et al. (2023): Botrytis hypersensitive response inducing protein 1 triggers noncanonical PTI to induce plant cell death. *Plant physiology* 191 (1), S. 125–141. DOI: 10.1093/plphys/kiac476.

Jones, Jonathan D. G.; Dangl, Jeffery L. (2006): The plant immune system. *Nature* 444 (7117), S. 323–329. DOI: 10.1038/nature05286.

Kars, Ilona; Krooshof, Geja H.; Wagemakers, Lia; Joosten, Rob; Benen, Jacques A. E.; van Kan, Jan A. L. (2005): Necrotizing activity of five Botrytis cinerea endopolygalacturonases produced in Pichia pastoris. *The Plant journal: for cell and molecular biology* 43 (2), S. 213–225. DOI: 10.1111/j.1365-313X.2005.02436.x.

Kliebenstein, D. J.; Rowe H.C. (2008): Ecological costs of biotrophic versus necrotrophic pathogen resistance, the hypersensitive response and signal transduction. *Plant Science* 174.6, S. 551–556.

Klug, Klaus; Zhu, Pinkuan; Pattar, Patrick; Mueller, Tobias; Safari, Nassim; Sommer, Frederik et al. (2024): Genome Comparisons between Botrytis fabae and the Closely Related Gray Mold Fungus Botrytis cinerea Reveal Possible Explanations for Their Contrasting Host Ranges. *Journal of Fungi* 10 (3). DOI: 10.3390/jof10030216.

Lai, Zhibing; Wang, Fei; Zheng, Zuyu; Fan, Baofang; Chen, Zhixiang (2011): A critical role of autophagy in plant resistance to necrotrophic fungal pathogens. *The Plant journal: for cell and molecular biology* 66 (6), S. 953–968. DOI: 10.1111/j.1365-313X.2011.04553.x.

Lampropoulos, Athanasios; Sutikovic, Zoran; Wenzl, Christian; Maegele, Ira; Lohmann, Jan U.; Forner, Joachim (2013): GreenGate---a novel, versatile, and efficient cloning system for plant transgenesis. *PloS one* 8 (12), e83043. DOI: 10.1371/journal.pone.0083043.

Leisen, Thomas; Bietz, Fabian; Werner, Janina; Wegner, Alex; Schaffrath, Ulrich; Scheuring, David et al. (2020): CRISPR/Cas with ribonucleoprotein complexes and transiently selected telomere vectors allows highly efficient marker-free and multiple genome editing in Botrytis cinerea. *PLoS Pathogens* 16 (8), e1008326. DOI: 10.1371/journal.ppat.1008326.

Leisen, Thomas; Werner, Janina; Pattar, Patrick; Safari, Nassim; Ymeri, Edita; Sommer, Frederik et al. (2022): Multiple knockout mutants reveal a high redundancy of phytotoxic compounds contributing to necrotrophic pathogenesis of Botrytis cinerea. Kaiserslautern: Technische Universität Kaiserslautern, Kaiserslautern - Fachbereich Biologie.

Lenarčič, Tea; Albert, Isabell; Böhm, Hannah; Hodnik, Vesna; Pirc, Katja; Zavec, Apolonija B. et al. (2017): Eudicot plant-specific sphingolipids determine host selectivity of microbial NLP cytolysins. *Science (New York, N.Y.)* 358 (6369), S. 1431–1434. DOI: 10.1126/science.aan6874.

Liang, Yong; Bi, Kai; Sharon, Amir (2024): The Botrytis cinerea transglycosylase BcCrh4 is a cell death-inducing protein with cell death-promoting and -suppressing domains. *Plant, cell & environment* 47 (1), S. 354–371. DOI: 10.1111/pce.14740.

Liebrand, T.W.H.; van den Burg, H. A.; Joosten, M.H.A.J. (2014): Two for all: receptor-associated kinases SOBIR1 and BAK1. *Trends in plant science* 19.2., S. 123–132.

Maddi, Abhiram; Free, Stephen J. (2010): α-1,6-Mannosylation of N-linked oligosaccharide present on cell wall proteins is required for their incorporation into the cell wall in the filamentous fungus Neurospora crassa. *Eukaryotic cell* 9 (11), S. 1766–1775. DOI: 10.1128/EC.00134-10.

Mali, Prashant; Yang, Luhan; Esvelt, Kevin M.; Aach, John; Guell, Marc; DiCarlo, James E. et al. (2013): RNA-guided human genome engineering via Cas9. *Science (New York, N.Y.)* 339 (6121), S. 823–826. DOI: 10.1126/science.1232033.

Müller, Nathalie; Leroch, Michaela; Schumacher, Julia; Zimmer, David; Könnel, Anne; Klug, Klaus et al. (2018): Investigations on VELVET regulatory mutants confirm the role of host tissue acidification and secretion of proteins in the pathogenesis of Botrytis cinerea. *The New phytologist* 219 (3), S. 1062–1074. DOI: 10.1111/nph.15221.

Newman, Toby E.; Kim, Haseong; Khentry, Yuphin; Sohn, Kee Hoon; Derbyshire, Mark C.; Kamphuis, Lars G. (2023): The broad host range pathogen Sclerotinia sclerotiorum produces multiple effector proteins that induce host cell death intracellularly. *Molecular plant pathology* 24 (8), S. 866–881. DOI: 10.1111/mpp.13333.

Ngou, Bruno Pok Man; Ding, Pingtao; Jones, Jonathan D. G. (2022): Thirty years of resistance: Zig-zag through the plant immune system. *The Plant cell* 34 (5), S. 1447–1478. DOI: 10.1093/plcell/koac041.

Nie, Jiajun; Zhou, Wenjing; Liu, Jianying; Tan, Ni; Zhou, Jian-Min; Huang, Lili (2021): A receptor-like protein from Nicotiana benthamiana mediates VmE02 PAMP-triggered immunity. *The New phytologist* 229 (4), S. 2260–2272. DOI: 10.1111/nph.16995.

Noda, Judith; Brito, Nélida; González, Celedonio (2010): The Botrytis cinerea xylanase Xyn11A contributes to virulence with its necrotizing activity, not with its catalytic activity. *BMC plant biology* 10, S. 38. DOI: 10.1186/1471-2229-10-38.

Nødvig, Christina S.; Nielsen, Jakob B.; Kogle, Martin E.; Mortensen, Uffe H. (2015): A CRISPR-Cas9 System for Genetic Engineering of Filamentous Fungi. *PloS one* 10 (7), e0133085. DOI: 10.1371/journal.pone.0133085.

Ottmann, Christian; Luberacki, Borries; Küfner, Isabell; Koch, Wolfgang; Brunner, Frédéric; Weyand, Michael et al. (2009): A common toxin fold mediates microbial attack and plant defence. *Proceedings of the National Academy of Sciences of the United States of America* 106 (25), S. 10359–10364. DOI: 10.1073/pnas.0902362106.

Pinedo, Cristina; Wang, Chieh-Mei; Pradier, Jean-Marc; Dalmais, Bérengère; Choquer, Mathias; Le Pêcheur, Pascal et al. (2008): Sesquiterpene synthase from the botrydial biosynthetic gene cluster of the phytopathogen Botrytis cinerea. *ACS chemical biology* 3 (12), S. 791–801. DOI: 10.1021/cb800225v.

Porquier, Antoine; Moraga, Javier; Morgant, Guillaume; Dalmais, Bérengère; Simon, Adeline; Sghyer, Hind et al. (2019): Botcinic acid biosynthesis in Botrytis cinerea relies on a subtelomeric gene cluster surrounded by relics of transposons and is regulated by the Zn2Cys6 transcription factor BcBoa13. *Current genetics* 65 (4), S. 965–980. DOI: 10.1007/s00294-019-00952-4.

Porquier, Antoine; Morgant, Guillaume; Moraga, Javier; Dalmais, Bérengère; Luyten, Isabelle; Simon, Adeline et al. (2016): The botrydial biosynthetic gene cluster of Botrytis cinerea displays a bipartite genomic structure and is positively regulated by the putative Zn(II)2Cys6 transcription factor BcBot6. *Fungal genetics and biology: FG & B* 96, S. 33–46. DOI: 10.1016/j.fgb.2016.10.003.

Porquier, Antoine; Tisserant, Constance; Salinas, Francisco; Glassl, Carla; Wange, Lucas; Enard, Wolfgang et al. (2021): Retrotransposons as pathogenicity factors of the plant pathogenic fungus Botrytis cinerea. *Genome biology* 22 (1), S. 225. DOI: 10.1186/s13059-021-02446-4.

Porquier, Antoine; Tisserant, Constance; Salinas, Francisco; Glassl, Carla; Wange, Lucas; Enard, Wolfgang et al. (2021): Retrotransposons as pathogenicity factors of the plant pathogenic fungus Botrytis cinerea. *Genome biology* 22 (1), S. 225. DOI: 10.1186/s13059-021-02446-4.

Qin, Si; Veloso, Javier; Baak, Mirna; Boogmans, Britt; Bosman, Tim; Puccetti, Guido et al. (2023): Molecular characterization reveals no functional evidence for naturally occurring cross-kingdom RNA interference in the early stages of Botrytis cinerea-tomato interaction. *Molecular plant pathology* 24 (1), S. 3–15. DOI: 10.1111/mpp.13269.

Qutob, Dinah; Kemmerling, Birgit; Brunner, Frédéric; Küfner, Isabell; Engelhardt, Stefan; Gust, Andrea A. et al. (2006): Phytotoxicity and innate immune responses induced by Nep1-like proteins. *The Plant cell* 18 (12), S. 3721–3744. DOI: 10.1105/tpc.106.044180.

Ron, Mily; Avni, Adi (2004): The Receptor for the Fungal Elicitor Ethylene-Inducing Xylanase Is a Member of a Resistance-Like Gene Family in Tomato. *The Plant cell* 16 (6), S. 1604–1615. DOI: 10.1105/tpc.022475.

Rowe, Heather C.; Kliebenstein, Daniel J. (2007): Elevated genetic variation within virulence-associated Botrytis cinerea polygalacturonase loci. *Molecular plant-microbe interactions: MPMI* 20 (9), S. 1126–1137. DOI: 10.1094/MPMI-20-9-1126.

Schouten, Alexander; van Baarlen, Peter; van Kan, Jan A. L. (2008): Phytotoxic Nep1-like proteins from the necrotrophic fungus Botrytis cinerea associate with membranes and the nucleus of plant cells. *The New phytologist* 177 (2), S. 493–505. DOI: 10.1111/j.1469-8137.2007.02274. x.

Schuster, Mariana; Kahmann, Regine (2019): CRISPR-Cas9 genome editing approaches in filamentous fungi and oomycetes. *Fungal genetics and biology: FG & B* 130, S. 43–53. DOI: 10.1016/j.fgb.2019.04.016.

Seidl, Michael F.; van den Ackerveken, Guido (2019): Activity and Phylogenetics of the Broadly Occurring Family of Microbial Nep1-Like Proteins. *Annual review of phytopathology*. DOI: 10.1146/annurev-phyto-082718-100054.

Seifbarghi, Shirin; Borhan, Mohammad Hossein; Wei, Yangdou; Ma, Lisong; Coutu, Cathy; Bekkaoui, Diana; Hegedus, Dwayne D. (2020): Receptor-Like Kinases BAK1 and SOBIR1 Are Required for Necrotizing Activity of a Novel Group of Sclerotinia sclerotiorum Necrosis-Inducing Effectors. *Frontiers in plant science* 11. DOI: 10.3389/fpls.2020.01021.

Shalem, Ophir; Sanjana, Neville E.; Hartenian, Ella; Shi, Xi; Scott, David A.; Mikkelson, Tarjei et al. (2014): Genome-scale CRISPR-Cas9 knockout screening in human cells. *Science (New York, N.Y.)* 343 (6166), S. 84–87. DOI: 10.1126/science.1247005.

Sharon, Amir et al. (2024): A secreted Botrytis cinerea stage-specific effector promotes virulence by targeting the plant ROS-generating machinery. *Research Square (preprint)*. DOI: 10.21203/rs.3.rs-4918366/v1.

Shlezinger, Neta; Goldfinger, Nir; Sharon, Amir (2012): Apoptotic-like programed cell death in fungi: the benefits in filamentous species. *Frontiers in oncology* 2, S. 97. DOI: 10.3389/fonc.2012.00097.

Song, Tianqiao; Zhang, You; Zhang, Qi; Zhang, Xiong; Shen, Danyu; Yu, Junjie et al. (2021): The N-terminus of an Ustilaginoidea virens Ser-Thr-rich glycosylphosphatidylinositol-anchored protein elicits plant immunity as a MAMP. *Nature communications* 12 (1), S. 2451. DOI: 10.1038/s41467-021-22660-9.

Spada, Maria; Pugliesi, Claudio; Fambrini, Marco; Pecchia, Susanna (2024): Challenges and Opportunities Arising from Host-Botrytis cinerea Interactions to Outline Novel and Sustainable Control Strategies: The Key Role of RNA Interference. *International journal of molecular sciences* 25 (12). DOI: 10.3390/ijms25126798.

van Kan, Jan A. L. (2006): Licensed to kill: the lifestyle of a necrotrophic plant pathogen. *Trends in plant science* 11 (5), S. 247–253. DOI: 10.1016/j.tplants.2006.03.005.

Veloso, Javier; van Kan, Jan A. L. (2018): Many Shades of Grey in Botrytis-Host Plant Interactions. *Trends in plant science* 23 (7), S. 613–622. DOI: 10.1016/j.tplants.2018.03.016.

Vignatti, Paulina; Gonzalez, María E.; Jofré, Edgardo C.; Bolívar-Anillo, Hernando J.; Moraga, Javier; Viaud, Muriel et al. (2020): Botrydial confers Botrytis cinerea the ability to antagonize soil and phyllospheric bacteria. *Fungal biology* 124 (1), S. 54–64. DOI: 10.1016/j.funbio.2019.11.003.

Wang, Xuli; Jiang, Nan; Liu, Jinling; Liu, Wende; Wang, Guo-Liang (2014): The role of effectors and host immunity in plant-necrotrophic fungal interactions. *Virulence* 5 (7), S. 722–732. DOI: 10.4161/viru.29798.

Wang, Pei; Wang, Yabo; Hu, Yawen; Chen, Ziyang; Han, Lili; Zhu, Wenjun et al. (2024): Plant hypersensitive induced reaction protein facilitates cell death induced by secreted xylanase associated with the pathogenicity of Sclerotinia sclerotiorum. *The Plant journal: for cell and molecular biology* 118 (1), S. 90–105. DOI: 10.1111/tpj.16593.

Wang, Ming; Weiberg, Arne; Lin, Feng-Mao; Thomma, Bart P. H. J.; Huang, Hsien-Da; Jin, Hailing (2016): Bidirectional cross-kingdom RNAi and fungal uptake of external RNAs confer plant protection. *Nature plants* 2, S. 16151. DOI: 10.1038/nplants.2016.151.

Wang, Yan; Xu, Yuanpeng; Sun, Yujing; Wang, Huibin; Qi, Jiaming; Wan, Bowen et al. (2018): Leucine-rich repeat receptor-like gene screen reveals that Nicotiana RXEG1 regulates glycoside hydrolase 12 MAMP detection. *Nature communications* 9 (1), S. 594. DOI: 10.1038/s41467-018-03010-8.

Webster, John; Weber, Roland (2009): Introduction to fungi. 3. ed., repr. Cambridge: Cambridge Univ. Press. http://www.loc.gov/catdir/enhancements/fy0703/2006036496-d.html.

Wei, Jinfeng; Zhou, Qian; Zhang, Jing; Wu, Mingde; Li, Guoqing; Yang, Long (2024): Dual RNA-seq reveals distinct families of co-regulated and structurally conserved effectors in Botrytis cinerea infection of Arabidopsis thaliana. *BMC biology* 22 (1), S. 239. DOI: 10.1186/s12915-024-02043-4.

Weiberg, Arne; Wang, Ming; Lin, Feng-Mao; Zhao, Hongwei; Zhang, Zhihong; Kaloshian, Isgouhi et al. (2013): Fungal small RNAs suppress plant immunity by hijacking host RNA interference pathways. *Science (New York, N.Y.)* 342 (6154), S. 118–123. DOI: 10.1126/science.1239705.

Wiermer, Marcel; Feys, Bart J.; Parker, Jane E. (2005): Plant immunity: the EDS1 regulatory node. *Current opinion in plant biology* 8 (4), S. 383–389. DOI: 10.1016/j.pbi.2005.05.010.

Williamson, Brian; Tudzynski, Bettina; Tudzynski, Paul; van Kan, Jan A. L. (2007): Botrytis cinerea: the cause of grey mould disease. *Molecular plant pathology* 8 (5), S. 561–580. DOI: 10.1111/j.1364-3703.2007.00417.x.

Yang, Yuankun; Yang, Xiufen; Dong, Yijie; Qiu, Dewen (2018a): The Botrytis cinerea Xylanase BcXyl1 Modulates Plant Immunity. *Frontiers in microbiology* 9, S. 2535. DOI: 10.3389/fmicb.2018.02535.

Yang, Chenyu; Liang, Yingbo; Qiu, Dewen; Zeng, Hongmei; Yuan, Jingjing; Yang, Xiufen (2018b): Lignin metabolism involves Botrytis cinerea BcGs1- induced defence response in tomato. *BMC plant biology* 18. DOI: 10.1186/s12870-018-1319-0.

Yarrington, Robert M.; Verma, Surbhi; Schwartz, Shaina; Trautman, Jonathan K.; Carroll, Dana (2018): Nucleosomes inhibit target cleavage by CRISPR-Cas9 in vivo. *Proceedings of the National Academy of Sciences of the United States of America* 115 (38), S. 9351–9358. DOI: 10.1073/pnas.1810062115.

Zhang, Weiguo; Fraiture, Malou; Kolb, Dagmar; Löffelhardt, Birgit; Desaki, Yoshitake; Boutrot, Freddy F. G. et al. (2013): Arabidopsis receptor-like protein30 and receptor-like kinase suppressor of BIR1-1/EVERSHED mediate innate immunity to necrotrophic fungi. *The Plant cell* 25 (10), S. 4227–4241. DOI: 10.1105/tpc.113.117010.

Zhang, Lisha; Kars, Ilona; Essenstam, Bert; Liebrand, Thomas W. H.; Wagemakers, Lia; Elberse, Joyce et al. (2014): Fungal endopolygalacturonases are recognized as microbe-associated molecular patterns by the arabidopsis receptor-like protein RESPONSIVENESS TO BOTRYTIS POLYGALACTURONASES1. *Plant physiology* 164 (1), S. 352–364. DOI: 10.1104/pp.113.230698.

Zhang, Yi; Zhang, Yunhua; Qiu, Dewen; Zeng, Hongmei; Guo, Lihua; Yang, Xiufen (2015): BcGs1, a glycoprotein from Botrytis cinerea, elicits defence response and improves disease resistance in host plants. *Biochemical and biophysical research communications* 457 (4), S. 627–634. DOI: 10.1016/j.bbrc.2015.01.038.

Zhang, Meixiang; Chiang, Yi-Hsuan; Toruño, Tania Y.; Lee, DongHyuk; Ma, Miaomiao; Liang, Xiangxiu et al. (2018): The MAP4 Kinase SIK1 Ensures Robust Extracellular ROS Burst and Antibacterial Immunity in Plants. *Cell host & microbe* 24 (3), 379-391.e5. DOI: 10.1016/j.chom.2018.08.007.

Zhang, Lisha; Hua, Chenlei; Pruitt, Rory N.; Qin, Si; Wang, Lei; Albert, Isabell et al. (2021): Distinct immune sensor systems for fungal endopolygalacturonases in closely related Brassicaceae. *Nature plants* 7 (9), S. 1254–1263. DOI: 10.1038/s41477-021-00982-2.

Zhang, Xiaokang; Zhang, Zhanquan; Chen, Tong; Chen, Yong; Li, Boqiang; Tian, Shiping (2024): Characterization of two SGNH family cell death-inducing proteins from the horticulturally important fungal pathogen Botrytis cinerea based on the optimized prokaryotic expression system. *Molecular Horticulture* 4(1), S. 1–16. DOI: 10.1186/s43897-024-00086-3.

Zhang, Y.; Chen, X.; Li, G.; Qin, Q.; Zhang, M.; Qin, J. (2025): CBC Complex Regulates Hyphal Growth, Sclerotial Quantity, and Pathogenicity in the Necrotrophic Fungus Botrytis cinerea. *Journal of Fungi* (11), S. 429. DOI: 10.3390/jof11060429.

Zhu, Wenjun; Ronen, Mordechi; Gur, Yonatan; Minz-Dub, Anna; Masrati, Gal; Ben-Tal, Nir et al. (2017): BcXYG1, a Secreted Xyloglucanase from Botrytis cinerea, Triggers Both Cell Death and Plant Immune Responses. *Plant physiology* 175 (1), S. 438–456. DOI: 10.1104/pp.17.00375.

Zhu, Wenjun; Wei, Wei; Wu, Yayun; Zhou, Yang; Peng, Fang; Zhang, Shaopeng et al. (2017): BcCFEM1, a CFEM Domain-Containing Protein with Putative GPI-Anchored Site, Is Involved in Pathogenicity, Conidial Production, and Stress Tolerance in Botrytis cinerea. *Frontiers in microbiology* 8, S. 1807. DOI: 10.3389/fmicb.2017.01807.

Zhu, Wenjun; Yu, Mengxue; Xu, Ran; Bi, Kai; Yu, Shuang; Xiong, Chao et al. (2022): Botrytis cinerea BcSSP2 protein is a late infection phase, cytotoxic effector. *Environmental microbiology* 24 (8), S. 3420–3435. DOI: 10.1111/1462-2920.15919.

Zhu, Wenjun; Dong, Huange; Xu, Ran; You, Jingmao; Yan, Da-zhong; Xiong, Chao et al. (2023): Botrytis cinerea BcCDI1 protein triggers both plant cell death and immune response. *Frontiers in plant science* 14. DOI: 10.3389/fpls.2023.1136463.

Zipfel, Cyril (2008) Pattern-recognition receptors in plant innate immunity. *Current Opinion in immunology* 20 (1), S. 10-16. DOI: 10.1016/j.coi.2007.11.003.

Zönnchen, Josua; Gantner, Johannes; Lapin, Dmitry; Barthel, Karen; Eschen-Lippold, Lennart; Erickson, Jessica L. et al. (2022): EDS1 complexes are not required for PRR responses and execute TNL-ETI from the nucleus in Nicotiana benthamiana. *The New phytologist* 236 (6), S. 2249–2264. DOI: 10.1111/nph.18511.

10. Curriculum Vitae

Personal Details

Name: Nassim Safari
Address (work):
RPTU Kaiserslautern-Landau
AG Phytopathologie
Paul-Ehrlich-Straße 22; Raum 111
67663 Kaiserslautern
Email: safari@rptu.de - nassim.safari@gmail.com

EDUCATION

PhD candidate
in Plant Pathology
Since 2021
Thesis: „ Addressing the redundant roles of phytotoxic proteins in the necrotrophic infection of *Botrytis cinerea* by multi-knockout mutagenesis."
RPTU Kaiserslautern-Landau

Master of Science
in Plant Pathology
2011 – 2014
Thesis: „ Effects of essential oil–based nanoparticles for controlling apple blue mould (*Penicillium expansum*)"
Prize: Excellent master thesis
University of Zanjan

Bachelor of Science
in Plant Pathology
2005 – 2009
Thesis: „ Identification of beneficial rhizobacteria and their effects on plant growth and disease suppression"
Tehran University

RESEARCH EXPERIENCE

Research Assistant

Herbi Pharmed Institute, Tehran, Iran | 2019 – 2021

- Developed strategies for controlling *Aspergillus* and aflatoxin contamination in pistachios using natural compounds and optimized storage management techniques.

University of Rome La Sapienza, Rome, Italy | 2019

- Investigated aflatoxin inhibition mechanisms in fungal pathogens.

Herbi Pharmed Institute, Tehran, Iran | 2013 – 2019

11. Acknowledgments

First and foremost, I express my heartfelt gratitude to my supervisor, Prof. Dr. Matthias Hahn, for his unwavering support and invaluable guidance throughout my PhD journey. Words cannot adequately convey my appreciation for his mentorship, trust, and encouragement, allowing me the freedom to explore my ideas and fostering my independent growth. His insightful advice, both academic and personal, was a constant inspiration. I am especially grateful for the meticulous care he invested in reviewing and refining my thesis. It has truly been an honor and privilege to be one of his PhD students.

My sincere thanks to Prof. Dr. Ekkehard Neuhaus for generously serving as the second reviewer on my thesis committee, his kind and approachable manner, and the generous support from his research group.

My gratitude also goes to Prof. Dr. Michael Schroda, who graciously chaired my thesis defense committee.

Special thanks to Dr. David Scheuring for the insightful and engaging discussions throughout.

I warmly acknowledge my dear friends, colleagues, and collaborators, Keyvan Mahjoory, Alejandra Vielba Fernandez, Lea Sommer, Shekhar Chole, Sabrina Kaiser, Jonas Müller, Tobias Müller, and Muhammad Saeed, for their invaluable support and camaraderie. Ale and Lea, your friendship made tough times easier and happy moments even better.

Patrick Pattar, thank you for your active involvement, especially in the experiments central to my thesis. Your positive spirit and genuine kindness made the journey enjoyable and memorable.

Christa Jung, I cannot thank you enough for your constant comfort, kindness, and unfailing assistance. You've been a steady presence, and I'll always hold a special place in my heart for you.

Finally, my deepest gratitude goes to my family, whose love and encouragement have always been my foundation. To my beloved father, though you are no longer physically here, your strength, unwavering belief, and quiet guidance have carried me through each step. Your enduring presence in my heart made this possible. I dedicate this work to your memory, with love and endless thanks.

Thank you all for being integral to my journey and for the unforgettable and meaningful moments we've shared.

12. Darlegung des Eigenanteils

Nassim Safari

Thema: Addressing the redundant roles of phytotoxic proteins in the necrotrophic infection of *Botrytis cinerea* by multi-knockout mutagenesis

Die Konzeption und Planung der Arbeit wurde von **Prof. Dr. Matthias Hahn** initiiert und während der Dissertation gemeinsam weitergeführt. Die Etablierung neuer Methoden, Entwicklung der Versuchsdesigns, sowie Interpretation der Ergebnisse erfolgte ebenfalls gemeinsam. Die Erhebung experimenteller Daten, inklusive Analyse und Aufbereitung sowie das Verfassen der Dissertation wurden von **Nassim Safari** durchgeführt. Die Ergebnisse in folgenden Abbildungen wurden gemeinsam mit Dritten erhoben:
Patrick Pattar war an den Transformationsversuchen mit Botrytis beteiligt.
Gabriel Lück und Marcel Dittmann konstruierten im Rahmen eines Laborpraktikums die Vektoren pBc22x-H2B-Nep1 und pBc22x-His3-Nep1 zur Transformation von *B. cinerea*.
Shekhar Chule, dessen Masterarbeit unter meiner Betreuung durchgeführt wurde, war verantwortlich für die Analyse der Experimente mit *B. cinerea*-Stämmen, die Nep1 überexprimieren.
Andrea T. Herreño in der Arbeitsgruppe von **Prof. Remco Stam** führte das Whole-Genome Sequencing an der Christian-Albrechts-Universität zu Kiel durch.
Dr. Frederik Sommer in der Arbeitsgruppe von **Prof. Michael Schroda** in unserem Fachbereich führte die Massenspektrometrie-Analysen (MS/MS) zur Proteomanalyse an der RPTU Kaiserslautern durch.
Dr. Alejandra Vielba Fernández führte die Infektionstests an Arabidopsis Wildtyp- und Mutantenlinien mit *B. cinerea* Wildtyp und dem Mutantenstamm Bc18x durch.
RNA-Sequenzierungsdaten wurden uns von **Prof. Jan van Kan** (Wageningen University, Niederlande) zur Verfügung gestellt.

Die vorliegende Einschätzung über die erbrachte Leistung von Dritten wurde mit den genannten Personen einvernehmlich abgestimmt.

Datum, Unterschrift Doktorand/in Datum, Unterschrift Betreuer/in

13. Darlegung aller benutzten Hilfsmittel und Hilfestellungen

Nassim Safari

Thema: Addressing the redundant roles of phytotoxic proteins in the necrotrophic infection of *Botrytis cinerea* by multi-knockout mutagenesis

Alle visuellen Auswertungen wurden analysiert mit ImageJ (Fiji). Datenberechnungen und die Erstellung der Dissertation erfolgten mit Microsoft Office-Anwendungen. Für das in silico Klonieren, Erstellen von Primern und Aufrufen von Genkarten wurde SnapGene (GSL Biotech) verwendet. DeepTMHMM (BioLib) wurde eingesetzt, um die Transmembrandomänen der in dieser Studie untersuchten Proteine vorherzusagen. Statistische Analysen und grafische Datenaufbereitung wurden mit GraphPad Prism 5 (Dotmatics) durchgeführt. Für das Design der guide-RNAs wurden die Online-Tools GPP sgRNA Designer (Broad Institute) und CHOPCHOP verwendet. Zur Überprüfung möglicher Off-target-Effekte wurden BLASTn-Suchen gegen die Pilzgenom-Datenbank Ensembl Fungi – *Botrytis cinerea* durchgeführt. Für gelegentliche Übersetzungen vom Deutschen ins Englische oder umgekehrt wurden Google Übersetzer (Google), DeepL (DeepL SE) und ChatGPT (OpenAI) verwendet. Bei der Erstellung von Illustrationen wurde bioRENDER (BioRender) benutzt.

Datum, Unterschrift Doktorand/in